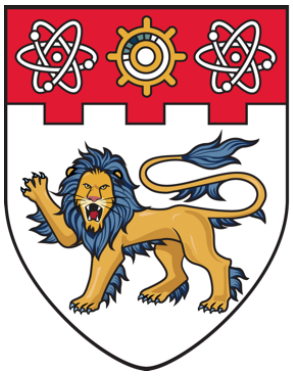

NANYANG TECHNOLOGICAL UNIVERSITY
SINGAPORE

NANOFORMULATION OF METAL COMPLEXES: INTELLIGENT STIMULI-RESPONSIVE PLATFORMS FOR BIOMEDICAL APPLICATIONS

HU MING

SCHOOL OF PHYSICAL AND MATHEMATICAL SCIENCES

2018

Nanoformulation of Metal Complexes: Intelligent Stimuli-responsive Platforms for Biomedical Applications

HU Ming

School of Physical and Mathematical Sciences

A thesis submitted to the Nanyang Technological University in partial fulfilment of the requirement for the degree of Doctor of Philosophy

2018

Statement of Originality

I hereby certify that the work embodied in this thesis is the result of original research done by me except where otherwise stated in this thesis. The thesis work has not been submitted for a degree or professional qualification to any other university or institution. I declare that this thesis is written by myself and is free of plagiarism and of sufficient grammatical clarity to be examined. I confirm that the investigations were conducted in accord with the ethics policies and integrity standards of Nanyang Technological University and that the research data are presented honestly and without prejudice.

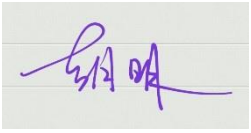

May 7th 2019

. . . . . .
Date

. . . . . .
HU Ming

Supervisor Declaration Statement

I have reviewed the content and presentation style of this thesis and declare it of sufficient grammatical clarity to be examined. To the best of my knowledge, the thesis is free of plagiarism and the research and writing are those of the candidate's except as acknowledged in the Author Attribution Statement. I confirm that the investigations were conducted in accord with the ethics policies and integrity standards of Nanyang Technological University and that the research data are presented honestly and without prejudice.

May 7th 2019

. . . . . .
Date

. . . . . .
XING Bengang

Authorship Attribution Statement

This thesis contains material from 2 paper(s) published in the following peer-reviewed journal(s) / from papers accepted at conferences in which I am listed as an author.

Chapter 1 is published as HU M., AI X., WANG Z., ZHANG Z., CHEONG H., ZHANG W., LIN J., LI J., YANG H. and XING B., Nanoformulation of metal complexes: Intelligent stimuliresponsive platforms for precision therapeutics, *Nano Research* **2018,** *11***,** 5474**.** DOI: 10.1007/s12274-018-2138-1

The contributions of the co-authors are as follows:

- Prof XING revised and edited the manuscript.
- HU M. and AI X. co-design the outline and logic flow of the manuscript.
- HU M. prepare the manuscript draft.
- The manuscript was revised by all the co-authors including HU M., AI X., WANG Z., ZHANG Z., CHEONG H., ZHANG W., LIN J., LI J., YANG H., XING B.

Chapter 2 is published as HU M., ZHAO J., AI X., BUDANOVIC M., MU J., WEBSTER R.D., CAO Q., MAO Z., XING B., Near infrared light-mediated photoactivation of cytotoxic Re(I) complexes by using lanthanidedoped upconversion nanoparticles, *Dalton Transactions* **2016**, *45*, 14101. DOI: 10.1039/c6dt01569g

The contributions of the co-authors are as follows:

- Prof XING provided the initial project direction, revised and edited the manuscript.
- HU M. prepared the manuscript draft. The manuscript was revised by HU M., ZHAO J., AI X., BUDANOVIC M., MU J., WEBSTER R.D., CAO Q., MAO Z., XING B.
- HU M. co-designed the study with AI X. and performed all the laboratory work at the school of physical and mathematical science. HU M. also analyzed the data.
- The preparation and characterization of Re complex were conducted by ZHAO J.
- BUDANOVIC M. and WEBSTER R.D. conducted ICP-MS experiment.

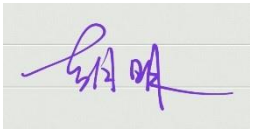

May 7th 2019

. . . . . .
Date

. . . . . .
HU Ming

Abstract

So far, precise theranostic demonstrated great possibility for effective therapeutics and diagnosis towards a variety of human diseases. As one type of commonly used agent, metal complexes have gained considerable successes in clinical applications for their rich and versatile properties for instance rich redox states, coordination numbers, preferential ligand and photo-induced ligand exchange processes etc. which can facilitate the rational design of therapeutic and sensing agents. In spite of these, limitations such as severe side effects, lack of specificity and inevitable toxicity have largely hampered their biomedical applications. To this end, innovative strategies to improve the pharmacokinetics as well as specificity of therapeutic and sensing agents based on traditional metal complex are highly demanded. Recently, nanotechnology has gained considerable attentions mainly due to their ability to reduce drug's side effect as well as enhanced pharmacokinetics and drug loading efficiency. Due to the favorable physical and chemical properties of nanostructures, the nanoformulation of metal complex has been demonstrated effective approaches to address the issues of currently used metal complex, especially those based on the stimuli-responsive therapeutic strategies allow on-demand treatment and imaging of diseases with excellent control over time, space and dosage. In this dissertation, we introduced some strategies which endowed traditional metal complex with stimuli-responsive properties for further advance their application as therapeutic and sensing agents.

Firstly, a NIR-light mediated strategy was developed to activated photo-sensitive Re(I) complex for its cytotoxic effect. To this end, the metal complex was incorporated onto light converting nanoparticles. Owing to the great spatial-temporal resolution of light irradiation, upon NIR stimulation, Re(I) complex can be locally activated within pathological side by upconverted UV light from nanoparticles and exert cytotoxic effect for precise treatment

against both drug-susceptible and drug-resistant cancer cells, minimizing unwanted photo damage.

Secondly, we introduced another stimuli-sensitive strategy for selective sensing illicit drug Gamma-hydroxybutyric acid (GHB). Upon substrate-specific enzyme recognition of GHB, reduced nicotinamide adenine dinucleotide (NADH) would be generated. As an ubiquitous reducing agent, the resulting NADH molecule can promote the reduction of gold(III) complex and form gold nanoparticles (AuNPs). The distinct transformation from molecular metal complex into nanoscaled particles can be easily monitored through either spectrometer or naked-eye observation, allowing specific sensing of GHB.

Thirdly, we designed a strategy for long term sensing and imaging in response to reducing cellular environment. Typically, we designed a lanthanide based molecular probe which can respond to reducing environment. Once reduced, this lanthanide probe would undergo inter-molecular cross linking and form dimer structure. The resulted dimer would subsequently assemble into nanoscaled particles which can potentially accumulate within cells for long term intracellular sensing and imaging purpose.

Lastly, we provided an effective approach to site-specifically localize luminescent complex on cell surface through metabolic labelling and biorthogonal reaction. Upon stimulation by NIR illumination, the intense emission from the complex could activate the light-responsive membrane channel and allow precise manipulation of ion flux both in vitro and in vivo. This strategy could not only provide new strategies towards the manipulation of membrane activities and relevant biological processes in vitro and in vivo, and it would also promote in-depth understanding of the physiological roles of cell membrane in live settings.

In summary, these proposed intelligent system in this dissertation could provide new prospectives for the precision therapeutics and diagnosis based on their stimuli-responsive

properties. We believe these current work could promote innovations in this research field and facilitate the advance in biomedical research and scientific community.

Acknowledgements

I would like to express my gratitude to Nanyang Technological University to the financial support and this opportunity to learn and explore within a great atmosphere.

I would like to express my deep gratitude to my supervisor Assoc. Prof. XING Bengang for the encouragement and support throughout all these four years. I'm grateful for his not giving up and still being patient to guide me through all the problems in experiment, paper preparation, presentation, especially in logical thinking. In addition, his commitment to excellence and passion for his career greatly inspired me and help me build up a proper career aspiration.

I would like to thank my collaborators Prof. MAO Zongwan, Assoc. Prof. LOH Zhiheng, Dr. CAO Qian, Dr. TONG Yan, Ms. DONG shuo, Mr. FU Afu, Mr. LOW Peiiang for their kind help and suggestions.

I would also express my thanks to my fellow group members and friends from other groups, Dr. AI Xiangzhao, Dr. MU Jing, Dr. AW Junxin, Dr. LYU Linna, Dr. ZHANG Zhijun, Dr. ZHANG Wenmin, Dr. SHINYA Ariyasu, Mr. WANG Zhimin, Mr. CHEONG Haolun, Mr. HAYASHI Hirohito, Ms. CHAN Huiling, Dr WU Xiangyang, Dr. LU Shentao, Ms NG Shuemei, Ms WANG Jin for their kind assistance and helpful discussion.

I would like to thank my friends Ms. HE Lei, Mr. WU Liuhai, Mr. ZHUO Shitian, Ms. LI Xirui, Mr. ZHANG Qiuchi, Dr. SHU Zhiyu, Mr. WANG Yong for all the support and joy they brought to me.

I would also express my special thanks to Mr. John LEE Yungchun for the inspiration and support he brought to me.

Last but not least, I want to express my deepest gratitude to my family. Thank you for taking care of everything so that I can do my PhD without much worries. Thank you for sharing my happy thoughts and difficult moments for the past 29 years. Thank you for always being with me. I would not be able to go this far without the love, warmth and peace in the family.

Table of Contents

Abstract iv

Acknowledgements 1

Table of Contents 3

List of abbreviations 6

Chapter 1: General introduction 8

1.1 Introduction 8

1.2 pH-responsive nanoplatforms for precise delivery of metal complexes 11

1.3 Redox-responsive nanoplatforms for metal complex activation 16

1.4. Enzyme-responsive nanoplatforms for controlled release of metal complex 20

1.5. Light-responsive platforms for precision therapeutics 22

1.6. Magnetic stimuli-responsive platforms for precision therapeutics 40

1.7 Research goals 43

1.8 Reference 44

Chapter 2: Near infrared light-mediated photoactivation of cytotoxic Re(I) complex by lanthanide-doped upconversion nanoparticles 64

2.1 Introduction 64

2.2 Experimental 66

2.3 Results and discussion 70

2.4 Conclusions 80

2.5 Reference 81

Chapter 3: A bioinspired strategy for selective sensing of illicit date rape drug GHB 86

3.1 Introduction 86

3.2 Materials and methods 88

3.3 Results and discussion 89

3.4 Conclusion 97

3.5 Future work 98

3.6 Reference 98

Chapter 4: Nanoformulation of lanthanide complex, smart probe for persistent imaging in tumor cells 100

4.1 Introduction 100

4.2 Materials and methods 102

4.3 Results and discussions 109

4.4 Conclusion 115

4.5 Future work 115

4.6 Reference 115

Chapter 5: NIR-responsive metal Complexes for Precise Cell Activity Regulation 117

5.1 Introduction 117

5.2 Materials and methods 120

5.3 Results and discussion 126

5.4 Conclusion 135

5.5 Reference 136

Chapter 6: Conclusion 138

Publications 140

List of abbreviations

ACN	Acetonitrile
Ac4ManNAz	Peracetylated N-azidoacetylmannosamine
Boc	tert-Butyloxycarbonyl
DCM	Dichloromethane
DIPEA	*N*,*N*-diisopropylethylamine
DLS	Dynamic light scattering
DMEM	Dulbecco's modified Eagle's medium
DMF	Dimethylformamide
DMSO	Dimethyl sulfoxide
EDC·HCl	*N*-(3-dimethylaminopropyl)-*N'*-ethylcarbodiimide hydrochloride
FBS	fetal bovine serum
Fmoc	Fluorenylmethyloxycarbonyl
HBTU	*O*-(benzotriazol-1-yl)-*N,N,N',N'*-tetramethyluronium hexafluoro-phosphate
MS	Mass spectrometry
PBS	Phosphate buffered saline
^{1}H NMR	Proton nuclear magnetic resonance spectroscopy
RP-HPLC	Reversed phase-high performance liquid chromatography
TEM	Transmission electron microscopy
TFA	Trifluoroacetic acid
TIPS	Triisopropylsilane
UCNP	Upconversion nanoparticles

UV	Ultraviolet
λ_{ex}	Excitation maximum
λ_{em}	Emission maximum

Chapter 1: General introduction

1.1 Introduction

Currently, precision therapeutics has attracted considerable attentions in clinical practice owing to its extraordinary roles in the battle against diverse diseases including cancer, neurological disorders, cardiovascular diseases, as well as bacterial infections [1]. The success of precision therapeutics/treatment not only relies on the efficient therapeutic agents. In addition, it requires robust and reliable analytical approaches which can facilitate the diagnosis of disease and posttreatment monitoring of the patients, to evaluate the therapeutic efficacy. Among the commonly used agents, metal complexes have been widely used in clinics, mainly because of the versatile roles of metal ions in biological process [1]. What's more, some of these metal compounds exhibit advantageous properties such as specific metal-ligand interactions, multiple redox states, photo-induced ligand exchange processes, as well as preferential ligand and coordination numbers etc. which allow them to interact with biomolecules, for instance DNA or proteins, in a multiplexing manner, and interfere with cellular pathways, therefore exerting their therapeutic effects in disease treatment [2]. Currently, a variety of drugs based on metal complexes (e.g. Platinum complexes, Gold complexes, Bismuth complexes etc.) have been extensively designed and developed for the treatment of diverse health threating ailments[3]. However, despite their great successes, the use of these metal complexes during the treatment processes has been mostly associated with severe side effects such as inevitable toxicity and limited specificity.[4] In addition, the rapid clearance and short half-life in circulation system have largely affected their *in vivo* therapeutic efficacy.[5] Therefore, the development of new metallodrugs based on rational design of novel metal complexes with potent

therapeutic effects, enhanced specificity as well as improved pharmacokinetics still remain a significant challenge.

In recent decades, the remarkable advance of nanomedicine based on the extensive usage of nanotechnologies has gained considerable attention and greatly promote the integration of metal complexes and nanomaterials for reduced side-effect, and improved pharmacokinetics. Such innovative platform greatly promotes the application in precise and effective therapeutics of various diseases, mainly due to the unique physical and chemical properties of diverse nanoagents in terms of the nanoscale size effect and high surface-to-volume ratio which allow efficient drug loading[6]. In addition, facile and versatile surface functionalization of nanoagents can greatly improve the solubility as well as bioavailability of metallodrugs. By right, several nanoplatforms for drug delivery purpose have been established by direct loading of therapeutic metal complexes on the surface or in the cavity of nanostructures mainly for their abilities to accumulate within diseased sites through enhanced permeability and retention effect (EPR effect)[7]. In spite of their initial success, the lack of specificity and uncontrolled drug release within targeted diseased sites remain challenging issues which heavily restrict their future clinical applications.[8] Effective and robust approaches, which can deposit therapeutic payload into targeted location on-demand with minimum off-target leakage, would be highly desirable and can be potentially used for precise therapeutics in clinics.

To bring such a vision of precision therapeutics into biomedical practice, extensive efforts have been devoted. Inspired by the responsiveness of living organisms, stimuli-responsive nanoplatforms are

emerging as a feasible and promising strategy for precision therapeutics with excellent spatial, temporal and dosage control.[9] Basically, such innovative platform would trigger payload (e.g. metal complex etc.) release or activation to exert cytotoxic effect in response to stimulation within targeted regions, thus minimizing nonspecific off-target leakage and improving the therapeutic efficacy. Until now, various stimuli-responsive therapeutic platforms which are sensitive to endogenous properties of diseased microenvironment including pH gradient, redox and enzyme activities, have been extensively investigated for the treatment of neoplastic diseases. In addition, extracorporeal physical stimuli including light, magnetic field etc. can be also applied to facilitate the studies of their precise therapeutic effect on pathological situations (e.g. ischemia, inflammatory diseases, infections etc.).[8, 10]

By right, the field of nanoconstructs functionalized with metal complex for administering therapeutic agents has been extensively studied. Relevant advance on this topic has already been discussed[7]. In this review, we mainly focus on the specificity and environment-responsiveness of nanoformulation of metallodrugs in disease treatment, and summarized the latest advances on the integration of therapeutic metal complexes with various stimuli-responsive intelligent platforms which respond to either endogenous signals (e.g. pH, redox conditions, enzyme activities etc.) or external triggers (such as light irradiation and magnetic field manipulation) for precise therapeutic purpose. These approaches provide great inspiration and excellent means for more specific and effective treatment of various human diseases through the use of improved metallodrugs in future clinical practice. Last but not least we also discuss the potential challenge and perspective of metallodrugs and their nanoformulations for future development towards precise disease treatment with potent therapeutic effect as well as improved specificity and minimized side effect.

1.2 pH-responsive nanoplatforms for precise delivery of metal complexes

Among diverse environmental triggers, pH gradients have been commonly exploited to design intelligent responsive therapeutic nanoplatforms. Compared to normal tissues, the diseased sites have been demonstrated to display altered pH conditions. For example, the pH states tend to be more acidic in tumor regions (with a median pH value about 7.0) than normal tissue (pH~7.4).[11] The acidic microenvironment of tumor areas is caused mainly by the overproduction of lactic acid which mostly arises from the elevated glucose uptake and reduced oxidative phosphorylation.[12] What's more, the poor lymphatic drainage and insufficient blood supply also play crucial roles contributing to the acidic tumor microenvironment.[13] Such notable difference of pH among normal tissue and pathological tissue inspired researchers to exploit local pH as natural triggers for controlled release of drug at targeted area to achieve high drug concentrations and minimize systemic exposure.[14]

1.2.1 Approaches based on disassociation of pH-sensitive bond

To achieve precise therapeutics through pH-responsive nanoplatform, one commonly used strategy is to utilize the pH-sensitive bond which can be cleaved under acidic conditions and allow targeted drug release within pathological region. For instance, Gu and Xu et al. reported a supramolecular dendritic system with PEGylated platinum derivatives coordinated to the carboxyl groups on the surface of the polymer. The polymer greatly enhanced the biodistribution and pharmacokinetics of platinum-based drug due to the stable nanostructure and PEG shell during blood circulation. Upon internalization into tumor cells, the low intracellular pH within tumor region triggers rapid degradation of the polymer owing to acid-sensitive coordinate bond. Therefore, the surface functionalized platinum drug can be released to exert antitumor activities. *In vivo* studies demonstrated that such system not only provided

antitumor efficacy which is comparable to the clinically used cisplatin. In addition, it exhibited reduced side-effect such as renal toxicity than platinum complex-based drugs. Moreover, the encapsulated NIR dye allows tracking the fate of such theranostic nanoplatforms and monitoring real-time drug metabolism both *in vitro* and *in vivo*. [15]

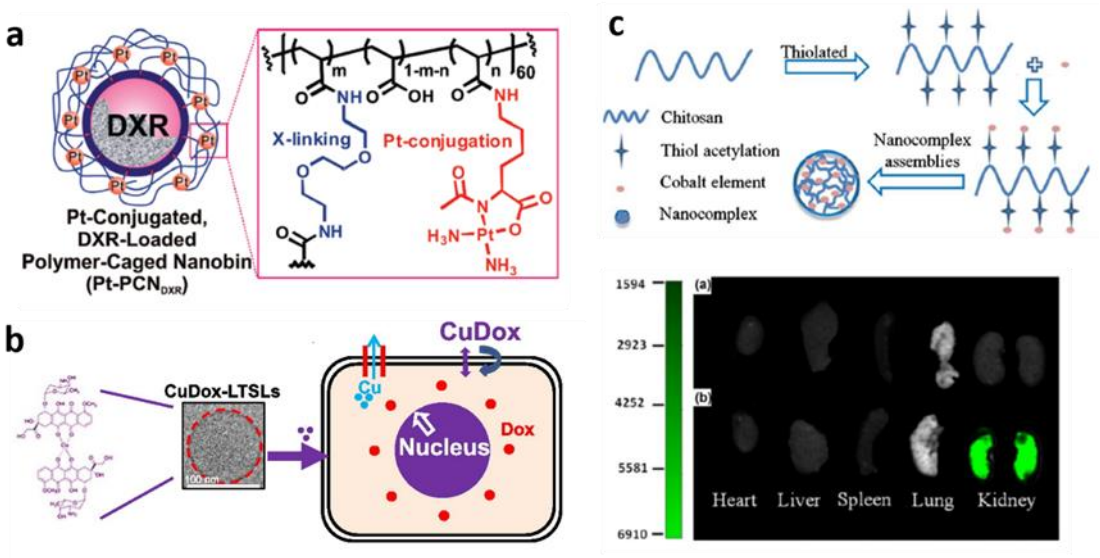

Figure 1 Illustration of pH-responsive platforms for precision therapeutics. (a) pH-sensitive polymer-caged nanobin [31]. (b) a pH-responsive copper-doxorubicin (CuDox) cargo loaded in lysolipid-based liposome [35]. (c) Co(II) chitosan nanocomplex as pH-responsive renal fibrosis targeting drugs[36].

In addition to single drug delivery, pH-responsive nanoplatforms also exhibited potential for multi drug delivery in synergistic therapy. Nguyen and O'Halloran et al. demonstrated a polymer-caged nanobin (PCN) to achieve dual drugs delivery of doxorubicin and cisplatin (Fig. 1(a)). The PCN is composed of doxorubicin-encapsulated core-structure, which is surrounded by pH-responsive platinum prodrug loaded shell. Platinum complex release observed under acidic tumor environment, can be attributed to the acidic lability of the N α-acetylamido ligand which is protonated by acid and detached

from the metal center. In the meantime, the protonation of core structure liposome composed of amine-modified lipid will lead to simultaneous release of doxorubicin. As such, both drugs can be delivered to the disease sites through a pH-controlled manner and exert synergistic effect to enhance the overall cytotoxicity against cancer cells at reduced doses.[16] Recently, to provide safe and effective strategy for delivery of therapeutic drug for cancer treatment, especially those with drug resistant properties, Wang's team has designed core-shell-corona nanoparticles $^{+}$NP/Pt@PPC-DA. To facilitate the rapid drug accumulation within drug-resistant cancer cell, positively charged core particle $^{+}$NP/Pt was prepared for its efficient cellular uptake. However, under *in vivo* condition, the positively charged nanoparticles are likely to be rapidly cleared from blood circulation, due to nonspecific interaction with serum. To circumvent this issue, acid-sensitive polymer PPC-DA was decorated on the surface of $^{+}$NP/Pt particles. Exposure of $^{+}$NP/Pt@PPC-DA to slight acid condition at pH 6.8 triggered the degradation of amide bonds of PPC-DA and generated positively charged groups, which subsequently lead to electrostatic repulsion to release positively charged $^{+}$NP/Pt. *In vitro* and *in vivo* studies on cisplatin-resistant tumor model demonstrated that $^{+}$NP/Pt@PPC-DA exhibited prolonged blood circulation and enhanced platinum drug accumulation in tumors. In the meantime, the response to pH led to the release of positively charged $^{+}$NP/Pt nanoparticles and hence further promoted nanoparticle internalization by cisplatin-resistant tumor cells *in vivo*. Furthermore, $^{+}$NP/Pt rapidly released cisplatin in the intracellular environment. Therefore, successful inhibition of cisplatin-resistant tumor growth was achieved in the murine xenograft model.[17] Apart from platinum complex, copper-based complexes have also been applied for the precise treatment of diseases. For instance, Farrara's team reported the delivery of metallodrug complex (CuDox) though activatable liposomes (Fig. 1(b))[18]. The complexation of Cu^{2+}

and doxorubicin in liposomes can effectively extend drug retention in blood, maintain the treatment efficacy and reduce the accumulation of drug in sensitive tissue and organ such as heart. The drug-metal complex is highly stable under physiological condition and rapidly releases the drug at acidic environment associated with lysosomes. Such rationally designed liposomes with drug-metal complex can facilitate the effective drug release in response to tumor environment. Moreover, the complexation of drug and Cu^{2+} in liposomes can minimize the side effect of clinically used DOX by reducing the formation of free radicals which arise from the interaction of drug with metal ions *in vivo*. What's more, the delivery of therapeutic metal complexes through pH-sensitive nanoplatform has been exploited to target diverse pathological conditions such as renal fibrosis, chronic inflammation etc[19]. Recently, Hu and coworkers reported chitosan cobalt nanocomplexes as pH-responsive renal fibrosis targeting drugs (Fig. 1(c)) [19a]. Tubulointerstitial fibrosis is considered the common pathway of chronic progressive kidney disease. Cobalt chloride has been reported to be able to attenuate renal fibrosis. However, it exhibited obvious toxicity and could cause unwanted damage to healthy tissue. Chitosan, as a widely used natural drug carrier, possessed superior biocompatibility and coordination ability. The nanocomplex formed by chitosan and cobalt is stable in circulation system (pH 7.4) and able to accumulate in proximal tubule. The pH-dependent cleavage of coordinate bond between cobalt and chitosan under acidic condition in lysosomes can trigger rapid release of drug exhibiting the potential as a kidney-targeting drug for the treatment against renal fibrosis.

1.2.2 Approaches based on rupture of pH-sensitive carrier

In addition to bond breaking, another commonly used strategy based on pH dependent hydrophobic to hydrophilic transitions of nanocarriers have also been well investigated for precise drug delivery

through the polymer matrix collapse. For instance, Nie and Wang et al. formulated a class of smart nanostructure with ultrasensitive size switching effect in response to pH change within tumor microenvironment for enhanced tumor penetration and efficient *in vivo* drug delivery. The nanostructure was constructed through amphiphilic polymer directed assembly of platinum-prodrug conjugated polyamidoamine (PAMAM) dendrimers, in which the amphiphilic polymer contains ionizable amine groups for rapid pH-responsiveness. The size of this nanostructure at neutral pH conditions (e.g. blood circulation) is ~80 nm. Once enter the slightly acidic tumor environment, where pH is 6.5−7.0, the nanostructures would undergo an obvious and sharp size transformation within a narrow range of acidity (less than 0.1−0.2 pH units) and dissociate instantaneously within seconds into the building blocks (~ less than 10 nm in diameter). Such rapid size-switching property will not only be beneficial to accumulation in tumor region via the enhanced permeability and retention effect, but also allow more efficient tumor penetration. Further studies of both pH-sensitive and insensitive nanostructures which resemble in size, surface charge, and chemical composition were carried out on both multicellular spheroids and poorly permeable BxPC-3 pancreatic tumor models. The results suggested that the pH-triggered size switching is a viable strategy for improving drug penetration and therapeutic efficacy.[20] In another study, Wang and Du et al. reported a responsive nanocarrier which is able to spatially target both tumor-associated macrophages and tumor cells for chemo-immunotherapy. To achieve optimized therapeutic efficacy, a system, which is able to deliver multiple therapeutic agents differentially to target cells, would be highly desirable. Therefore, they developed an immunostimulatory nanocarrier (BLZ‑945SCNs/Pt) which could spatially target tumor-associated macrophages (TAMs) and tumor cells for cancer chemoimmunotherapy. At pH of 6.7-6.8, the ionization of amine group on the

amphiphilic polymer would induce the hydrophobic to hydrophilic transition and eventually leads to structure collapse of the carrier within the prevascular regions of tumor tissues, thus enabling the concurrent release of both platinum-prodrug nano-conjugates and small molecule inhibitor BLZ-945 for colony stimulating factor 1 receptor (CSF-1R) of TAMs. The released inhibitor in the extracellular environment can be taken up by TAMs and cause TAMs depletion from tumor tissues. In the meantime, the Pt-prodrug containing small particles would allow deep tumor penetration as well as intracellularly specific drug release and exert cytotoxic effect against cancer cells. Further mechanistic studies revealed that the customized pH-sensitive co-delivery nanocarriers not only induce tumor cell apoptosis but also modulate the tumor immune environment and eventually augment the antitumor effect of $CD8^+$ cytotoxic T cells through TAMs depletion.[21]

1.3 Redox-responsive nanoplatforms for metal complex activation

In addition to pH-responsive delivery of metal complex, another well-established strategy for precise therapeutics involves redox-responsive platforms which utilize the local redox properties within diseased regions to activate metal complex agents. The concept of redox-responsive therapeutics arises from the steep reductive gradient between the extracellular and intracellular compartment of cells, and the accentuated upregulation of reductive species in cancer cells. The highly reductive environment in the intracellular milieu is mainly due to the presence of glutathione tri-peptide, ɤ-glutamyl-cysteinyl-glycine (GSH), which is the most abundant small molecule reducing agent.[22] Within normal cells, the concentration of GSH is higher inside of the cell (e.g. ~ 2-10 mM) compared to outside (e.g. ~ 2-20 mM).[23] In addition to the reductive nature of intracellular environment, tumor cells are endowed with an even more reductive microenvironment, since their intracellular GSH concentration is four-times

higher than that of normal cells.[24] Exploiting this cancer-specific chemical cue, one commonly strategy is to utilize the transformation of inert prodrug into its bioactive form under such reducing condition. Recently, Lippard and Dai et al. devised a redox-sensitive delivery system based on soluble single-walled carbon nanotubes (SWNTs) and platinum (IV) prodrug. Such SWNTs can effectively deliver the Pt(IV) prodrug into tumor cells. Under the reducing intracellular microenvironment of tumor cells, the Pt(IV) prodrug can be converted into cytotoxic Pt(II) species. Through this strategy, a substantial increase in cytotoxicity was achieved in comparison to cisplatin and the free Pt(IV) complex.[25] For targeting of folate receptors which are overexpressed on cancer cells, the Pt(IV) prodrug was conjugated to folate through axial ligand. With the assistance of folate, Pt(IV) prodrug can be effectively and specifically delivered into cancer cells and showed enhanced cell killing properties by up to 9-fold compared to cisplatin itself.[26] Based on the strategy of intracellular reduction of Pt(IV), several groups have reported redox-sensitive nanosystem for tumor-specific and controlled drug delivery. Inspired by the ligand dissociation property of Pt(IV) prodrug under reducing environment, extensive studies have been exploited to fully utilize such feature for multi drug delivery to achieve synergistic treatment of diseases. For instance, Liang's team designed a dual drug backboned shattering polymeric nanomedicine (Fig. 2(a)) [27]. Demethylcantharidin (DMC), which can improve anticancer activity of DNA-damaging drugs without evident toxicity, was introduced to Pt(IV) prodrug. The interaction between DMC and Pt center based on metal-ligand coordination allows precise control of drug ratio to optimize therapeutic efficacy. What's more, the prodrug was further reacted with linker ethylenediamine and self-assembled into polymeric nanoparticles. Under reductive and acidic tumor microenvironment, the nanoscale polymers can be site-specifically chain-shattered through the

transformation of Pt(IV) into Pt(II) and hydrolysis of DMC precursor, releasing both drug to exert synergistic antitumor effect in a controlled manner. Moreover, the *in vivo* experiment on a high-fidelity patient-derived lung cancer model demonstrated the potential application of such personalized nanomedicine with precisely controlled composition in disease treatment. Moreover, to overcome the drug resistance in cancer treatment, nano-scaled metal-organic frameworks (MOFs) have been also applied for co-delivery of therapeutic metal complex prodrugs and siRNA (Fig. 2(b))[28]. MOFs are emerging types of porous materials which are constructed through self-assembly of molecular building blocks[29]. Typically, nanosized MOFs possess advantages such as well-defined pore aperture, high loading capacity, and intrinsic biodegradability. In addition, the size, composition and morphology of engineered MOFs can be fine-tuned to optimize their properties for drug loading and controlled release, thus exhibiting the great potential to serve as promising platforms for drug delivery and disease treatment [30].For instance, Lin and coworkers designed an UiO MOF nanostructure with high porosity and surface binding sites. Redox-sensitive Pt(IV) prodrug and MDR gene silencing siRNA are efficiently loaded into UiO MOFs. The UiO carrier can protect siRNAs from nuclease degradation, enhance siRNA uptake, thus improving the MDR gene silencing effect and leading to an order-of-magnitude enhancement in therapeutic efficacy of metallodrugs.

In addition to drug delivery, the redox-responsive drug delivery properties have also been combined with multi-modal imaging modalities for diagnosis and evaluation of therapeutic outcomes. Recently, Guo and Wang et al. reported a superparamagnetic iron oxide nanoparticles (SPIONs) based nanocomposite loaded with Pt(IV) prodrug as targeted theranostic agents for effective cancer treatment. Together with the promising magnetic targeting and anti-proliferative properties, such intelligent

platform exhibited minimum toxic effect over normal cells. More importantly, unlike most commonly used chemotherapeutic agent cisplatin, which is prone to inactivation in the presence of GSH, such therapeutic platform displayed increased cytotoxicity upon GSH treatment, suggesting a different mechanism action of the nanocomposite, compared to well-established paradigm for Pt drugs.[31]

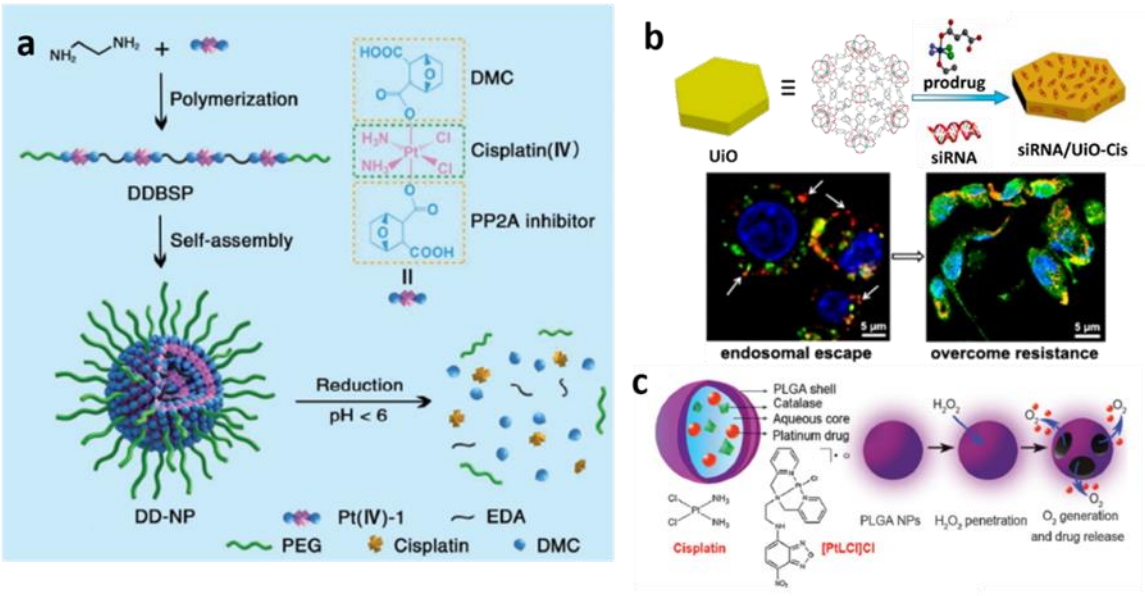

Figure 2 Schematic illustration of Redox-responsive platforms for precision therapeutics. (a) Dual drug backboned shattering polymeric theranostic nanomedicine (DDBSP) [47]. (b) Redox-responsive MOFs (siRNA/UiO-Cis) [48]. (c) ROS-responsive PLGA NPs structure and the mechanism of intracellular drug release[56].

In addition to the highly reductive properties, the redox environment in pathophysiological conditions is also characterized by upregulated reactive oxygen species (ROS), which accumulate in inflammatory tissues to create an oxidative stress[32]. Accumulating evidence suggests that the misregulation of ROS is associated with diverse diseases, such as cancer, atherosclerosis, and asthma.[33]

Therefore ROS-derived redox condition has been well-explored as a chemical trigger for stimuli-responsive therapeutics. For instance, Guo and He et al. proposed a ROS-responsive nanocarrier for controlled dual-release of Pt(II) drug and O_2 against cisplatin-resistant cancer cells (Fig. 2(c)). In their typical design, PLGA nanoparticles were chosen as a degradable carrier, and platinum drugs together with catalase which served as oxygen generating agent were incorporated into the particles. Facilitated by catalase, oxygen was generated when intracellular ROS penetrate into the particles, thus leading to the rupture of the carrier and subsequent release of encapsulated drugs. Moreover, the generated oxygen helped relieve hypoxia-induced multidrug resistance and enhance the efficacy of chemotherapy.[34] Similarly, Liu and Feng et al. reported a redox-sensitive liposome loaded with catalase and Pt(IV) prodrug for enhanced chemo-radiotherapy against tumor under hypoxic conditions. Such system could catalyze the decomposition of hydrogen peroxide produced by tumor cells, thereby providing oxygen source to relieve hypoxia and remarkably enhance the therapeutic efficacy of chemo-radiotherapy.[35]

1.4. Enzyme-responsive nanoplatforms for controlled release of metal complex

Although nanoplatforms in response to pH and redox signal have been well investigated for controlled release and activation of metal complexes for precise therapeutics, the inherent pH gradient and pervasive reductants in both healthy and diseased tissues may potentially compromise the specificity during treatment. Therefore, alternative approaches which allow more selective on-demand treatment in response to specific triggers in diseased sites are highly desirable. Recently, strategy based on enzyme-responsive nanoplatform has emerging as one promising option for precise delivery of metal complex for disease treatment. As one type of specific endogenous molecules, enzymes play critical roles in all biological and metabolic processes. The misregulation of enzyme expression and activity

underpins the pathology of many diseases.[36] Exploiting enzymes as triggers can be an advantageous strategy in therapeutics not only for their ability to promote chemical reactions under physiological conditions.[37] Moreover, enzymes exhibit extraordinary selectivity for their substrates allowing for specific, sophisticated therapeutic modality within desired biological targets.[38] In the past few years, a number of nano-scaled materials have been employed for the design of enzyme-responsive systems including polymer materials, phospholipids and inorganic materials. The integration of nanomaterials with enzymatic responses can endow the delivery of metal complex with bio-specificity and selectivity, allowing for promising applications in biomedical fields. For example, Chen and coworkers have constructed a biocompatible DNA origami nanostructure for the delivery of anticancer ruthenium complex (Fig. 3). The unique tetrahedral DNA nanocages facilitate the intercalation with Ru(II) complex, enhancing the loading efficiency of therapeutic agents. Further conjugation with biotin allows specific cellular uptake of the DNA nanocarrier against HepG2 cells through receptor-mediated targeting. Moreover, different from free Ru(II) complex or nanocage alone, such system translocated to cell nucleus upon internalization and would degrade in response to DNases, thus leading to controlled drug release and subsequent induction of effective cell apoptosis through ROS-mediated signaling pathways.[39]

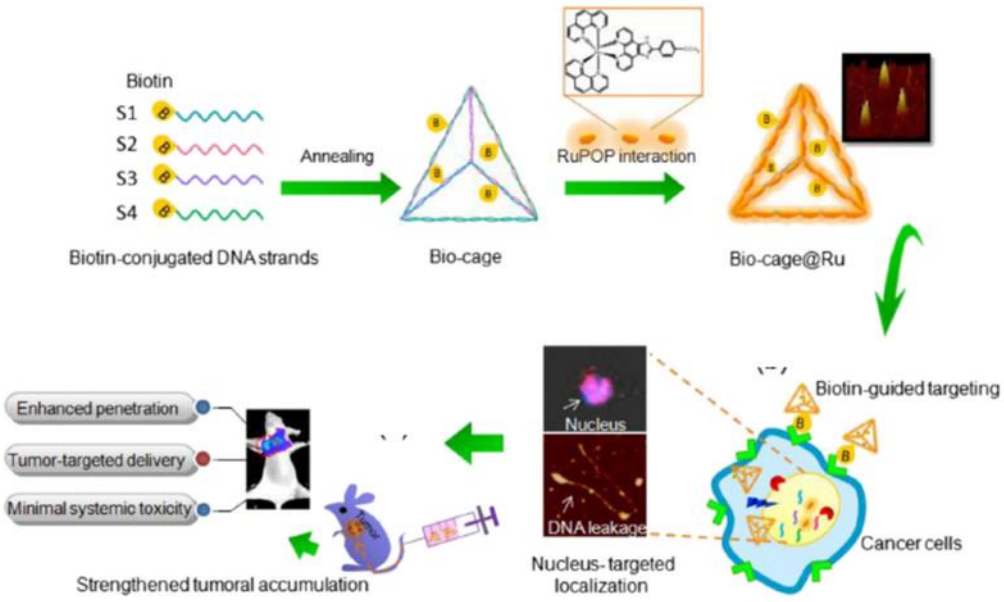

Figure 3 Enzyme-mediated precision therapeutics. Illustration of multifunctional Bio-cage@Ru nanostructure for enhanced tumor treatment and reduced systemic toxicity [62].

1.5. Light-responsive platforms for precision therapeutics

Compared to intrinsic stimuli (e.g. pH gradient, redox environment and enzyme activity etc.) external stimuli (e.g. light trigger, magnetic field etc.) also display advantages of user-defined control over time and space without interference from complex biological environment. Therefore, therapeutic platforms which respond to external stimuli would allow for more precise regulation of timed release of therapeutic agents within highly confined area of interest for precision treatment. Among diverse external stimuli, light trigger strategy is gaining increasing attention because of its great opportunity for on-demand therapeutics in well-delimited sites, which arise from the non-invasive and spatiotemporally precise mode of action upon light irradiation. [40] So far, a variety of photo-sensitive therapeutic systems have been studied for light-responsive drug release, photodynamic therapy and photothermal therapy

under living conditions.[41] Until now, the most widely used light sources for therapeutic purpose are based on UV-visible light, whose penetration depth has been limited by the absorption and scattering of endogenous molecules such as water, lipids and proteins inside living systems.[42] Therefore, efforts to improve tissue penetration depth towards pathological sites that located deep beneath the skin are highly desirable. By right, one of the key strategies for a deeper tissue penetration is the use of near-infrared (NIR) light within the range of NIR window (e.g. ~ 650 – 1350 nm). Light within this range exhibits better tissue penetration depth (e.g. < 10 cm) than UV-visible light (e.g. < 1 cm), due to lower absorption coefficient of water, lipids and proteins. In addition, compared to short-wavelength UV-visible light, long-wavelength NIR light is expected to have minimal photodamage to biomolecules, cells and tissues. To this end, a burgeoning number of drug molecules and bioprobes which respond to NIR light have been devised.[43] However, the laborious synthetic procedures, poor aqueous solubility and limited accumulation within pathological area have restricted their future applications. Thanks to the advance of chemistry and nanotechnology, some novel nanomaterials (e.g. upconversion nanoparticles, UCNPs, gold nanoparticles, AuNPs, carbon nanomaterials, CNMs, etc) which display large NIR absorption coefficients, have gained increasing attention for their ability to absorb NIR light and facilitate the generation of bioactive species (e.g. drug, ROS etc) for treatment of diseased situated in deep tissue.[44] Moreover, these promising materials can serve as useful platforms for integration of multiple functions in one single system, which could greatly promote the simultaneous disease diagnosis, treatment and real-time imaging *in vitro* and *in vivo*.

1.5.1 UV-visible light-mediated precision therapeutics

Currently, the most commonly used strategies to achieve light-responsive therapeutics involve the stimulation by UV-visible light, through which photolabile and photoactivatable moieties triggered to induce controlled therapy as well as imaging at targeted sites. In this part, the rational design through controlled photo-release of bioactive molecules and activation of prodrug through light irradiation will be discussed.

1.5.1.1 UV-visible light triggered drug-release

Carbon monoxide (CO) is known for its toxicity which arises from its strong affinity towards hemoglobin. However, recent studies revealed that it can also function as an important cell signaling mediator in response to stress and inflammation[45]. Beside, CO is known to exert protective role through its anti-inflammatory, anti-apoptotic and anti-proliferative properties.[46] However, its systemic toxicity and control of the location, dosage and timing of gaseous molecule delivery are two major challenges for the controlled CO release. As such photoactive CO-releasing metal complexes have been studied and exhibited promising potential for intracellular CO delivery, due to their ability to store CO in solid state that can be liberated upon external light stimulations. However, these compounds may have issues for their rapid diffusion, which may lead to unwanted toxicity to healthy tissue.[47] The integration of CO-releasing complexes and nanomaterials is one of the promising strategies to achieve localized on-demand delivery of CO for therapeutic purpose. Therefore, considerable efforts have been devoted to this area.[48] For instance, Mascharak's group has developed a nanocarrier based on mesoporous silica nanoparticles (MSNs) entrapped with a tailored photoCORM for rapid eradication of human breast cancer cells through trackable light-triggered CO delivery.[49] Initially, this group prepared a photoCORM (fac-[$Re(CO)_3$(pbt) (PPh_3)](CF_3SO_3)) which could not only releases CO upon illumination

with low-power UV light (e.g. 305 nm, 5 mW•cm^{-2}). In addition, the photoCORM also exhibited "turn-off" fluorescence signal change upon release of CO ligand. Such property provided a convenient strategy for tracking the CO release event. Upon integration with MSNs, the photoCORM could be effectively internalized into live cells. In the presence of light stimulation, the fluorescence signal of the photoCORM rapidly decreased as CO released from the photoCORM to exert cytotoxic effect against malignant cancer cells. Moreover, Ueno's team has developed a photoactive CO-releasing protein cage for dose-regulated delivery in living cells[48a]. In their studies, they synthesized a composite of protein with photoCORMs (e,g, Mn-carbonyl complexes etc) by designing a protein mutant which could stabilize the CO-releasing complexes within the *in vivo* environment. Further studies revealed that, the cellular uptake and light-induced (e.g. 456 nm light etc.) CO-releasing properties of such protein cage contribute to the activation of nuclear factor-kB (NF-kB) in mammalian cells as well as the tumor necrosis factor a (TNF-a), which suggested the potential of protein cage to uncover the role and mechanism of action of CO within living systems.

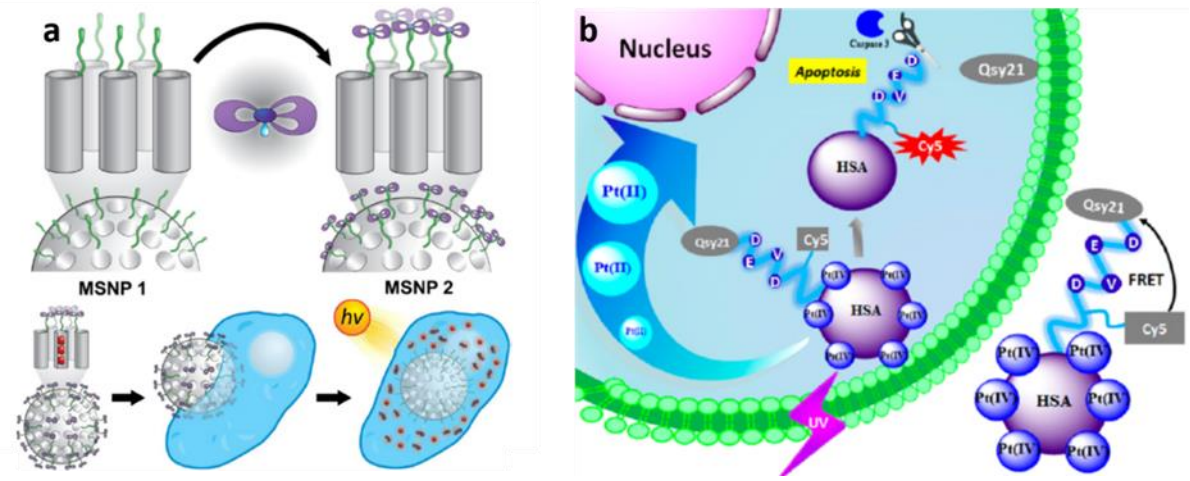

Figure 4 UV-Visible light-mediated therapeutic strategies. (a) Scheme of visible light-controlled drug delivery through photoactivation Ru(II)-dppz complexes modified MSNs[85]. (b) Human transport protein carrier for controlled photoactivation of antitumor prodrug and real-time intracellular tumor imaging[86].

1.5.1.2 UV-visible light triggered photo-activation of prodrug

In addition to light-triggered release of gaseous signaling mediator, one alternative approach in UV-vis light-mediated therapeutics is the photo-activation of prodrug. In this case, upon light treatment, some photoactive metal complex-based prodrugs which are non-toxic can be converted into their active form and exert cytotoxic effect for therapeutic purpose.[50] Therefore, delivery of complex with such property would allow controlled prodrug activation within targeted diseased area upon light stimulation. For instance, Frasconi et al. recently developed a novel platform MSNPs2 through covalent linkage between Ru(II) complex and MSNPs (Fig. 4(a)). Upon light treatment, the Ru(II) complexes were rapidly released and transformed into cytotoxic aqua complex which subsequently formed monoadducts

with DNA. Moreover, through rational design chemotherapy medication, paclitaxel, can form caged-prodrug with Ru(II) complex loaded on MSNPs. In the presence of visible light irradiation, paclitaxel can be released in a light controlled manner and inhibit the mitotic progression and cell proliferation for cancer treatment.[51] Moreover, Xing etc. demonstrated a novel human serum albumin (HSA) protein-based nanocarrier, which combined the photoactivatable Pt(IV) antitumor prodrug for controlled release and fluorescent light-up probe for evaluations of drug action and efficacy (Fig. 4(b)). The constructed Pt(IV)-probe@HSA platform could be locally activated by UV irradiation to release the active Pt species, which led to enhanced cell death in both drug-sensitive A2780 and cisplatin-resistant A2780cis cell lines, when compared to free prodrug molecules alone. In the meantime, the cytotoxicity caused by light controlled drug release would further lead to the cellular apoptosis and trigger the activation of caspases 3, one typical protease enzyme responsible for executing programmed cell death, which can be visualized through the apoptosis-sensitive probe on the platform. Such unique design offered a successful strategy for controlled drug delivery through biocompatible protein based nanocarrier to enhance therapeutic efficacy. In the meantime, it also provided real-time monitoring of antitumor drug efficacy at the earlier stage, which may greatly benefit personalized cancer chemotherapy *in vitro* and *in vivo*.[52]

1.5.2 NIR light-mediated precision therapeutics

So far, the strategies that based on light-triggered therapeutics have gained considerable attention for their specificity and spatiotemporal precision. In most cases, the excitation sources for light-mediated therapeutics are mainly based on radiations within UV-visible rage. Although their initial

success, short-wavelength light irradiations (e.g. UV-visible light etc.) may have certain drawbacks such as limited tissue penetration and unwanted photodamage to cells and tissue.[53] Hence, strategies which allow precise light-mediated therapeutics with deep tissue penetration and minimum photo toxicity would be highly desired. Recently, an alternative strategy based on excitation through light within NIR window (e.g. 650-1350 nm) had emerged to fulfill the demand in clinics.[54] Endogenous light absorbers such as water, lipids and protein molecules exhibit minimum light absorption within NIR window. Such property contributes to unique advantages of NIR excitation such as deeper tissue penetration, minimized autofluorescence background as well as limited light scattering or absorbance from endogenous biomolecules and less photodamage, which are beneficial for light-mediated therapeutics in living systems. By far, several strategies have been demonstrated for effective therapy and imaging based on NIR-light mediated platforms.[55] One frequently used method of NIR light-mediated therapeutics is to develop light-responsive drug delivery systems which allow precise control of drug release into through light-promoted reactions. Another wide studied approach, termed as photodynamic therapy (PDT), based on the nanocomposite integrated with photosensitizer (PS) [56]. In the presence of NIR light stimulation, PS molecules would generate reactive oxygen species (ROS) for treatment of disease owing to their unique photo-physical and photo-chemical properties. In addition, another well-established method for light-induced therapeutics involves the application of photothermal therapy (PTT), which convert NIR radiation into heat through the intense absorption of thermal-sensitive agents[57]. Herein, in this section, we will briefly introduce the NIR-light mediated therapeutics approaches based on light-mediated drug delivery, PDT and PTT for precise therapeutics *in vitro* and *in vivo*.

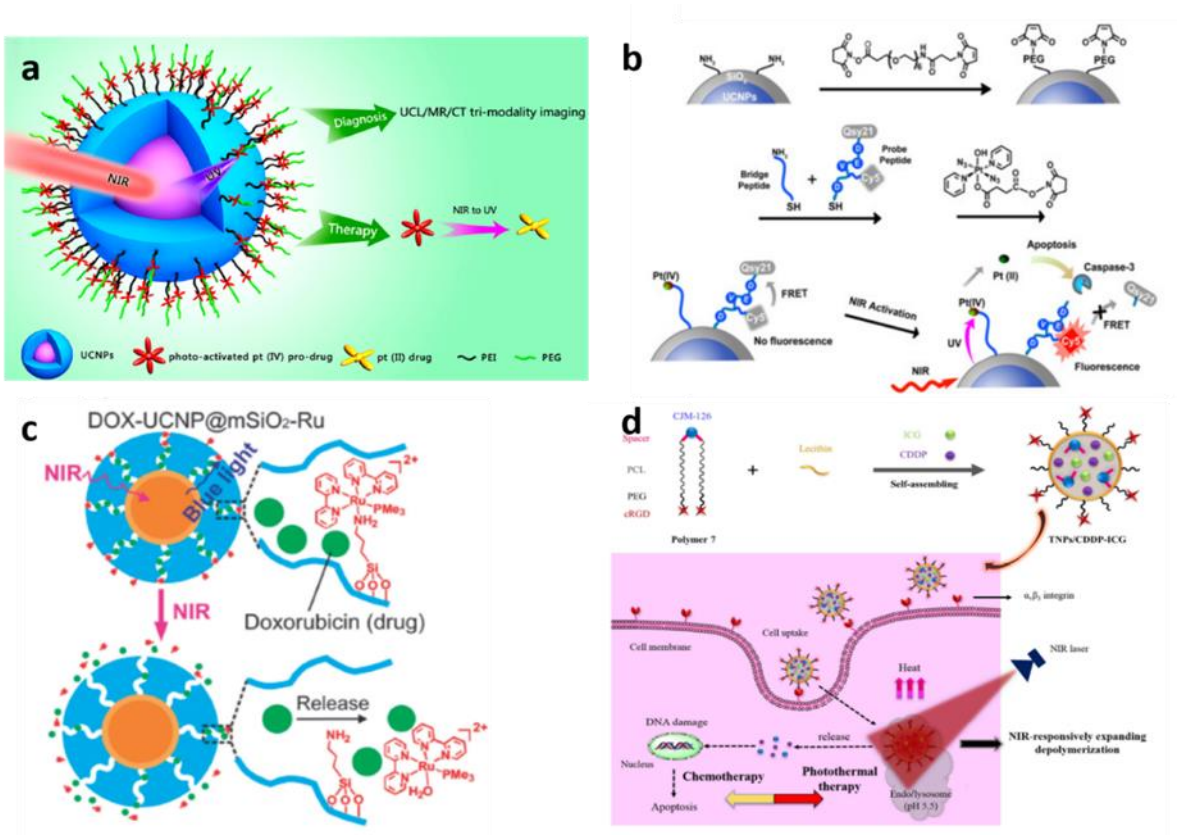

Figure 5 NIR light-triggered drug delivery strategies. (a) Scheme of NIR light-mediated UCNPs nanoplatform for Pt(IV) prodrug-based therapy and multimodal imaging[113]. (b) 980 nm light-induced Pt(IV) prodrug photoactivation and intracellular apoptosis monitoring[114]. (c)Upconverted blue luminescence triggers cleavage of Ru complexes and release of doxorubicin from DOX-UCNP@mSiO2-Ru nanoparticles [115]. (d) NIR-responsive binary-drug loaded photothermal conversion nanoparticles for drug delivery [120].

1.5.2.1 NIR light triggered drug delivery

Currently, the most noteworthy light-mediated treatment approach is the NIR light-triggered drug delivery system, which is emerging as effective technique for solid tumor treatment in recent years.[58]

Typically, NIR light will be applied to either promote photochemical reaction of caged-drug or by NIR-light induced heat generation for controlled drug delivery within diseased sites. To this end, one commonly used method is to involve rational design of prodrug by integration of light-sensitive agent with multifunctional nanoplatforms. Under light trigger, the nanoplatform can be activated and induce the structure change of prodrug, thus effectively activating the prodrug for precise therapeutics. Meanwhile, the nanoplatform can serve as intelligent carrier to enhance treatment efficacy through enhanced permeability and retention (EPR) effect to accumulate high dose of drugs within targeted area. So far, a variety of NIR light-responsive drug delivery platforms based on nanomaterials, such as UCNPs[59], carbon nanomaterials[44] and gold nanomaterials[60] etc. have been extensively investigated for NIR light-mediated delivery of drugs.

Among various nanomaterials for NIR light-mediated therapeutics, UCNP, an unique rare-earth lanthanide-doped nanoplatform, has attracted much attention owing to its impressive photophysical properties.[61] Generally, UCNPs are able to convert low-energy NIR light irradiation (e.g. 808 nm or 980 nm, etc.) into high-energy UV or visible light.[61c, 62] The upconverted emissions within UV or visible window can effectively trigger the photo-release of bioactive molecules or the photo-activation of light-sensitive prodrugs.[63] For instance, recently, both Xing's team and Lin's lab have independently devised novel NIR light-mediated delivery system based on UCNPs for light-controlled activation of Pt(IV) anticancer prodrug. In Lin's work, a newly designed Pt(IV) prodrug trans, trans, trans-$[Pt(N_3)_2(NH_3)(py)(O_2CCH_2CH_2COOH)_2]$ was conjugated to core-shell UCNPs (Fig. 5(a)). This photoactive system can not only displayed significant *in vivo* antitumor efficacy upon 980 nm laser irradiation, but also served as multifunctional tri-modality imaging contrast agents for cancer treatment

in living animals.[64] While, in Xing's design, a photo-sensitive Pt(IV) prodrug trans, trans, trans-[$Pt(N_3)_2(py)_2(OH)(O_2CCH_2CH_2COOH)$] together with an apoptosis sensing probe are conjugated to silica-coated UCNPs (Fig. 5(b)). In the presence of light stimulation (e.g. 980 nm), the Pt(IV) prodrug can be activated through upconverted UV emission and exert cytotoxic effect within cancer cells. Moreover, caspase protease enzymes triggered by the cytotoxicity of activated Pt drug can interact with the peptide-based apoptosis sensing probe, leading to the fluorescence light up for real-time cell imaging and earlier evaluation of antitumor therapeutic efficacy.[65] Apart from photo-activation of prodrug, another effective approach to control the drug delivery with deep tissue penetration depends on the photo-triggered release of biologically active molecules.[66] For example, Xing's group recently demonstrated NIR light-mediated activation of cytotoxic Re(I) complexes by using lanthanide-doped UCNPs. Typically, UCNPs can be used to activate the complex with upconversion luminescence triggered by NIR. Upon NIR irradiation, the Re(I) complex can be locally activated and generate biologically ROS and CO molecules. Such system exhibited enhanced cytotoxicity against both drug susceptible A2780 cells demonstrating that NIR irradiation combined with such system can achieve potent photoactivated cytotoxicity while minimizing unwanted photodamage to cells [63b]. In another study, Wu and coworkers have fabricated a light-responsive drug delivery system by loading of mesoporous silica coated UCNPs with doxorubicin (DOX) (Fig. 5(c)). To achieve light-controlled release and prevent non-specific drug leakage, photo-sensitive Ru(II) complexes are grafted on the surface of nanoparticles as molecular valves [66a]. Upon NIR light trigger, upconverted emissions from UCNPs could induce the cleavage of molecular valves on particle's surface, thus allowing the on-demand release of loaded drugs in a light-dependent manner. In addition to strategies based on photo-

triggered release and photo-activation of prodrug, heat produced by specific NIR light-sensitive materials has been also widely investigated as an alternative approach for light-mediated drug delivery. Generally, the rational design involved nanomaterial with unique optical properties which enabled the absorptions of NIR light and converted them into heat generation. The locally produced heat would induce temperature increase in the surrounding diseased area, therefore leading to rapid drug release from the nano-carrier. So far, a variety of light-to-heat transducer such as AuNPs[67], CuS[68], Pd@Au[69] has been reported for heat-induced drug delivery. For example, Sun and co-workers constructed a platform for NIR light-induced dual drug release via the photothermal effect of polymeric carrier loaded with ICG dye (Fig. 5(d))[70]. The NIR light-sensitive dye ICG allows light to heat conversion which accelerated the expanding depolymerization of nanoparticles when exposed to 808 nm NIR light. Subsequently, the loaded drug DOX and CDDP could be released to exert cytotoxic effect due to the degradation of the nanoparticles. Yeh's group recently developed an oligonucleotides-assembled Au nanorods for NIR light-triggered dual drug delivery. In their design, single-stranded DNAs were assembled onto the surface of Au nanorods. The complementary DNA strand which was conjugated to Pt(IV) prodrug were hybridized. The resulting double stranded DNA sequences facilitate the loading of anticancer drug DOX. Upon heating by 808nm NIR light, dehybridization of double-stranded DNA leads to rapid release of both drug within intracellular environment for effective cancer treatment.[67]

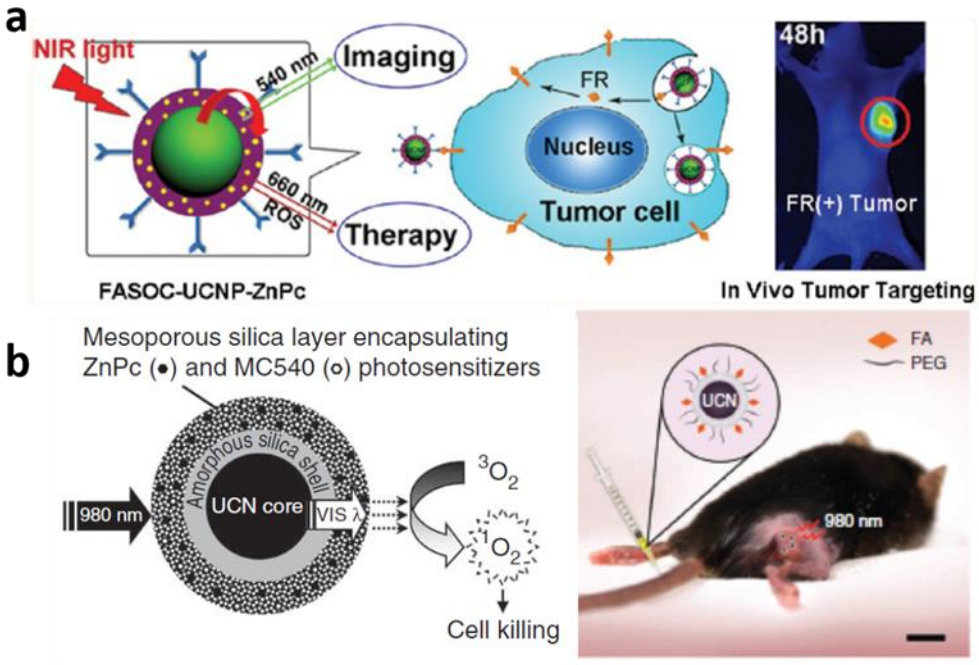

Figure 6 NIR light-mediated PDT strategies. (a) FA/PEG modified UCNPs@mSiO$_2$ loaded with ZnPc and MC540 for PDT[137]. (b) FA and ZnPc modified FASOC-UCNP-ZnPc nanoconstruct for PDT and simultaneous UCL imaging applications[138].

In addition to drug release, light-responsive nano-formulated complex also demonstrated to regulate cellular events[71]. For instance, Qu and coworkers have developed an intelligent spiropyran-upconversion (SP-UCNPs) based light-activatable nanosystem for accurate regulation of zinc signaling in living cells at precise times and locations. By varying the duration of NIR irradiation, the magnitude of zinc release can be simply manipulated to regulate downstream biological event, such as protein activity. This promising strategy can potentially enable the precise control of specific signaling pathways of metal ions while minimizing cellular damage, facilitating the advanced manipulation of cellular dynamics.

1.5.2.2 NIR light triggered photodynamic therapy

So far, NIR light-mediated drug delivery systems have been well recognized as effective approaches for the treatment of diseases. In addition to the methods based on the light-activatable prodrug or photo-triggered drug release, another well-established therapeutic modality is photodynamic therapy (PDT), which relies on photosensitizer to produce ROS (e.g., hydrogen peroxide, hydroxyl radical, singlet oxygen etc.) after light irradiation. These highly reactive oxygen species are usually associated with oxidative stress and subsequently cause significant cellular damage by reaction with the components in cells, such as DNA and proteins.[72] Compared to traditional therapeutic modalities (e.g. chemotherapy etc), PDT displays unique advantages especially in cancer therapy owing to the intrinsically non-invasive safety and spatiotemporal precision upon light treatment. Therefore, PDT has been well developed as a promising therapeutic approach for effective cancer treatment and been approved by the FDA.[73]

Currently, a variety of metal complexes based photosensitizers (e.g. ZnPc, Ir complexes etc.) have been developed owing to their promising efficiency of singlet oxygen generation.[74] For instance, Huang's team developed a novel type of phosphorescent polymer dots (Pdots) containing Ir(III) complex. The excited state energy transfer from Pdots to molecular oxygen facilitated the optical sensing of oxygen with high sensitivity. In addition, upon 488 nm light stimulation, these Pdots are capable of generating singlet oxygen for effective inhibition of tumor cells *in vitro*.[75] Despite the initial success, their extensive usage in clinics could be restricted by two challenges. Firstly, most PS molecules applied in PDT are hydrophobic which may lead to limited accumulation within diseased sites due to their lack of aqueous solubility. To this end, various carriers based on nanomaterials have

been demonstrated to deliver PS agents to targeted diseased area for improved PDT efficacy. Another drawback of traditional PDT is the limited tissue penetration as most PS agents only respond to short-wavelength light. To these ends, extensive efforts have been made to explore the feasibility of NIR light for PDT mainly for their ability for deeper tissue penetration, which could greatly improve the safety of PDT treatment by effectively reducing the possible light-induced cytotoxicity in living systems. Although various NIR light-responsive PS molecules have been developed for PDT in clinics, some drawbacks including laborious synthesis procedures, poor aqueous solubility and limited accumulation in diseased area etc, have restricted their application in deep-tissue therapeutics. In recent years, various types of nanomaterials with large extinction coefficient in NIR window, including organic NPs (e.g. polymeric NPs[76], liposomes [77], etc) and inorganic NPs (e.g. carbon-based NPs[78], gold-based NPs[79], UCNPs[80], etc), have been extensively investigated for PDT applications both *in vitro* and *in vivo*.

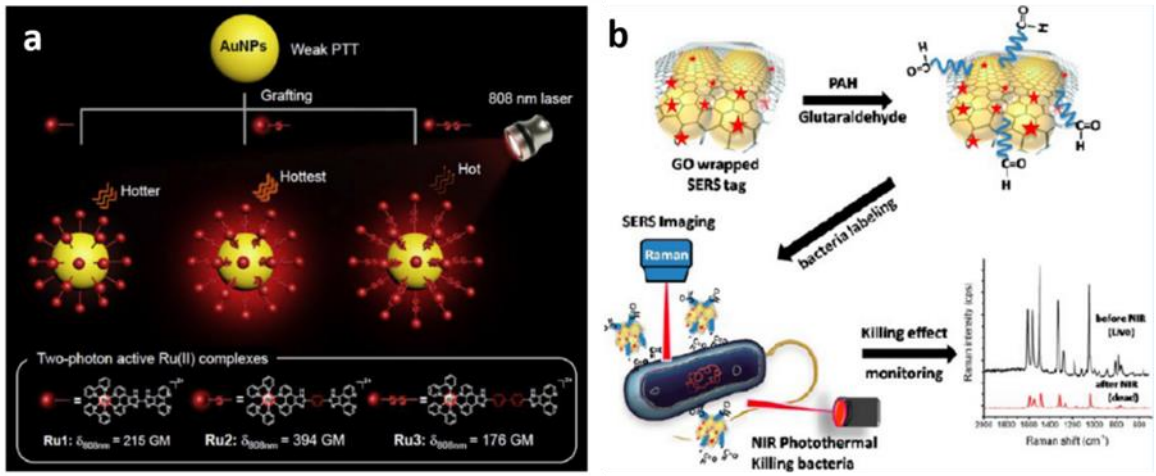

Figure 7 NIR light-mediated PTT strategies. (a) Illustration of gold nanoparticles grafted with Ru(II) complexes for PTT[146]. (b) Au@Ru(bpy)/GO for PTT and simultaneous SERS imaging applications[151].

As a promising candidate, lanthanide-dopedUCNPs, which are able to convert NIR light into broad UV/visible emission, can serve as a powerful tool to overcome the major limitations of current PDT strategies through NIR light illumination. For instance, Zhang and coworkers have first reported 980 nm light-triggered PDT in living cells by using UCNPs as light transducer to activate PS agents.[81] Similarly, Gu and Cui et al. have also demonstrated *in vivo* deep-tissue PDT through NIR light triggered UCNPs. Typically, a well-established metal complex-based photosensitizer ZnPC was loaded on to UCNPs through the surface functionalized polymer chitosan (Fig. 6(a)). This system can not only display significant *in vivo* antitumor efficacy upon 980 nm laser irradiation, but also served as multifunctional upconversion luminescence (UCL) imaging contrast agents for cancer treatment in living animals.[82] Moreover, Zhang's team presented an intelligent UCNP-based PDT strategy. In their

design, two photosensitizers ZnPc and MC540 were incorporated into one single UCNP platform (Fig. 6(b)). Upon NIR light trigger, the upconverted emissions (e.g. at ~540nm and ~660nm) can activate both types of PS molecules respectively, thus greatly enhanced the PDT efficacy. Moreover, by surface coating of tumor targeting ligand such as folic acid, the UCNPs platform displayed effective tumor accumulation for promising NIR light-mediated in vivo PDT treatment.[83]

1.5.2.3 NIR light triggered photothermal therapy

Over the past decade, NIR light-mediated drug delivery and PDT therapeutic approaches have been extensively studied for effective diseases treatment in living system. In addition, another promising therapeutic modality, photothermal therapy (PTT), has also attracted much attention in recent years. Basically, PTT utilizes photothermal conversion agents (PTCAs) to convert NIR light into heat within localized region. The localized heat generation will lead to the overheating of diseased sites, facilitating the damage of surrounding biological species and cause subsequent cell death.[84] Generally, the ideal PTCAs can be featured as the following advantages: 1) strong NIR light absorption; 2) excellent photothermal conversion efficiency; 3) good biocompatibility and biodegradability etc. By far, a variety of promising PTCAs, including inorganic nanomaterials[85] and organic polymers[86], have been developed for effective NIR light-triggered PTT treatment *in vitro* and *in vivo*. For instance, Chao's team recently demonstrated gold nanoparticles with Ru(II) complexes grafted on the surface of nanoparticles (Fig. 7(a)). The Ru(II) complexes which displayed strong NIR absorption were utilized as antenna molecules to effectively harvest NIR photons, thus greatly improved the photothermal efficiency of the Au nanomaterials *in vitro* and *in vivo*.[87] In addition to their successful application in cancer treatment, metal

complexes also exhibit efficient antimicrobial effect against bacterial infections through various strategies including damaging bacterial cell walls, photothermal inactivation etc[88]. For instance, Chen and Wang et al. proposed an in situ synthesis strategy for graphene oxide (GO) wrapped gold SERS tags by using Ru(bpy)/GO nanohybrid as Raman reporter (Fig. 7(b)). Such nanomaterial could serve as a multifunctional platform which not only allowed sensitive Raman imaging of both gram-positive (e.g. *Staphylococcus aureus etc*) and gram-negative (e.g. *Escherichia coli* etc) bacteria. Moreover, effective photothermal eradication of both type of bacteria can be also achieved upon NIR light treatment. Moreover, the correlation between SERS signal intensity and bacteria survival rate enables simultaneous monitoring of light triggered antimicrobial efficacy.[89]

Table 1 Representative examples of light-responsive platforms for precision therapeutics

Wavelength range	Wavelength	Delivery system	Size	Mode of action	Loading capacity	Loaded complex	Ref.
UV light	305 nm	MCM-41	100 nm	drug release	0.97%	Re(I) complex	83
UV light	365 nm	HSA NPs	200 nm	photoactivation of prodrug	4.10%	Pt(IV) complex	86
Visible light	456 nm	protein assembly	12 nm	drug release	–	Mn(I) complex	79
Visible light	–	MCM-41	120 nm	photoactivation of prodrug	–	Ru(II) complex	85
Visible light	488 nm	polymeric NPs	19 nm	PDT	8%	Ir(III) complex	128
NIR light	980 nm	UCNPs	65 nm	photoactivation of prodrug	2.60%	Pt(IV) complex	113
NIR light	980 nm	UCNPs	35 nm	photoactivation of prodrug	3.50%	Pt(IV) complex	114
NIR light	980 nm	UCNPs	118 nm	drug release	6.14%	Re(I) complex	109
NIR light	980 nm	UCNPs	92 nm	drug release	0.76%	Ru(II) complex	115
NIR light	808 nm	polymeric NPs	88.9 nm	drug release	9.52%	cisplatin	120
NIR light	808 nm	AuNRs	38.5 nm (H)* 9.5 nm(W)	drug release	–	Pt(IV) complex	117
NIR light	980 nm	UCNPs	50-60 nm	PDT	up to 10%	ZnPc	137, 138
NIR light	808 nm	AuNPs	45.0± 1.5 nm	PTT	–	Ru(II) complex	146
NIR light	785 nm	GO	192.8 nm	PTT	–	Ru(II) complex	151
NIR light	808 nm	chitosan NPs	89 nm	PTT	–	Cu(II) complex	155

Although, these nanomaterials based on inorganic structures exhibited great therapeutic effects, concerns over their non-biodegradable properties and long-term biosafety may potentially restrict their future applications *in vivo* and in clinics. Therefore, several type of PTT materials such as NIR dye

loaded liposomes[90], polymers[91] and micelles[57a, 92]etc, have been extensively studied over the past decades. For instance, Zhang and Sun et al. have demonstrated a facile and feasible approach for enhancing 808 nm photothermal conversion effect of d orbits transition Cu(II) ions by forming Cu-carboxylate complexes. The coordination with carboxylate groups greatly enhanced the splitting energy gap of Cu(II) and the capability of electron transition, thus improving the absorption in near-infrared region. Further loading of the cupreous complex into biocompatible chitosan NPs enabled photothermal therapy of human oral epithelial carcinoma (KB) cells *in vitro* and *in vivo*. Such nanoplatform not only greatly inhibited tumor growth through effective PTT. In addition, the released cupreous complexes could also serve as chemotherapeutic agent for tumor treatment.[93]

1.6. Magnetic stimuli-responsive platforms for precision therapeutics

Although light-responsive therapeutic approaches enabled precise intervention of treatment process, the use of high power laser has raised safety concern for its potential damage to tissues. Therefore, alternative stimuli-responsive strategy with minimum damage to biological samples is highly desirable for precision therapeutics[94]. Similar to light-simulation strategy, magnetism is an external non-invasive method of activation that has attractive capabilities because it can be controlled in a temporal and spatial manner. In addition, magnetic stimuli have been considered to be one promising option for the design of precision therapeutics owing to the fact that magnetic fields rarely interact with the patient's body in comparison to other traditional stimuli, e.g. pH, light etc.[95] So far, various strategies based on magnetically responsive systems for precision therapeutics have been reported mainly for their ability to achieve magnetically guided targeting and hyperthermia-induced drug release triggered by

alternating magnetic field.[96] Typically, magnetic guidance can be obtained by focusing an external magnetic field on the targeted diseased site during the administration of magnetically-responsive nano-systems. The interaction between the magnetic field and nano-system would facilitate the targeting and accumulation of nanocarriers within diseased regions.[97] Furthermore, once the carrier reaches the biological target, by applying an external oscillating or alternating magnetic field (AMF) onto the region of interest, the magnetically-active nanosystems can serve as a transducer to produce heat in the surrounding environment for controlled drug release or thermal therapy.[98] By combining these properties, a broad spectrum of system for on-demand drug delivery has been proposed. For instance, Janiak and Kunz et al. reported manipulation of CO-gasotransmitter release triggered by magnetic signal. As a proof-of-concept, a CO-releasing molecule (CORM) (e.g. [RuCl(CO_3)-(l-DOPA)]) as precursor of CO-gasotransmitter were conjugated to nano-magnet (Fe_2O_3 nanoparticles) (Fig. 8(a)). Upon heating within AMF, the locally increased temperature would facilitate the rapid CO release from the Ru(II) complex within targeted region.[99] In addition, Zhang and coworkers presented (a multifunctional theranostic platform for precise therapy and simultaneous magnetic resonance imaging (MRI). In their design, on the surface of a core-shell magnetic mesoporous silica nanoparticle (Fe_3O_4@MSN), β-cyclodextrin (β-CD) was conjugated on the silica shell as gatekeeper through a Pt (IV) prodrug (Fig. 8(b)). Upon administration, the nanoparticles could accumulate at cancer regions through magnetic targeting enhanced EPR effect. Once internalized by tumor cell, the reducing microenvironment would induce the reduction of Pt(IV) prodrug and remove the gatekeeper β-CD, thus promoting the release of loaded anticancer agent DOX for precise therapy. Moreover, the magnetic properties of the nanoparticles enabled simultaneous MRI imaging modality for theranostic purpose.[100] In another study,

Kim and Ishikawa et al. designed magnetically active theranostic platform for effective treatment of cancer. Concerning the potential biosafety issue of conventional inorganic magnetic nanoparticles, the platform was mainly based on polymeric nanoassembly loaded with simple magnetic metal complex (Fig. 8(c)). The simple complex Fe(salen) could serve as antitumor agent owing to its intrinsic antitumor activity. Moreover, the ubiquitous magnetic properties of this versatile complex not only rendered the nanoassembly favorable magnet-guided targeting ability and MRI imaging modality. More importantly, the magneto-thermal properties could trigger the release of encapsulated dual drug (Fe(Salen) and DOX) for precise drug delivery to achieve enhanced tumor treatment *in vivo*, demonstrating its great potential as theranostic platform in future preclinical applications.[101]

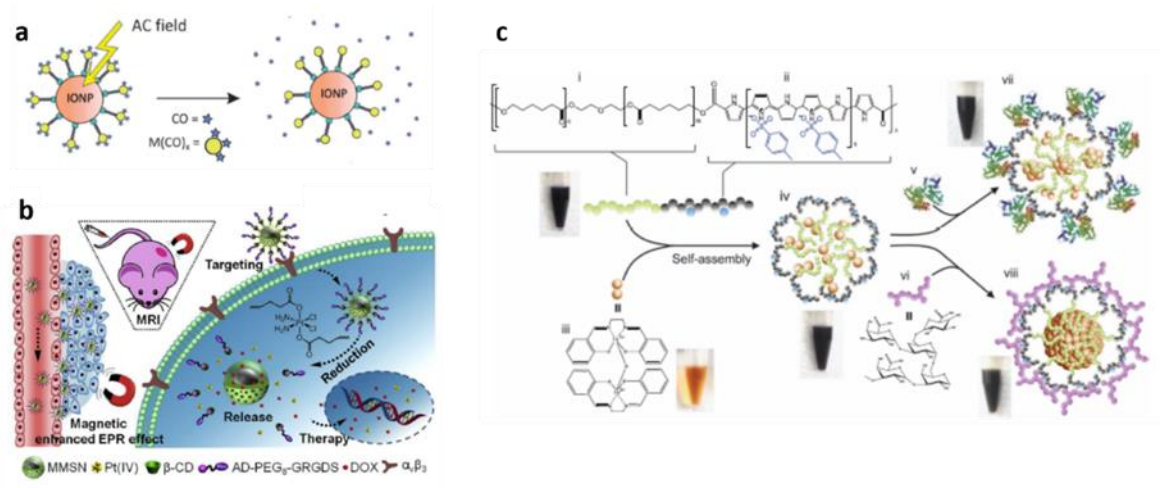

Figure 8 Magnetic stimuli mediated precision therapeutics. (a) Illustration of induced CO-release from CORM-functionalized IONP through an alternating magnetic field [164]. (b) The design and proposed mechanism of the multifunctional MMSNs for tumor-targeted MRI and precise therapy [165]. (c)

Preparation of Fe(salen)-loaded polypyrrole (PPy)-polycaprolactone (PCL) core–shell nanoassembled composites for a single-drug anticancer platform[166].

1.7 Research goals

By now, nanotechnology exhibits unique advantages for research and development of effect and safer therapeutic and diagnostic modalities mainly for its ability to improve drug loading efficiency, pharmacokinetics as well as to minimize side effects. Considering the unique and desirable properties of different nanostructures, nanoformulation of traditional metal complex has been demonstrated promising strategy to solve the issues of currently used metal complex as therapeutic and sensing agents. In this dissertation, some intelligent platform were built based on stimuli-responsiveness of metal complex and nanostructures to facilitate the future advance of precise therapeutics and diagnostics.

In chapter 2, photo-sensitive Re(I) complex was incorporated onto light converting nanoparticles to construct a light mediated system which is capable of activating cytotoxic Re(I) complex for therapeutic purpose. Owing to the great spatial-temporal resolution of light irradiation, upon NIR stimulation, Re(I) complex can be locally activated within pathological side by upconverted UV light from nanoparticles and exert cytotoxic effect for precise treatment against both drug-susceptible and drug-resistant cancer cells, minimizing unwanted photo damage.

In chapter 3, to selectively detect illicit drug Gamma-hydroxybutyric acid (GHB), we provide a bioinspired strategy based on stimuli-responsive formulation of AuNPs from Au(III) complex. Upon substrate-specific enzyme recognition of GHB, reduced nicotinamide adenine dinucleotide (NADH) would be generated and promoted the reduction of gold(III) complex to form gold nanoparticles. Thus allowing selective sensing of GHB through both spectroscopic analysis and naked-eye observation.

In chapter 4, to develop a probe for long term sensing and imaging in response to reducing cellular environment, we introduced a strategy based on nanoformulation of lanthanide complex which can respond to reducing environment. Within reducing environment, the lanthanide complex would undergo inter-molecular cross linking and form dimer structure. Further self-assembly of the lanthanide dimer yield luminescent nanoscaled particles which can potentially accumulate within cells for long term intracellular sensing and imaging purpose.

In chapter 5, we provided a light induced strategy for remote manipulation of cell membrane activity. To precisely regulate membrane event, we started with site-specifically localize luminescent complex on cell surface through metabolic labelling and biorthogonal reaction. The luminescence of the metal complex could activate the light-sensitive ion channel on cell membrane and allow remote regulation of cation influx under both in vitro and in vivo settings. Such strategy can serve as a useful toolbox for accurate perturbation of biological event and promote in-depth understanding of the diverse biological processes in biomedical studies.

1.8 Reference

1. (a) Friedman, A. A.; Letai, A.; Fisher, D. E.; Flaherty, K. T., Precision medicine for cancer with next-generation functional diagnostics. *Nat. Rev. Cancer* **2015,** *15* (12), 747; (b) Arnedos, M.; Vicier, C.; Loi, S.; Lefebvre, C.; Michiels, S.; Bonnefoi, H.; Andre, F., Precision medicine for metastatic breast cancer—limitations and solutions. *Nat. Rev. Clin. Oncol.* **2015,** *12* (12), 693.

2. Mjos, K. D.; Orvig, C., Metallodrugs in medicinal inorganic chemistry. *Chem. Rev.* **2014,** *114* (8), 4540-4563.

3. (a) Yang, Y.; Ouyang, R.; Xu, L.; Guo, N.; Li, W.; Feng, K.; Ouyang, L.; Yang, Z.; Zhou, S.; Miao, Y., Bismuth complexes: synthesis and applications in biomedicine. *J. Coord. Chem.* **2015,** *68* (3), 379-397; (b) Pricker, S. P., Medical uses of gold compounds: past, present and future. *Gold bulletin* **1996,** *29* (2), 53-60; (c) Bruijnincx, P. C.; Sadler, P. J., New trends for metal complexes with anticancer activity. *Curr. Opin. Chem. Biol.* **2008,** *12* (2), 197-206; (d) Romero-Canelón, I.; Sadler, P. J., Next-generation metal anticancer complexes: multitargeting via redox modulation. *Inorg. Chem.* **2013,** *52* (21), 12276-12291.

4. (a) Siddik, Z. H., Cisplatin: mode of cytotoxic action and molecular basis of resistance. *Oncogene* **2003,** *22* (47), 7265; (b) Wang, X.; Wang, X.; Guo, Z., Functionalization of platinum complexes for biomedical applications. *Acc. Chem. Res.* **2015,** *48* (9), 2622-2631.

5. Dhar, S.; Kolishetti, N.; Lippard, S. J.; Farokhzad, O. C., Targeted delivery of a cisplatin prodrug for safer and more effective prostate cancer therapy in vivo. *Proc. Natl. Acad. Sci.* **2011,** *108* (5), 1850-1855.

6. (a) Mout, R.; Moyano, D. F.; Rana, S.; Rotello, V. M., Surface functionalization of nanoparticles for nanomedicine. *Chem. Soc. Rev.* **2012,** *41* (7), 2539-2544; (b) Mehdi, A.; Reye, C.; Corriu, R., From molecular chemistry to hybrid nanomaterials. Design and functionalization. *Chem. Soc. Rev.* **2011,** *40* (2), 563-574; (c) Dobrovolskaia, M. A.; McNeil, S. E., Immunological properties of engineered nanomaterials. *Nat. Nanotechnol.* **2007,** *2* (8), 469; (d) Barreto, J. A.; O'Malley, W.; Kubeil, M.; Graham, B.; Stephan, H.; Spiccia, L., Nanomaterials: applications in cancer imaging and therapy. *Adv. Mater.* **2011,** *23* (12), H18-H40; (e) Qin, H.; Zhao, C.; Sun, Y.; Ren, J.; Qu, X., Metallo-supramolecular complexes enantioselectively eradicate cancer stem

cells in vivo. *J. Am. Chem. Soc.* **2017,** *139* (45), 16201-16209; (f) Liang, C.; Xu, L.; Song, G.; Liu, Z., Emerging nanomedicine approaches fighting tumor metastasis: animal models, metastasis-targeted drug delivery, phototherapy, and immunotherapy. *Chem. Soc. Rev.* **2016,** *45* (22), 6250-6269.

7. Wani, W. A.; Prashar, S.; Shreaz, S.; Gómez-Ruiz, S., Nanostructured materials functionalized with metal complexes: in search of alternatives for administering anticancer metallodrugs. *Coord. Chem. Rev.* **2016,** *312*, 67-98.

8. Mura, S.; Nicolas, J.; Couvreur, P., Stimuli-responsive nanocarriers for drug delivery. *Nat. Mater.* **2013,** *12* (11), 991.

9. (a) Son, S.; Shin, E.; Kim, B.-S., Light-responsive micelles of spiropyran initiated hyperbranched polyglycerol for smart drug delivery. *Biomacromolecules* **2014,** *15* (2), 628-634; (b) Lu, Y.; Aimetti, A. A.; Langer, R.; Gu, Z., Bioresponsive materials. *Nat. Rev. Mater.* **2017,** *2* (1), 16075.

10.(a) Yang, P.; Gai, S.; Lin, J., Functionalized mesoporous silica materials for controlled drug delivery. *Chem. Soc. Rev.* **2012,** *41* (9), 3679-3698; (b) Meng, F.; Zhong, Z.; Feijen, J., Stimuli-responsive polymersomes for programmed drug delivery. *Biomacromolecules* **2009,** *10* (2), 197-209; (c) Ganta, S.; Devalapally, H.; Shahiwala, A.; Amiji, M., A review of stimuli-responsive nanocarriers for drug and gene delivery. *J. Control. Release* **2008,** *126* (3), 187-204; (d) Schmaljohann, D., Thermo-and pH-responsive polymers in drug delivery. *Adv. Drug Del. Rev.* **2006,** *58* (15), 1655-1670; (e) Zhang, Y.; Yu, J.; Bomba, H. N.; Zhu, Y.; Gu, Z., Mechanical force-triggered drug delivery. *Chem. Rev.* **2016,** *116* (19), 12536-12563.

11.Wike-Hooley, J.; Haveman, J.; Reinhold, H., The relevance of tumour pH to the treatment of malignant disease. *Radiother. Oncol.* **1984,** *2* (4), 343-366.

12.Kim, J.-w.; Dang, C. V., Cancer's molecular sweet tooth and the Warburg effect. *Cancer Res.* **2006,** *66* (18), 8927-8930.

13.Brahimi-Horn, M. C.; Pouysségur, J., Oxygen, a source of life and stress. *FEBS Lett.* **2007,** *581* (19), 3582-3591.

14.Lee, E. S.; Gao, Z.; Bae, Y. H., Recent progress in tumor pH targeting nanotechnology. *J. Control. Release* **2008,** *132* (3), 164-170.

15.Li, Y.; Li, Y.; Zhang, X.; Xu, X.; Zhang, Z.; Hu, C.; He, Y.; Gu, Z., Supramolecular PEGylated dendritic systems as pH/redox dual-responsive theranostic nanoplatforms for platinum drug delivery and NIR imaging. *Theranostics* **2016,** *6* (9), 1293.

16.(a) Lee, S.-M.; O'Halloran, T. V.; Nguyen, S. T., Polymer-caged nanobins for synergistic cisplatin−doxorubicin combination chemotherapy. *J. Am. Chem. Soc.* **2010,** *132* (48), 17130-17138; (b) Lee, S.-M.; Chen, H.; O'Halloran, T. V.; Nguyen, S. T., "Clickable" polymer-caged nanobins as a modular drug delivery platform. *J. Am. Chem. Soc.* **2009,** *131* (26), 9311-9320; (c) Lee, S.-M.; Chen, H.; Dettmer, C. M.; O'Halloran, T. V.; Nguyen, S. T., Polymer-caged lipsomes: a pH-responsive delivery system with high stability. *J. Am. Chem. Soc.* **2007,** *129* (49), 15096-15097.

17.Yang, X. Z.; Du, X. J.; Liu, Y.; Zhu, Y. H.; Liu, Y. Z.; Li, Y. P.; Wang, J., Rational design of polyion complex nanoparticles to overcome cisplatin resistance in cancer therapy. *Adv. Mater.* **2014,** *26* (6), 931-936.

18.Kheirolomoom, A.; Ingham, E. S.; Commisso, J.; Abushaban, N.; Ferrara, K. W., Intracellular trafficking of a pH-responsive drug metal complex. *J. Control. Release* **2016,** *243*, 232-242.

19.(a) Li, M.; Tan, L.; Tang, L.; Li, A.; Hu, J., Hydrosoluble 50% N-acetylation-thiolated chitosan complex with cobalt as a pH-responsive renal fibrosis targeting drugs. *J. Biomater. Sci. Polym. Ed.* **2016,** *27* (10), 972-985; (b) Mavuso, S.; Choonara, Y. E.; Marimuthu, T.; Kumar, P.; du Toit, L. C.; Kondiah, P. P.; Pillay, V., A dual pH/Redox responsive copper-ligand nanoliposome bioactive complex for the treatment of chronic inflammation. *Int. J. Pharm.* **2016,** *509* (1-2), 348-359.

20.Li, H.-J.; Du, J.-Z.; Liu, J.; Du, X.-J.; Shen, S.; Zhu, Y.-H.; Wang, X.; Ye, X.; Nie, S.; Wang, J., Smart superstructures with ultrahigh pH-sensitivity for targeting acidic tumor microenvironment: instantaneous size switching and improved tumor penetration. *ACS nano* **2016,** *10* (7), 6753-6761.

21.Shen, S.; Li, H.-J.; Chen, K.-G.; Wang, Y.-C.; Yang, X.-Z.; Lian, Z.-X.; Du, J.-Z.; Wang, J., Spatial Targeting of Tumor-Associated Macrophages and Tumor Cells with a pH-Sensitive Cluster Nanocarrier for Cancer Chemoimmunotherapy. *Nano Lett.* **2017,** *17* (6), 3822-3829.

22.(a) Meng, F.; Hennink, W. E.; Zhong, Z., Reduction-sensitive polymers and bioconjugates for biomedical applications. *Biomaterials* **2009,** *30* (12), 2180-2198; (b) Gauthier, M. A., Redox-responsive drug delivery. Mary Ann Liebert, Inc. 140 Huguenot Street, 3rd Floor New Rochelle, NY 10801 USA: 2014.

23.Schafer, F. Q.; Buettner, G. R., Redox environment of the cell as viewed through the redox state of the glutathione disulfide/glutathione couple. *Free Radic. Biol. Med.* **2001,** *30* (11), 1191-1212.

24.(a) Balendiran, G. K.; Dabur, R.; Fraser, D., The role of glutathione in cancer. *Cell Biochem. Funct.* **2004,** *22* (6), 343-352; (b) Saito, G.; Swanson, J. A.; Lee, K.-D., Drug delivery strategy utilizing conjugation via reversible disulfide linkages: role and site of cellular reducing activities. *Adv. Drug Del. Rev.* **2003,** *55* (2), 199-215.

25.Feazell, R. P.; Nakayama-Ratchford, N.; Dai, H.; Lippard, S. J., Soluble single-walled carbon nanotubes as longboat delivery systems for platinum (IV) anticancer drug design. *J. Am. Chem. Soc.* **2007,** *129* (27), 8438-8439.

26.Dhar, S.; Liu, Z.; Thomale, J.; Dai, H.; Lippard, S. J., Targeted single-wall carbon nanotube-mediated Pt (IV) prodrug delivery using folate as a homing device. *J. Am. Chem. Soc.* **2008,** *130* (34), 11467-11476.

27.Cong, Y.; Xiao, H.; Xiong, H.; Wang, Z.; Ding, J.; Li, C.; Chen, X.; Liang, X. J.; Zhou, D.; Huang, Y., Dual Drug Backboned Shattering Polymeric Theranostic Nanomedicine for Synergistic Eradication of Patient‐Derived Lung Cancer. *Adv. Mater.* **2018,** *30*, 1706220.

28.He, C.; Lu, K.; Liu, D.; Lin, W., Nanoscale metal–organic frameworks for the co-delivery of cisplatin and pooled siRNAs to enhance therapeutic efficacy in drug-resistant ovarian cancer cells. *J. Am. Chem. Soc.* **2014,** *136* (14), 5181-5184.

29.Della Rocca, J.; Liu, D.; Lin, W., Nanoscale metal–organic frameworks for biomedical imaging and drug delivery. *Acc. Chem. Res.* **2011,** *44* (10), 957-968.

30.Wu, M. X.; Yang, Y. W., Metal–Organic Framework (MOF)‐Based Drug/Cargo Delivery and Cancer Therapy. *Adv. Mater.* **2017,** *29*, 1606134.

31.Zhu, Z.; Wang, Z.; Hao, Y.; Zhu, C.; Jiao, Y.; Chen, H.; Wang, Y.-M.; Yan, J.; Guo, Z.; Wang, X., Glutathione boosting the cytotoxicity of a magnetic platinum (IV) nano-prodrug in tumor cells. *Chem. Sci.* **2016,** *7* (4), 2864-2869.

32.Giorgio, M.; Trinei, M.; Migliaccio, E.; Pelicci, P. G., Hydrogen peroxide: a metabolic by-product or a common mediator of ageing signals? *Nature reviews Molecular cell biology* **2007,** *8* (9), 722.

33.(a) Shim, M. S.; Xia, Y., A reactive oxygen species (ROS)‐responsive polymer for safe, efficient, and targeted gene delivery in cancer cells. *Angew. Chem. Int. Ed.* **2013,** *52* (27), 6926-6929; (b) Gupta, M. K.; Meyer, T. A.; Nelson, C. E.; Duvall, C. L., Poly (PS-b-DMA) micelles for reactive oxygen species triggered drug release. *J. Control. Release* **2012,** *162* (3), 591-598; (c) Chung, M.-F.; Chia, W.-T.; Wan, W.-L.; Lin, Y.-J.; Sung, H.-W., Controlled release of an anti-inflammatory drug using an ultrasensitive ROS-responsive gas-generating carrier for localized inflammation inhibition. *J. Am. Chem. Soc.* **2015,** *137* (39), 12462-12465.

34.Chen, H.; He, W.; Guo, Z., An H 2 O 2-responsive nanocarrier for dual-release of platinum anticancer drugs and O 2: controlled release and enhanced cytotoxicity against cisplatin resistant cancer cells. *Chem. Commun.* **2014,** *50* (68), 9714-9717.

35.Zhang, R.; Song, X.; Liang, C.; Yi, X.; Song, G.; Chao, Y.; Yang, Y.; Yang, K.; Feng, L.; Liu, Z., Catalase-loaded cisplatin-prodrug-constructed liposomes to overcome tumor hypoxia for enhanced chemo-radiotherapy of cancer. *Biomaterials* **2017,** *138*, 13-21.

36.Rodríguez, D.; Morrison, C. J.; Overall, C. M., Matrix metalloproteinases: what do they not do? New substrates and biological roles identified by murine models and proteomics. *Biochim. Biophys. Acta-Mol. Cell Res.* **2010,** *1803* (1), 39-54.

37.(a) Hu, J.; Zhang, G.; Liu, S., Enzyme-responsive polymeric assemblies, nanoparticles and hydrogels. *Chem. Soc. Rev.* **2012,** *41* (18), 5933-5949; (b) Ulijn, R. V., Enzyme-responsive materials: a new class of smart biomaterials. *J. Mater. Chem.* **2006,** *16* (23), 2217-2225.

38.De La Rica, R.; Aili, D.; Stevens, M. M., Enzyme-responsive nanoparticles for drug release and diagnostics. *Adv. Drug Del. Rev.* **2012,** *64* (11), 967-978.

39.Huang, Y.; Huang, W.; Chan, L.; Zhou, B.; Chen, T., A multifunctional DNA origami as carrier of metal complexes to achieve enhanced tumoral delivery and nullified systemic toxicity. *Biomaterials* **2016,** *103*, 183-196.

40.(a) Huang, P.; Lin, J.; Wang, X.; Wang, Z.; Zhang, C.; He, M.; Wang, K.; Chen, F.; Li, Z.; Shen, G., Light‐triggered theranostics based on photosensitizer‐conjugated carbon dots for simultaneous enhanced‐fluorescence imaging and photodynamic therapy. *Adv. Mater.* **2012,** *24* (37), 5104-5110; (b) Ding, X.; Liow, C. H.; Zhang, M.; Huang, R.; Li, C.; Shen, H.; Liu, M.; Zou, Y.; Gao, N.; Zhang, Z., Surface plasmon resonance enhanced light absorption and photothermal therapy in the second near-infrared window. *J. Am. Chem. Soc.* **2014,** *136* (44), 15684-15693; (c) Zhao, J.; Lin, S.; Huang, Y.; Zhao, J.; Chen, P. R., Mechanism-based design of a photoactivatable firefly luciferase. *J. Am. Chem. Soc.* **2013,** *135* (20), 7410-7413.

41.(a) Nomoto, T.; Fukushima, S.; Kumagai, M.; Machitani, K.; Matsumoto, Y.; Oba, M.; Miyata, K.; Osada, K.; Nishiyama, N.; Kataoka, K., Three-layered polyplex micelle as a multifunctional nanocarrier platform for light-induced systemic gene transfer. *Nat. Commun.* **2014,** *5*, 3545; (b) Tian, J.; Ding, L.; Ju, H.; Yang, Y.; Li, X.; Shen, Z.; Zhu, Z.; Yu, J. S.; Yang, C. J., A Multifunctional Nanomicelle for Real‐Time Targeted Imaging and Precise Near‐Infrared Cancer Therapy. *Angew. Chem. Int. Ed.* **2014,** *53* (36), 9544-9549; (c) Huang, L.; Zhao, Y.; Zhang, H.; Huang, K.; Yang, J.; Han, G., Expanding Anti‐Stokes Shifting in Triplet–Triplet Annihilation Upconversion for In Vivo Anticancer Prodrug Activation. *Angew. Chem. Int. Ed.* **2017,** *56* (46), 14400-14404.

42.(a) Kobayashi, H.; Ogawa, M.; Alford, R.; Choyke, P. L.; Urano, Y., New strategies for fluorescent probe design in medical diagnostic imaging. *Chem. Rev.* **2009,** *110* (5), 2620-2640; (b) Shen, J.; Chen, G.; Vu, A. M.; Fan, W.; Bilsel, O. S.; Chang, C. C.; Han, G., Engineering the Upconversion Nanoparticle Excitation Wavelength: Cascade Sensitization of Tri‐doped Upconversion Colloidal Nanoparticles at 800 nm. *Adv. Opt. Mater.* **2013,** *1* (9), 644-650; (c) Klohs, J.; Wunder, A.; Licha, K., Near-infrared fluorescent probes for imaging vascular pathophysiology. *Basic Res. Cardiol.* **2008,** *103* (2), 144-151.

43.(a) Jing, T.; Fu, L.; Liu, L.; Yan, L., A reduction-responsive polypeptide nanogel encapsulating NIR photosensitizer for imaging guided photodynamic therapy. *Polym. Chem.* **2016,** *7* (4), 951-957; (b) Deng, K.; Hou, Z.; Deng, X.; Yang, P.; Li, C.; Lin, J., Enhanced Antitumor Efficacy by 808 nm Laser‐Induced Synergistic Photothermal and Photodynamic Therapy Based on a Indocyanine‐Green‐Attached W18O49 Nanostructure. *Adv. Funct. Mater.* **2015,** *25* (47), 7280-7290; (c) Barth, B. M.; I. Altinoğlu, E.; Shanmugavelandy, S. S.; Kaiser, J. M.; Crespo-Gonzalez, D.; DiVittore, N. A.; McGovern, C.; Goff, T. M.; Keasey, N. R.; Adair, J. H., Targeted indocyanine-green-loaded calcium phosphosilicate nanoparticles for in vivo photodynamic therapy of leukemia. *Acs Nano* **2011,** *5* (7), 5325-5337.

44.Shanmugam, V.; Selvakumar, S.; Yeh, C.-S., Near-infrared light-responsive nanomaterials in cancer therapeutics. *Chem. Soc. Rev.* **2014,** *43* (17), 6254-6287.

45.Kim, H. P.; Ryter, S. W.; Choi, A. M., CO as a cellular signaling molecule. *Annu. Rev. Pharmacol. Toxicol.* **2006,** *46*, 411-449.

46.Motterlini, R.; Otterbein, L. E., The therapeutic potential of carbon monoxide. *Nat. Rev. Drug Discov.* **2010,** *9* (9), 728.

47.Matson, J. B.; Webber, M. J.; Tamboli, V. K.; Weber, B.; Stupp, S. I., A peptide-based material for therapeutic carbon monoxide delivery. *Soft matter* **2012,** *8* (25), 6689-6692.

48.(a) Fujita, K.; Tanaka, Y.; Abe, S.; Ueno, T., A Photoactive Carbon‐Monoxide‐Releasing Protein Cage for Dose‐Regulated Delivery in Living Cells. *Angew. Chem. Int. Ed.* **2016,** *55* (3), 1056-1060; (b) Nguyen, D.; Nguyen, T.-K.; Rice, S. A.; Boyer, C., CO-releasing polymers exert antimicrobial activity. *Biomacromolecules* **2015,** *16* (9), 2776-2786; (c) Govender, P.; Pai, S.; Schatzschneider, U.; Smith, G. S., Next generation PhotoCORMs: polynuclear tricarbonylmanganese (I)-functionalized polypyridyl metallodendrimers. *Inorg. Chem.* **2013,** *52* (9), 5470-5478; (d) Dördelmann, G.; Meinhardt, T.; Sowik, T.; Krueger, A.; Schatzschneider, U., CuAAC click functionalization of azide-modified nanodiamond with a photoactivatable CO-releasing molecule (PhotoCORM) based on [Mn (CO) 3 (tpm)]+. *Chem. Commun.* **2012,** *48* (94), 11528-11530.

49.Chakraborty, I.; Carrington, S. J.; Hauser, J.; Oliver, S. R.; Mascharak, P. K., Rapid eradication of human breast cancer cells through trackable light-triggered CO delivery by mesoporous silica nanoparticles packed with a designed photoCORM. *Chem. Mater.* **2015,** *27* (24), 8387-8397.

50.Mackay, F. S.; Woods, J. A.; Heringová, P.; Kašpárková, J.; Pizarro, A. M.; Moggach, S. A.; Parsons, S.; Brabec, V.; Sadler, P. J., A potent cytotoxic photoactivated platinum complex. *Proc. Natl. Acad. Sci.* **2007,** *104* (52), 20743-20748.

51.Frasconi, M.; Liu, Z.; Lei, J.; Wu, Y.; Strekalova, E.; Malin, D.; Ambrogio, M. W.; Chen, X.; Botros, Y. Y.; Cryns, V. L., Photoexpulsion of surface-grafted ruthenium complexes and subsequent release of cytotoxic cargos to cancer cells from mesoporous silica nanoparticles. *J. Am. Chem. Soc.* **2013,** *135* (31), 11603-11613.

52.Li, X.; Mu, J.; Liu, F.; Tan, E. W. P.; Khezri, B.; Webster, R. D.; Yeow, E. K. L.; Xing, B., Human transport protein carrier for controlled photoactivation of antitumor prodrug and real-time intracellular tumor imaging. *Bioconj. Chem.* **2015,** *26* (5), 955-961.

53.(a) Zirkin, S.; Fishman, S.; Sharim, H.; Michaeli, Y.; Don, J.; Ebenstein, Y., Lighting up individual DNA damage sites by in vitro repair synthesis. *J. Am. Chem. Soc.* **2014,** *136* (21), 7771-7776; (b) Schwarz, A.; Ständer, S.; Berneburg, M.; Böhm, M.; Kulms, D.; van Steeg, H.; Grosse-Heitmeyer, K.; Krutmann, J.; Schwarz, T., Interleukin-12 suppresses ultraviolet radiation-induced apoptosis by inducing DNA repair. *Nat. Cell Biol.* **2002,** *4* (1), 26.

54.(a) Wu, W.; Yao, L.; Yang, T.; Yin, R.; Li, F.; Yu, Y., NIR-light-induced deformation of cross-linked liquid-crystal polymers using upconversion nanophosphors. *J. Am. Chem. Soc.* **2011,** *133* (40), 15810-15813; (b) Carling, C.-J.; Boyer, J.-C.; Branda, N. R., Remote-control photoswitching using NIR light. *J. Am. Chem. Soc.* **2009,** *131* (31), 10838-10839.

55.(a) Dong, H.; Du, S.-R.; Zheng, X.-Y.; Lyu, G.-M.; Sun, L.-D.; Li, L.-D.; Zhang, P.-Z.; Zhang, C.; Yan, C.-H., Lanthanide nanoparticles: from design toward bioimaging and therapy. *Chem. Rev.* **2015,** *115* (19), 10725-10815; (b) Yang, D.; Hou, Z.; Cheng, Z.; Li, C.; Lin, J., Current advances in lanthanide ion (Ln 3+)-based upconversion nanomaterials for drug delivery. *Chem. Soc. Rev.* **2015,** *44* (6), 1416-1448.

56.(a) Hu, J.; Tang, Y. a.; Elmenoufy, A. H.; Xu, H.; Cheng, Z.; Yang, X., Nanocomposite ‐ based photodynamic therapy strategies for deep tumor treatment. *Small* **2015,** *11* (44), 5860-5887; (b) Ai, X.; Ho, C. J. H.; Aw, J.; Attia, A. B. E.; Mu, J.; Wang, Y.; Wang, X.; Wang, Y.; Liu, X.; Chen, H., In vivo covalent cross-

linking of photon-converted rare-earth nanostructures for tumour localization and theranostics. *Nat. Commun.* **2016,** *7*, 10432.

57.(a) Song, X.; Chen, Q.; Liu, Z., Recent advances in the development of organic photothermal nano-agents. *Nano Res.* **2015,** *8* (2), 340-354; (b) Cheng, L.; Wang, C.; Feng, L.; Yang, K.; Liu, Z., Functional nanomaterials for phototherapies of cancer. *Chem. Rev.* **2014,** *114* (21), 10869-10939.

58.Luo, D.; Carter, K. A.; Miranda, D.; Lovell, J. F., Chemophototherapy: an emerging treatment option for solid tumors. *Adv. Sci.* **2017,** *4* (1), 1600106.

59.Bansal, A.; Zhang, Y., Photocontrolled nanoparticle delivery systems for biomedical applications. *Acc. Chem. Res.* **2014,** *47* (10), 3052-3060.

60.(a) Yang, X.; Liu, Z.; Li, Z.; Pu, F.; Ren, J.; Qu, X., Near‐Infrared‐Controlled, Targeted Hydrophobic Drug‐Delivery System for Synergistic Cancer Therapy. *Chem. Eur. J.* **2013,** *19* (31), 10388-10394; (b) Xia, Y.; Li, W.; Cobley, C. M.; Chen, J.; Xia, X.; Zhang, Q.; Yang, M.; Cho, E. C.; Brown, P. K., Gold nanocages: from synthesis to theranostic applications. *Acc. Chem. Res.* **2011,** *44* (10), 914-924.

61.(a) Zheng, W.; Huang, P.; Tu, D.; Ma, E.; Zhu, H.; Chen, X., Lanthanide-doped upconversion nano-bioprobes: electronic structures, optical properties, and biodetection. *Chem. Soc. Rev.* **2015,** *44* (6), 1379-1415; (b) Liu, D.; Xu, X.; Du, Y.; Qin, X.; Zhang, Y.; Ma, C.; Wen, S.; Ren, W.; Goldys, E. M.; Piper, J. A., Three-dimensional controlled growth of monodisperse sub-50 nm heterogeneous nanocrystals. *Nat. Commun.* **2016,** *7*, 10254; (c) Li, X.; Zhang, F.; Zhao, D., Lab on upconversion nanoparticles: optical properties and applications engineering via designed nanostructure. *Chem. Soc. Rev.* **2015,** *44* (6), 1346-1378; (d) Dong, H.; Sun, L.-D.; Yan, C.-H., Energy transfer in lanthanide upconversion studies for extended optical applications. *Chem. Soc. Rev.*

2015, *44* (6), 1608-1634; (e) Yang, Y.; Shao, Q.; Deng, R.; Wang, C.; Teng, X.; Cheng, K.; Cheng, Z.; Huang, L.; Liu, Z.; Liu, X., In vitro and in vivo uncaging and bioluminescence imaging by using photocaged upconversion nanoparticles. *Angew. Chem. Int. Ed.* **2012,** *51* (13), 3125-3129.

62.(a) Idris, N. M.; Jayakumar, M. K. G.; Bansal, A.; Zhang, Y., Upconversion nanoparticles as versatile light nanotransducers for photoactivation applications. *Chem. Soc. Rev.* **2015,** *44* (6), 1449-1478; (b) Tsang, M.-K.; Bai, G.; Hao, J., Stimuli responsive upconversion luminescence nanomaterials and films for various applications. *Chem. Soc. Rev.* **2015,** *44* (6), 1585-1607.

63.(a) Pierri, A. E.; Huang, P.-J.; Garcia, J. V.; Stanfill, J. G.; Chui, M.; Wu, G.; Zheng, N.; Ford, P. C., A photoCORM nanocarrier for CO release using NIR light. *Chem. Commun.* **2015,** *51* (11), 2072-2075; (b) Hu, M.; Zhao, J.; Ai, X.; Budanovic, M.; Mu, J.; Webster, R. D.; Cao, Q.; Mao, Z.; Xing, B., Near infrared light-mediated photoactivation of cytotoxic Re (i) complexes by using lanthanide-doped upconversion nanoparticles. *Dalton Trans.* **2016,** *45* (36), 14101-14108; (c) Perfahl, S.; Natile, M. M.; Mohamad, H. S.; Helm, C. A.; Schulzke, C.; Natile, G.; Bednarski, P. J., Photoactivation of Diiodido–Pt (IV) Complexes Coupled to Upconverting Nanoparticles. *Mol. Pharm.* **2016,** *13* (7), 2346-2362; (d) Burks, P. T.; Garcia, J. V.; GonzalezIrias, R.; Tillman, J. T.; Niu, M.; Mikhailovsky, A. A.; Zhang, J.; Zhang, F.; Ford, P. C., Nitric oxide releasing materials triggered by near-infrared excitation through tissue filters. *J. Am. Chem. Soc.* **2013,** *135* (48), 18145-18152; (e) Garcia, J. V.; Yang, J.; Shen, D.; Yao, C.; Li, X.; Wang, R.; Stucky, G. D.; Zhao, D.; Ford, P. C.; Zhang, F., NIR‐triggered release of caged nitric oxide using upconverting nanostructured materials. *Small* **2012,** *8* (24), 3800-3805.

64.Dai, Y.; Xiao, H.; Liu, J.; Yuan, Q.; Ma, P. a.; Yang, D.; Li, C.; Cheng, Z.; Hou, Z.; Yang, P., In vivo multimodality imaging and cancer therapy by near-infrared light-triggered trans-platinum pro-drug-conjugated upconverison nanoparticles. *J. Am. Chem. Soc.* **2013,** *135* (50), 18920-18929.

65.Min, Y.; Li, J.; Liu, F.; Yeow, E. K.; Xing, B., Near‐Infrared Light‐Mediated Photoactivation of a Platinum Antitumor Prodrug and Simultaneous Cellular Apoptosis Imaging by Upconversion‐Luminescent Nanoparticles. *Angew. Chem.* **2014,** *126* (4), 1030-1034.

66.(a) He, S.; Krippes, K.; Ritz, S.; Chen, Z.; Best, A.; Butt, H.-J.; Mailänder, V.; Wu, S., Ultralow-intensity near-infrared light induces drug delivery by upconverting nanoparticles. *Chem. Commun.* **2015,** *51* (2), 431-434; (b) Zhang, Y.; Yu, Z.; Li, J.; Ao, Y.; Xue, J.; Zeng, Z.; Yang, X.; Tan, T. T. Y., Ultrasmall-Superbright Neodymium-Upconversion Nanoparticles via Energy Migration Manipulation and Lattice Modification: 808 nm-Activated Drug Release. *ACS nano* **2017,** *11* (3), 2846-2857.

67.Shanmugam, V.; Chien, Y.-H.; Cheng, Y.-S.; Liu, T.-Y.; Huang, C.-C.; Su, C.-H.; Chen, Y.-S.; Kumar, U.; Hsu, H.-F.; Yeh, C.-S., Oligonucleotides Assembled Au Nanorod-Assisted Cancer Photothermal Ablation and Combination Chemotherapy with Targeted Dual-Drug Delivery of Doxorubicin and Cisplatin Prodrug. *ACS Appl. Mater. Interfaces* **2014,** *6* (6), 4382-4393.

68.Bi, H.; Dai, Y.; Xu, J.; Lv, R.; He, F.; Gai, S.; Yang, D.; Yang, P., CuS–Pt (iv)–PEG–FA nanoparticles for targeted photothermal and chemotherapy. *J. Mat. Chem. B* **2016,** *4* (35), 5938-5946.

69.Shi, S.; Chen, X.; Wei, J.; Huang, Y.; Weng, J.; Zheng, N., Platinum (IV) prodrug conjugated Pd@ Au nanoplates for chemotherapy and photothermal therapy. *Nanoscale* **2016,** *8* (10), 5706-5713.

70.You, C.; Wu, H.; Wang, M.; Gao, Z.; Zhang, X.; Sun, B., Co-delivery of cisplatin and CJM-126 via photothermal conversion nanoparticles for enhanced synergistic antitumor efficacy. *Nanotechnology* **2017,** *29* (1), 015601.

71.Li, W.; Liu, Z.; Chen, Z.; Kang, L.; Guan, Y.; Ren, J.; Qu, X., An intelligent near-infrared light activatable nanosystem for accurate regulation of zinc signaling in living cells. *Nano Res.* **2017,** *10* (9), 3068-3076.

72.(a) Ai, F.; Ju, Q.; Zhang, X.; Chen, X.; Wang, F.; Zhu, G., A core-shell-shell nanoplatform upconverting near-infrared light at 808 nm for luminescence imaging and photodynamic therapy of cancer. *Sci. Rep.* **2015,** *5*, 10785; (b) Zou, W.; Visser, C.; Maduro, J. A.; Pshenichnikov, M. S.; Hummelen, J. C., Broadband dye-sensitized upconversion of near-infrared light. *Nat. Photonics* **2012,** *6* (8), 560; (c) Zhang, P.; Chiu, C. K.; Huang, H.; Lam, Y. P.; Habtemariam, A.; Malcomson, T.; Paterson, M. J.; Clarkson, G. J.; O'Connor, P. B.; Chao, H., Organoiridium Photosensitizers Induce Specific Oxidative Attack on Proteins within Cancer Cells. *Angew. Chem. Int. Ed.* **2017,** *56* (47), 14898-14902; (d) Ju, E.; Dong, K.; Chen, Z.; Liu, Z.; Liu, C.; Huang, Y.; Wang, Z.; Pu, F.; Ren, J.; Qu, X., Copper (II)–Graphitic Carbon Nitride Triggered Synergy: Improved ROS Generation and Reduced Glutathione Levels for Enhanced Photodynamic Therapy. *Angew. Chem.* **2016,** *128* (38), 11639-11643.

73.Lucky, S. S.; Soo, K. C.; Zhang, Y., Nanoparticles in photodynamic therapy. *Chem. Rev.* **2015,** *115* (4), 1990-2042.

74.(a) Leanne B, J.; Ross W, B., Photodynamic therapy and the development of metal-based photosensitisers. *Met.-Based Drugs* **2008,** *2008*, 276109; (b) Li, S. P.-Y.; Lau, C. T.-S.; Louie, M.-W.; Lam, Y.-W.; Cheng, S. H.;

Lo, K. K.-W., Mitochondria-targeting cyclometalated iridium (III)–PEG complexes with tunable photodynamic activity. *Biomaterials* **2013,** *34* (30), 7519-7532.

75.Shi, H.; Ma, X.; Zhao, Q.; Liu, B.; Qu, Q.; An, Z.; Zhao, Y.; Huang, W., Ultrasmall phosphorescent polymer dots for ratiometric oxygen sensing and photodynamic cancer therapy. *Adv. Funct. Mater.* **2014,** *24* (30), 4823-4830.

76.(a) Ding, X.; Han, B. H., Metallophthalocyanine‐Based Conjugated Microporous Polymers as Highly Efficient Photosensitizers for Singlet Oxygen Generation. *Angew. Chem.* **2015,** *127* (22), 6636-6639; (b) Huang, L.; Li, Z.; Zhao, Y.; Yang, J.; Yang, Y.; Pendharkar, A. I.; Zhang, Y.; Kelmar, S.; Chen, L.; Wu, W.; Zhao, J.; Han, G., Enhancing Photodynamic Therapy through Resonance Energy Transfer Constructed Near‐Infrared Photosensitized Nanoparticles. *Adv. Mater.* **2017,** *29* (28), 1604789.

77.Yuan, A.; Tang, X.; Qiu, X.; Jiang, K.; Wu, J.; Hu, Y., Activatable photodynamic destruction of cancer cells by NIR dye/photosensitizer loaded liposomes. *Chem. Commun.* **2015,** *51* (16), 3340-3342.

78.Ge, J.; Lan, M.; Zhou, B.; Liu, W.; Guo, L.; Wang, H.; Jia, Q.; Niu, G.; Huang, X.; Zhou, H., A graphene quantum dot photodynamic therapy agent with high singlet oxygen generation. *Nat. Commun.* **2014,** *5*, 4596.

79.Cheng, Y.; Doane, T. L.; Chuang, C. H.; Ziady, A.; Burda, C., Near infrared light‐triggered drug generation and release from gold nanoparticle carriers for photodynamic therapy. *Small* **2014,** *10* (9), 1799-1804.

80.Wang, C.; Cheng, L.; Liu, Z., Upconversion nanoparticles for photodynamic therapy and other cancer therapeutics. *Theranostics* **2013,** *3* (5), 317.

81.Zhang, P.; Steelant, W.; Kumar, M.; Scholfield, M., Versatile photosensitizers for photodynamic therapy at infrared excitation. *J. Am. Chem. Soc.* **2007,** *129* (15), 4526-4527.

82.Cui, S.; Yin, D.; Chen, Y.; Di, Y.; Chen, H.; Ma, Y.; Achilefu, S.; Gu, Y., In vivo targeted deep-tissue photodynamic therapy based on near-infrared light triggered upconversion nanoconstruct. *ACS nano* **2012,** *7* (1), 676-688.

83.Idris, N. M.; Gnanasammandhan, M. K.; Zhang, J.; Ho, P. C.; Mahendran, R.; Zhang, Y., In vivo photodynamic therapy using upconversion nanoparticles as remote-controlled nanotransducers. *Nat. Med.* **2012,** *18* (10), 1580.

84.Wang, X.; Wang, C.; Cheng, L.; Lee, S.-T.; Liu, Z., Noble metal coated single-walled carbon nanotubes for applications in surface enhanced Raman scattering imaging and photothermal therapy. *J. Am. Chem. Soc.* **2012,** *134* (17), 7414-7422.

85.(a) Huang, P.; Rong, P.; Lin, J.; Li, W.; Yan, X.; Zhang, M. G.; Nie, L.; Niu, G.; Lu, J.; Wang, W., Triphase interface synthesis of plasmonic gold bellflowers as near-infrared light mediated acoustic and thermal theranostics. *J. Am. Chem. Soc.* **2014,** *136* (23), 8307-8313; (b) Lin, J.; Wang, M.; Hu, H.; Yang, X.; Wen, B.; Wang, Z.; Jacobson, O.; Song, J.; Zhang, G.; Niu, G., Multimodal‐Imaging‐Guided Cancer Phototherapy by Versatile Biomimetic Theranostics with UV and γ‐Irradiation Protection. *Adv. Mater.* **2016,** *28* (17), 3273-3279; (c) Zhu, X.; Feng, W.; Chang, J.; Tan, Y.-W.; Li, J.; Chen, M.; Sun, Y.; Li, F., Temperature-feedback upconversion nanocomposite for accurate photothermal therapy at facile temperature. *Nat. Commun.* **2016,** *7*, 10437; (d) Zhang, L.; Chen, Y.; Li, Z.; Li, L.; Saint‐Cricq, P.; Li, C.; Lin, J.; Wang, C.; Su, Z.; Zink, J. I.,

Tailored Synthesis of Octopus‐type Janus Nanoparticles for Synergistic Actively‐Targeted and Chemo‐Photothermal Therapy. *Angew. Chem. Int. Ed.* **2016,** *55* (6), 2118-2121.

86.(a) Li, X.; Takashima, M.; Yuba, E.; Harada, A.; Kono, K., PEGylated PAMAM dendrimer–doxorubicin conjugate-hybridized gold nanorod for combined photothermal-chemotherapy. *Biomaterials* **2014,** *35* (24), 6576-6584; (b) Leung, S. J.; Kachur, X. M.; Bobnick, M. C.; Romanowski, M., Wavelength‐Selective Light‐Induced Release from Plasmon Resonant Liposomes. *Adv. Funct. Mater.* **2011,** *21* (6), 1113-1121.

87.Zhang, P.; Wang, J.; Huang, H.; Yu, B.; Qiu, K.; Huang, J.; Wang, S.; Jiang, L.; Gasser, G.; Ji, L.; Chao, H., Unexpected high photothemal conversion efficiency of gold nanospheres upon grafting with two-photon luminescent ruthenium (II) complexes: A way towards cancer therapy? *Biomaterials* **2015,** *63*, 102-114.

88.(a) Bello-Vieda, N. J.; Pastrana, H. F.; Garavito, M. F.; Ávila, A. G.; Celis, A. M.; Muñoz-Castro, A.; Restrepo, S.; Hurtado, J. J., Antibacterial Activities of Azole Complexes Combined with Silver Nanoparticles. *Molecules* **2018,** *23* (2), 361; (b) Albada, B.; Metzler-Nolte, N., Highly Potent Antibacterial Organometallic Peptide Conjugates. *Acc. Chem. Res.* **2017,** *50* (10), 2510-2518; (c) Chen, Z.; Ji, H.; Liu, C.; Bing, W.; Wang, Z.; Qu, X., A Multinuclear Metal Complex Based DNase‐Mimetic Artificial Enzyme: Matrix Cleavage for Combating Bacterial Biofilms. *Angew. Chem. Int. Ed.* **2016,** *55* (36), 10732-10736; (d) Azócar, M. I.; Gómez, G.; Levín, P.; Paez, M.; Muñoz, H.; Dinamarca, N., Antibacterial behavior of carboxylate silver (I) complexes. *J. Coord. Chem.* **2014,** *67* (23-24), 3840-3853.

89.Lin, D.; Qin, T.; Wang, Y.; Sun, X.; Chen, L., Graphene oxide wrapped SERS tags: multifunctional platforms toward optical labeling, photothermal ablation of bacteria, and the monitoring of killing effect. *ACS Appl. Mater. Interfaces* **2014,** *6* (2), 1320-1329.

90.Lovell, J. F.; Jin, C. S.; Huynh, E.; MacDonald, T. D.; Cao, W.; Zheng, G., Enzymatic regioselection for the synthesis and biodegradation of porphysome nanovesicles. *Angew. Chem. Int. Ed.* **2012,** *51* (10), 2429-2433.

91.Xu, L.; Cheng, L.; Wang, C.; Peng, R.; Liu, Z., Conjugated polymers for photothermal therapy of cancer. *Polym. Chem.* **2014,** *5* (5), 1573-1580.

92.Huang, P.; Gao, Y.; Lin, J.; Hu, H.; Liao, H.-S.; Yan, X.; Tang, Y.; Jin, A.; Song, J.; Niu, G., Tumor-specific formation of enzyme-instructed supramolecular self-assemblies as cancer theranostics. *ACS nano* **2015,** *9* (10), 9517-9527.

93.Lin, M.; Wang, D.; Liu, S.; Huang, T.; Sun, B.; Cui, Y.; Zhang, D.; Sun, H.; Zhang, H.; Sun, H., Cupreous complex-loaded chitosan nanoparticles for photothermal therapy and chemotherapy of oral epithelial carcinoma. *ACS Appl. Mater. Interfaces* **2015,** *7* (37), 20801-20812.

94.Khan, I.; Tang, E.; Arany, P., Molecular pathway of near-infrared laser phototoxicity involves ATF-4 orchestrated ER stress. *Sci. Rep.* **2015,** *5*, 10581.

95.Thévenot, J.; Oliveira, H.; Sandre, O.; Lecommandoux, S., Magnetic responsive polymer composite materials. *Chem. Soc. Rev.* **2013,** *42* (17), 7099-7116.

96.(a) Hao, R.; Xing, R.; Xu, Z.; Hou, Y.; Gao, S.; Sun, S., Synthesis, functionalization, and biomedical applications of multifunctional magnetic nanoparticles. *Adv. Mater.* **2010,** *22* (25), 2729-2742; (b) Gao, J.; Gu, H.; Xu, B., Multifunctional magnetic nanoparticles: design, synthesis, and biomedical applications. *Acc. Chem. Res.* **2009,** *42* (8), 1097-1107; (c) Sun, C.; Lee, J. S.; Zhang, M., Magnetic nanoparticles in MR imaging and drug delivery. *Adv. Drug Del. Rev.* **2008,** *60* (11), 1252-1265.

97.(a) Åkerman, M. E.; Chan, W. C.; Laakkonen, P.; Bhatia, S. N.; Ruoslahti, E., Nanocrystal targeting in vivo. *Proc. Natl. Acad. Sci.* **2002,** *99* (20), 12617-12621; (b) Zhao, W.; Gu, J.; Zhang, L.; Chen, H.; Shi, J., Fabrication of uniform magnetic nanocomposite spheres with a magnetic core/mesoporous silica shell structure. *J. Am. Chem. Soc.* **2005,** *127* (25), 8916-8917.

98.Kumar, C. S.; Mohammad, F., Magnetic nanomaterials for hyperthermia-based therapy and controlled drug delivery. *Adv. Drug Del. Rev.* **2011,** *63* (9), 789-808.

99.Kunz, P. C.; Meyer, H.; Barthel, J.; Sollazzo, S.; Schmidt, A. M.; Janiak, C., Metal carbonyls supported on iron oxide nanoparticles to trigger the CO-gasotransmitter release by magnetic heating. *Chem. Commun.* **2013,** *49* (43), 4896-4898.

100. Chen, W.-H.; Luo, G.-F.; Lei, Q.; Cao, F.-Y.; Fan, J.-X.; Qiu, W.-X.; Jia, H.-Z.; Hong, S.; Fang, F.; Zeng, X., Rational design of multifunctional magnetic mesoporous silica nanoparticle for tumor-targeted magnetic resonance imaging and precise therapy. *Biomaterials* **2016,** *76*, 87-101.

101. Kim, J.-H.; Eguchi, H.; Umemura, M.; Sato, I.; Yamada, S.; Hoshino, Y.; Masuda, T.; Aoki, I.; Sakurai, K.; Yamamoto, M., Magnetic metal-complex-conducting copolymer core–shell nanoassemblies for a single-drug anticancer platform. *NPG Asia Mater.* **2017,** *9* (3), e367.

Chapter 2: Near infrared light-mediated photoactivation of cytotoxic Re(I) complex by lanthanide-doped upconversion nanoparticles

2.1 Introduction

Transition metal based antitumor complexes, especially platinum drugs such as cisplatin, oxaliplatin and carboplatin have been studied for their abilities in cancer treatment for almost half a century.[1] Some of these complexes have gained worldwide applications in chemotherapy against various types of cancers. However, the use of these metal complexes in treatment process has been mostly associated with deficiencies such as limited tumor specificity, intrinsic or acquired multi-drug resistance.[2] Therefore, the rational design through the development of new alternatives with potent anticancer effect and improved specificity will be thus the main concern, and extensive studies have been carried out so far. [3-13] Recently, some photoactivatable Re(I) complexes which demonstrated the great potential to inactivate tumor growth based on increased tumor recognition have been investigated as possible candidates in chemotherapy.[14-19] In these cases, light irradiation, which has impressively high spatiaotemporal resolution, is required to activate the complexes for enhanced cytotoxicity within targeted tumor area. Despite their initial success, most of these photoactivatable Re(I) complexes are triggered by short-wavelength of light, such as UV, blue and green light. The application of short-wavelength light may cause undesired damage of tissue, protein and DNA.[20] In addition, limited penetration depth

in tissue making it difficult to reach tumors which locate beneath skin surface.[21] Therefore the application of short wavelength light in activating Re(I) complexes for better antitumor effect could be largely restricted. As comparison, long-wavelength light irradiation has been considered to cause less photo-damage and have deeper tissue penetration, making it more suitable for applications in biological system. Therefore, considering the potential significance of photoactive Re(I) complexes in antitumor treatment, the rational design of a simple yet specific strategy which allows activation of Re(I) complexes by long-wavelength light selectively in tumor region with minimum biological damage is highly desirable, and relevant investigations toward this direction still need to be further conducted. Recently, Lanthanide-doped upconversion nanoparticles (UCNPs) as a promising tool to gain precise control of light irradiation, have drawn much attention for its application in sensing[22-24], imaging[25-29], drug delivery[30-37], phototherapy[38-43] and theranostic[44-47] because of its unique optical properties. Generally, UCNPs can absorb long wavelength near infrared (NIR) light and give out multiple emission ranging from UV to visible and even NIR region[48-54]. Such appealing photo-physical property enable the local activation of photosensitive metal complex, such as complex of Pt, Ru, Fe, Zn, Cr and Mn, for therapeutic purpose by remotely controlled long-wavelength light irradiation which is suitable for living system[39, 55-67]. The successful NIR photoactivation by combination of UCNPs and Pt complex has been reported effective in suppressing the viability of cancer cells and inhibiting the tumor growth in living animals demonstrating that UCNPs can serve as a powerful platform for their remotely control in vitro and in vivo medical applications in biological system.[40, 45, 68] Herein, we demonstrate a system for NIR light controlled activation of Re(I) complex cytotoxicity by combining photoactivatable Re(I) complex with lanthanide-doped upconversion nanoparticles (Scheme 1). Upon NIR irradiation,

the Re(I) complex can be locally activated by upconverted UV light emitted from UCNPs and subsequently leads to enhanced cell lethality, therefore minimizing the potential side effect.

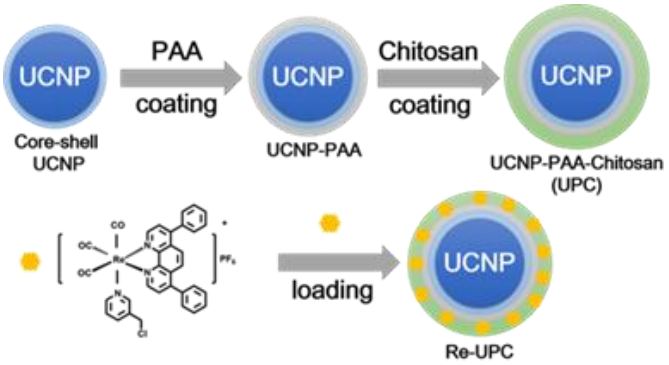

Scheme1 Schematic representation for the synthesis of Re(I) complex loaded UCNPs (Re-UPC).

2.2 Experimental

Instruments and general methods

^{1}HNMR spectrum was recorded on a Bruker AVANCE AV 300MHz spectrometer. ESI-MS spectrum was acquired on a Thermo LCQ DECA XP Liquid Chromatography-Mass Spectrometer. UV-VIS spectra were recorded on a SHIMAZU UV-1800 UV spectrophotometer. Fluorescence spectra were obtained on a SHIMAZU RF-5301PC spectro-fluorophotometer. The fluorescence emission spectra of UCNPs was recorded at an angle of 90° to the excitation laser (980 nm) and an optical SEC-2000 spectrometer coupled 2048 pixels CCD array (ALS Co., Ltd). Transmission electron microscope (TEM) images were recorded using a FEI EM208S TEM (Philips) operated at 100 kV. Dynamic light scattering (DLS) measurements were performed by Brookhaven 90 plus Nanoparticle Size Analyzer. Rhenium content was measured on an Agilent 7700 Inductively Coupled Plasma Mass Spectrometer (ICP-MS). Cell imaging was carried out on a fluorescence microscope (Nikon, Eclipse TE2000-E).

Synthetic procedure of [Re(DIP)(CO)$_3$(cpy)](PF$_6$):

Typically, the starting material, [Re(DIP)(CO)$_3$Cl] (DIP: 4,7-diphenyl-1,10-phenanthroline), was prepared according to a literature procedure.[69] The prepared molecule was then converted to [Re(DIP)(CO)$_3$](OTf). Basically, AgOTf (0.235 mmol) was added to a suspension of [Re(DIP)(CO)$_3$Cl] (0.157 mmol) in 50 mL of CH_3CN. The mixture was refluxed under nitrogen overnight in the dark. After removed off-white AgCl precipitate, CH_3CN was evaporated under reduced pressure. The resulting solid was dissolved in 50mL of THF containing 3-(Hydroxymethyl)pyridine (1.5 mmol) and refluxed under nitrogen atmosphere for 20 h in the dark. The mixture was then evaporated to dryness and the solid obtained was further dissolved in dichloromethane with 5 mL of thionyl chloride and heated to reflux under nitrogen atmosphere for 5 h. After removal of dichloromethane and excess amount of thionyl chloride by nitrogen flush, the resulting yellow solid was dissolved in CH_3CN and added dropwise into saturated NH_4PF_6 solution. The yellow precipitate was collected and washed with distilled water and diethylether followed by recrystallization from diethylether and dried under vacuum to afford the final product. (Yield: 77%) ^{1}H NMR (300 MHz, DMSO) δ 9.85 (d, *J* = 5.4 Hz, 2H; H of Ph$_2$-phen), 8.68 (s, 1H; H of pyridine), 8.52 (d, *J* = 4.9 Hz, 1H; H of pyridine), 8.22 (d, *J* = 5.4 Hz, 2H; H of Ph$_2$-phen), 8.14 (s, 2H; H of Ph$_2$-phen), 7.99 (d, *J* = 8.1 Hz, 1H;H of pyridine), 7.69 (s, 10H; C_6H_5 at Ph$_2$-phen), 7.42 (t, *J* = 7.9, 5.7 Hz, 1H;H of pyridine), 4.70 (s, 2H; CH_2). ESI-MS: m/z 729.9 [M-PF_6^-]$^+$ Elemental Analysis (%) Calcd: $C_{33}H_{22}ClF_6N_3O_3PRe\cdot 5H_2O$: C,41.06; H,3.34; N,4.35; C/N,9.41. Found: C ,39.79; H,2.97; N,4.11; C/N,9.68.

Preparation of NaYF$_4$:Yb^{3+}/Tm^{3+} core nanoparticles

$NaYF_4:Yb^{3+}/Tm^{3+}$ core nanoparticles were synthesized according to the method reported previously.[70] In general, 1 mmol of $RE(CH_3\ CO_2)_3$ (RE= 59.5% Y + 40% Yb + 0.5% Tm), 12 mmol of NaF, and 20 mL of oleic acid (OA)/1-octadecene (ODE) (v/v = 1:1) mixed solvent were added to the round bottom flask and heated to 110°C under vacuum with magnetic stirring for 30 min to remove residual water and oxygen. Then, the temperature was further increased to 320°C and kept for 1.5 h under nitrogen atmosphere. The resulting UCNPs were obtained by centrifugation for the following application.

Fabrication of $NaYF_4:Yb^{3+}/Tm^{3+}@NaYF_4$ core-shell nanoparticles

A cyclohexane solution of as-prepared $NaYF_4:Yb^{3+}/Tm^{3+}$ core nanoparticles and 20 mL mixture of OA and ODE (OA/ODE=v/v=1:1) were added to a round bottom flask and heated to 120°C under vacuum with magnetic stirring for 1 h and flushed with nitrogen. Then, the temperature was further heated to 310°C. The mixture of 3 mL of OA and ODE (OA/ODE= v/v = 1:1), $Y(CH_3CO_2)_3$ (1mmol) and $Na(CH_3CO_2)$ (1mmol) were added to the solution immediately. The reaction was kept at 310°C for 1 h under nitrogen atmosphere. The resulting core-shell UCNPs were isolated by centrifugation for the further surface modification.

Synthesis of PAA-functionalized UCNPs (UCNP-PAA)

A ligand exchange process was performed using poly(acrylic acid) (PAA) to replace the original hydrophobic ligands on the nanoparticle surface.[71] PAA (50 mg) was dissolved in ethanol (5 mL) and mixed with 2 mL of as-prepared core-shell UCNPs dispersion in chloroform (20 mg). The resulting mixture was kept overnight with magnetic stirring. The solution was then centrifuged at 2×10^4 rpm for 10 minutes. The precipitate was washed 3 times with ethanol to obtain the UCNP-PAA particles.

Surface coating of chitosan

The reagents EDC (28.7 mg) and NHS (11.6 mg) were added to an aqueous dispersion (10 mg, 2.5 mL) of as-prepared UCNP-PAA particles to activate carboxyl group on UCNP-PAA for 30min. Then an aqueous solution of chitosan (4 mg/ mL, 2.5 mL) was added and kept overnight with magnetic stirring. The solution was then centrifuged at 2×10^4 rpm for 10 minutes. The precipitate was washed 3 times with deionized water to obtain the UCNP-PAA-chitosan (UPC) particles.

Loading of Re(I) complex on UPC:

The previously prepared Re(I) complex (0.8 mg) was dissolved in CH_3CN 20μL to give a yellow solution. The resulting solution was added into PBS (1 mL, 10 mM, pH7.4) containing UCNP-PAA-chitosan particles (5.2 mg). The mixture was then stirred overnight. The resulting Re(I) loaded UCNPs (Re-UPC) was obtained by centrifugation at 2×10^4 rpm for 10 minutes and washed with PBS/CH_3CN (20:1) three times to remove excess amount of the Re(I) complex. Rhenium content was determined on an Agilent 7700 ICP-MS.

Stability evaluation of Re-UPC:

The Re-UPC (50 uM) were incubated with PBS (10 mM, pH 5.0 or 7.4) at 37 °C of different time intervals. Released Re(I) complex from Re-UPC was obtained by centrifugation at 2×10^4 rpm for 10 minutes. The amount of released Re(I) complex in the resulting supernatant was measured by fluorescence spectroscopy.

Cellular uptake

Cellular uptake was investigated by using fluorescence microscope. Drug susceptible human ovarian carcinoma A2780 cells or cisplatin resistant human ovarian carcinoma A2780cis cell were seeded at a density of 10^5 cells per well in a 35 mm u-dish (ibidi) containing RPMI 1640 medium (Gibco) supplemented with 10% fetal bovine serum (FBS, HyClone) and antibiotics (100 units/mL penicillin and 100 μg/mL

streptomycin) at 5% CO_2 and 37 °C for 24 hours prior to treatment with Re-UPC or Re(I) complex. After 2 hours incubation, the media were removed and cells were washed. The images were acquired on fluorescence microscope (Nikon Eclipse TE2000) with the excitation filter at 364nm.

Cell viability assay

In cell viability assay, cells were seeded in 96-wells plates with a density of 10^4 cells per well. After 24 hours of incubation at 5% CO_2 and 37°C, the medium was replaced with fresh medium containing Re(I) complex or UPC, Re-UPC. After another 24-hour incubation at 37°C, culture media were removed, cells were washed and then incubated with 3-(4,5-Dimethyl-2-thiazolyl)-2,5-diphenyl-2H-tetrazolium bromide (MTT) containing culture media. After 5 hours incubation, media were removed and 100 μL of DMSO was added. The absorbance at 570 nm was measured by a Tecan's Infinite M200 microplate reader. For NIR or UV light irradiation experiment, cells were incubated with Re-UPC for 2 hours. Subsequently, the drug-containing medium was replaced with fresh medium and cells were irradiated with NIR (980 nm, 1.5W/cm^2). After 24 hours of incubation cell viability was evaluated by standard MTT assays. In phototoxicity tests, cells were exposed to NIR for different period of time followed by 24 hours incubation and MTT assays to investigate cell viability.

2.3 Results and discussion

Synthesis and characterization of Re-UPC:

Scheme 1 illustrates the design of NIR-mediated activation of Re(I) complex on chitosan-coated UCNPs (UCNP-PAA-chitosan). The Re(I) complex was obtained through a facile synthesis by refluxing a mixture of $[Re(DIP)(CO)_3(CH_3CN)](PF_6)$ and 4-(Chloromethyl)pyridine in THF under nitrogen atmosphere. The bidentate N−N ligand tunes the lipophilicity of the compounds to facilitate the fast penetration into cells.

And the monodentate ligand is expected to contribute to the mitochondria affinity. The compound was characterized by ^{1}HNMR and ESI-MS. To establish our platform, first, $NaYF^{4}$:Yb^{3+}/Tm^{3+} core nanoparticles were prepared using thermal decomposition method, followed by coating of the $NaYF_4$ shell on the surface to afford the core-shell UCNPs. TEM images demonstrate that, the as-prepared core nanoparticles have a narrow size distribution of around 25 nm. After coating with $NaYF_4$, the size of particles increased to about 35 nm. The as-prepared core-shell particles are terminated with oleic ligands which is hydrophobic. To improve the solubility of particles in water, the core-shell UCNPs were transfer from nonpolar solvent to aqueous environment by using poly(acrylic acid) (PAA) as functional ligands to replace the hydrophobic oleic ligands.

Moreover, to facilitating the loading of Re(I) complex, as well as biocompatibility of the nanoparticles, carboxyl groups of PAA on the PAA-coated UCNPs (UCNP-PAA) were activated using EDC/NHS method, and followed by further conjugation with amine groups on amphiphilic chitosan structures. The size of the obtained PAA-coated UCNPs and chitosan-coated UCNPs were determined by dynamic light scattering (DLS) and transmission electron micrographs (TEM). As given in Fig 2.1, the obtained UCNPs (UCNP-PAA and UCNP-PAA-chitosan) have good mono-dispersity and uniform morphology. The inner core-shell structures of both UCNP-PAA and UCNP-PAA-chitosan were ~35 nm. The hydrodynamic diameter distribution, measured by DLS is ~76 nm for UCNP-PAA and ~118 nm for UCNP-PAA-chitosan, respectively. In addition, the successful coating of PAA and chitosan was further confirmed by Fourier transform infrared (FT-IR) spectra. As shown in Fig 2.2A disappearance of vibration of $-CH_3$ at 2927 cm^{-1} and 2855 cm^{-1} suggests the successful removal of oleic acid from particle surface. Further conjugation of chitosan on the particle surface can be confirmed by peaks situated at 1080 cm^{-1} and 1643 cm^{-1} corresponding to the C-O stretching and

formation of amide between carboxyl group on PAA and amine group on chitosan. Moreover, spectroscopy studies indicated that the absorption of the Re(I) complex overlaps the emission of UCNP-PAA-chitosan (Fig2.2B) at 291 nm ($^1I_6$-$^3H_6$), 350 nm ($^1I_6$-$^3F_4$) and 365 nm ($^1D_2$-$^3H_6$), suggesting that the as-prepared UCNP-PAA-chitosan can be utilized for activation of the Re(I) complex. Next, to afford the final product Re-UPC (Re(I) complex loaded UCNP-PAA-chitosan), the Re(I) complex was dissolved in aqueous solution (PBS/CH_3CN =50:1) in which UCNP-PAA-chitosan (UPC) was suspended to facilitate the incorporation of the complex onto the particles surface (UPC). Loading of the Re(I) complex was confirmed and quantified by fluorescence emission from the complex on Re-UPC. The amount of the complex on Re-UPC was determined to be 6.14 wt %, which is comparable to the value in the nano-platforms reported previously.[72] Furthermore, in order to exam the stability of Re-UPC under biological relevant condition, the possible release of the Re(I) complex was evaluated. In general, the aqueous suspensions containing Re-UPC were incubated at 37°C (pH 5.0 and 7.4) for different time duration within 24 hours. The release of Re(I) complex was quantified by measuring fluorescence intensity of the supernatant after centrifugation. As shown in Fig2.2c, the released Re(I) complex under both condition (37°C, pH 5.0 and 7.4) was less than 4% of the total amount loaded on Re-UPC, suggesting that Re-UPC is stable under biological conditions.

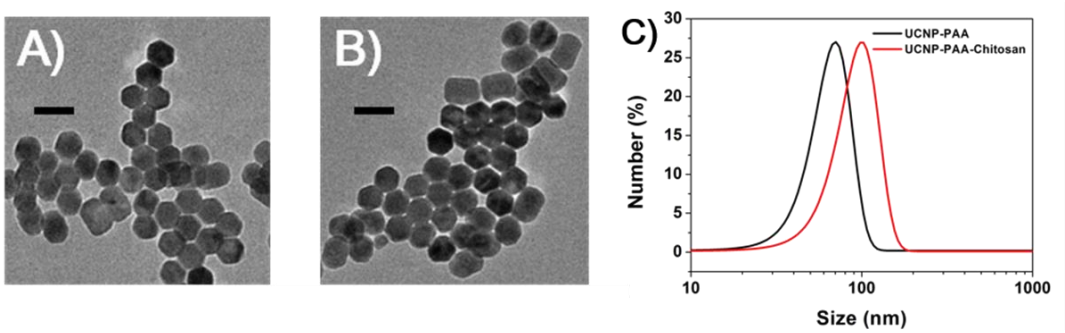

Fig 2.1 Characterization of prepared nanoparticles. A) and B) TEM images of PAA-coated UCNPs (UCNP-PAA) and chitosan-coated nanoparticles (UCNP-PAA-Chitosan, UPC), respectively. Scale bar =50 nm. C) Size distributions of the prepared UCNP-PAA and UCNP-PAA-Chitosan (UPC) determined by DLS.

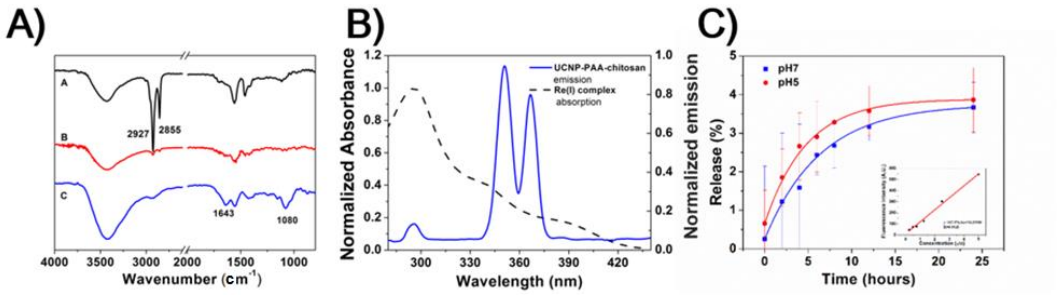

Fig2.2 A) FT-IR spectra of core-shell UCNP (black), UCNP-PAA (red) and UCNP-PAA-Chitosan(UPC) (blue). B) Absorbance spectra of the Re(I) complex (black dash line) and emission spectra of of UPC (blue line, λ_{ex}=980 nm). C) Cumulative release of Re(I) complex from Re-UPC at 37°C in PBS buffer. pH5.0 (red) and pH7.4 (blue). Inset: the calibration curve used to determine the concentration of released Re(I) complex.

Cellular uptake monitored by fluorescence microscopy:

To evaluate the cellular uptake of Re-UPC, fluorescence imaging study was carried out. In this typical study, A2780 cell, a well characterized cisplatin susceptible human ovarian carcinoma cell line, and its cisplatin resistant subline, A2780cis were chosen as the target cells. Both cells were incubated with Re-UPC (10 μM) in the dark for 2 hours before fluorescence imaging. As shown in Fig2.3 the green fluorescence signal of the Re(I) complex loaded on Re-UPC was observed within both cell lines, indicating the

successful internalization of Re-UPC into cells. To further investigate the possible mechanism of cellular uptake of Re-UPC, both type of cells were treated with Re-UPC (10 μM) at 4°C in the dark for 2 hours. It can be observed that (Fig2.3) at lower temperature (~4°C), there was little green fluorescence inside cells, suggesting the inhibited internalization of Re-UPC. These results indicated that the uptake of Re-UPC followed a temperature dependent endocytotic pathway.[73] Moreover, the uptake of free Re(I) complex was investigate as control. It can be observed that the fluorescence intensity of Re-UPC inside cell is much higher than that of free complex, demonstrating more cell uptake via Re-UPC. Moreover, it suggested that UPC can serve as a reliable platform for effective delivery of Re(I) complex, which can potentially lead to better antitumor effect in vitro and in living cells.

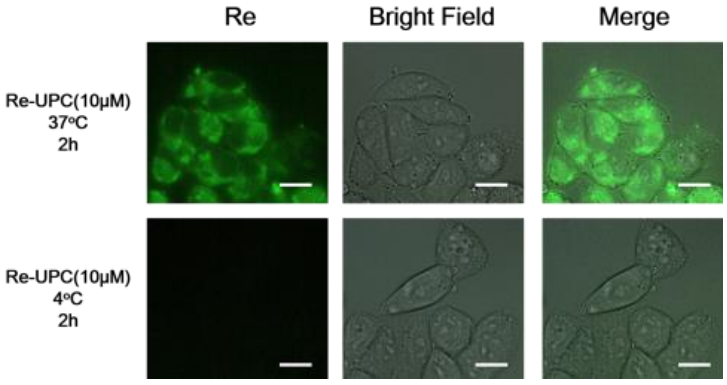

Fig 2.3 Fluorescence microscope images of A2780 cells incubated with Re-UPC (10 μM) at 37°C and 4°C for 2 h, λ_{ex}=364nm. All scale bars are 10 μm.

Cytotoxicity Assay upon Light Irradiation:

Moreover, we evaluated the cytotoxicity of our system in living cells. Both drug susceptible human ovarian carcinoma A2780 cells and its cisplatin resistant subline A2780cis were chosen as target cell lines. Basically, the two types of cells were treated with Re-UPC and 1 hour of NIR irradiation (980 nm) followed by 24 hours incubation before cell viability assays. Similar cellular incubation in the absence of NIR irradiation

was used as control. Tumor cells alone and cells treated with UPC were irradiated under NIR to assess the potential phototoxicity. As indicated in Fig2.4A and Fig2.4B, no significant toxicity was detected in Re-UPC treated A2780 cells and A2780cis cells without NIR irradiation. However, when cells were treated with Re-UPC and 1 h of NIR irradiation (at 980 nm) more potent cytotoxicity could be achieved. Cell viability of A2780 cells dramatically decreased from 89% to around 55% (0.5 μM) exhibiting enhanced cytotoxicity of Re-UPC upon NIR irradiation (Fig2.4A). Similarly, improved cell lethality was also achieved in cisplatin resistant cell line A2780cis. There was 47% cell viability observed in A2780cis cells treated with Re-UPC (1 μM) and NIR irradiation, which was much lower than (~ 74%) the similarly treated cells without NIR activation (Fig 2.4B). These results clearly suggested that NIR irradiation of Re-UPC is essential for activated cytotoxicity. In addition, the light-mediated cytotoxicity in both A2780 and A2780cis cell lines exhibited dependence on concentration of Re-UPC and duration of NIR irradiation. In particular, the increased cytotoxicity could be achieved when the higher concentration of Re-UPC was applied. As indicated in Fig 2.4A and Fig 2.4B, under 1h NIR light irradiation, Re-UPC (0.5 μM) was found to exhibit obvious cytotoxicity against both A2780 cells and A2780cis cells, and there were 55% and 86% cell viability detected respectively. Moreover, the more potent cell lethality (e.g. 32% and 47% cell viability) of A2780 and A2780cis cells was observed when the higher concentration of Re-UPC (1 μM) was used. Similarly, the more significant cell lethality could be also observed when the prolonged NIR irradiation was applied. It can be observed that (Fig 2.4C and Fig 2.4D) cell treated with 0.5 μM of Re-UPC under 2 h NIR irradiation exhibited more distinct toxicity towards A2780 and A2780cis cells with cell viability of 40% and 59% respectively than that under 1 h NIR illumination. The potent NIR-triggered cytotoxicity in both A2780 and A2780cis cells demonstrated that

Re-UPC can be successfully used in activating the Re(I) complex for effective inactivation of both drug susceptible and cisplatin-resistant tumor cells.

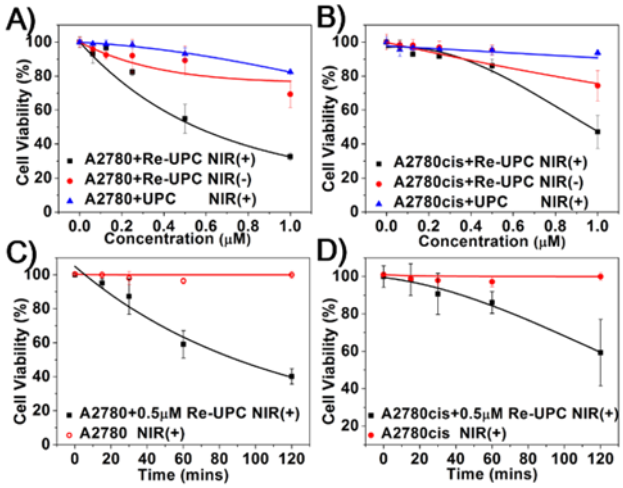

Fig 2.4 The cytotoxicity assays of the Re-UPC (black) and UPC (blue) at different concentration with 1 h of NIR irradiation (1.5 W/cm^2) in A) A2780 and B) cisplatin-resistant A2780cis cells. The cells treated with the Re-UPC but without light illumination were used as controls (red). C) A2780 cells and D) A2780cis cells under different exposure time of NIR with treatment of Re-UPC (0.5 μM, black) or without Re-UPC (red).

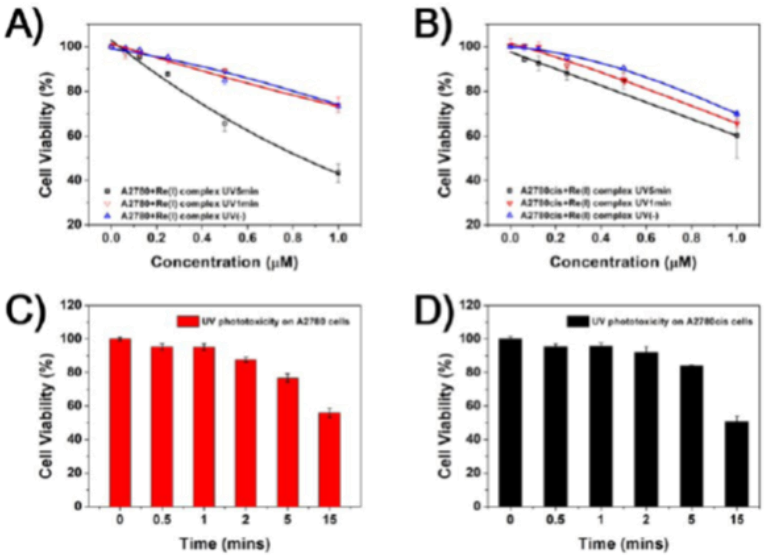

Fig 2.5 The cytotoxicity assays of free Re (I) complex in A2780 cells A) and A2780cis cells B) treated with UV light for different periods of time (0 minute (no,

UV irradiation, blue), 1 minute (pink) and 5 minutes (black). The phototoxicity of UV light over increasing time on C) A2780 cells (red) and D) A2780cis cells (black) respectively

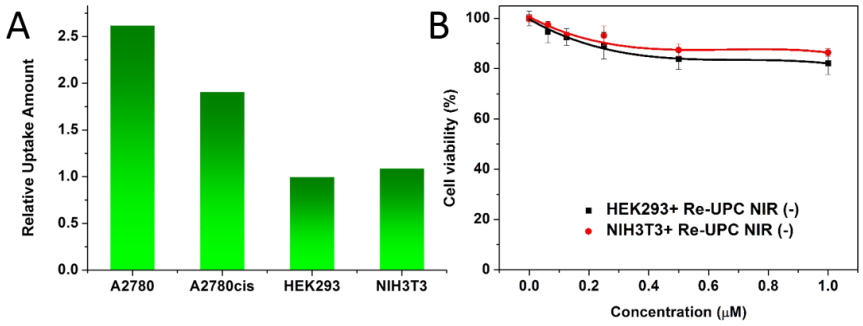

Fig 2.6 A) Cellular uptake of Re-UPC (10 μM) among different cell lines. B) The cytotoxicity assays of the Re-UPC at different concentration without light illumination in HEK293 and NIH3T3 cells.

As control, the similar free Re(I) complex under UV irradiation also exhibited photoactivatable cytotoxicity which was found to be dependent upon the concentration of the complex and duration of UV irradiation. (Fig 2.5 A and B). Although photoactivated cytotoxicity can be achieved by both NIR and UV irradiation, NIR activated Re-UPC showed slightly better antitumor effect in comparison to free Re(I) complex irradiated by UV light. For instance, A2780 cells incubated with 1μM of Re-UPC followed by 1 h NIR irradiation result in more obvious toxicity (32% cell viability, Fig 2.4A) than cells treated with 1 μM of Re(I) complex and 5 min UV illumination (43% cell viability Fig 2.5 A) Similarly in A2780cis cell line, 1 μM of Re-UPC with 1h NIR irradiation caused more cell death (47% cell viability, Fig 2.4B) than 1μM of Re(I) complex and 5 min UV illumination (60% cell viability Fig 2.5B). Despite the fact that it is possible to obtain improved cytotoxicity of Re(I) complex with prolonged UV irradiation, overexposure to UV light may cause drastic photo-damage to cells (Fig 2.5 C and D). In contrast, more potent cytotoxicity of Re-UPC can be achieved by prolonged

NIR irradiation (Fig 2.4C and Fig 2.4D) without obvious cell lethality. Therefore, these results suggested that the combination of UCNPs and photoactivatable Re(I) complex provide a promising strategy to remotely control the activation of cytotoxicity for inhibition of targeted tumor cells in both drug susceptible cells and cisplatin resistant cells. Moreover, the use of NIR illumination, compared to UV light, can largely reduce photo-damage to cells. What's more flow cytometry analysis (Fig 2.6 A) showed that showed that both A2780 and A2780cis cells exhibited higher uptake (A2780 2.62-fold and A2780cis 1.91-fold) than normal HEK293 cells. While normal cell line exhibit a relative lower amount of uptake (HEK293 1.00-fold, NIH3T3 1.09-fold.) In addition, Re-UPC did not exhibited significant toxicity to normal cells (Fig 2.6 B). Although, significant toxicity to normal cells may occur upon light stimulation. As the toxicity of Re-UPC is largely based on the activation through light irradiation. The light activation area can be precisely controlled through manipulation of NIR radiation with high spatial-temporal resolution, minimizing unwanted damage to normal tissue and cells.

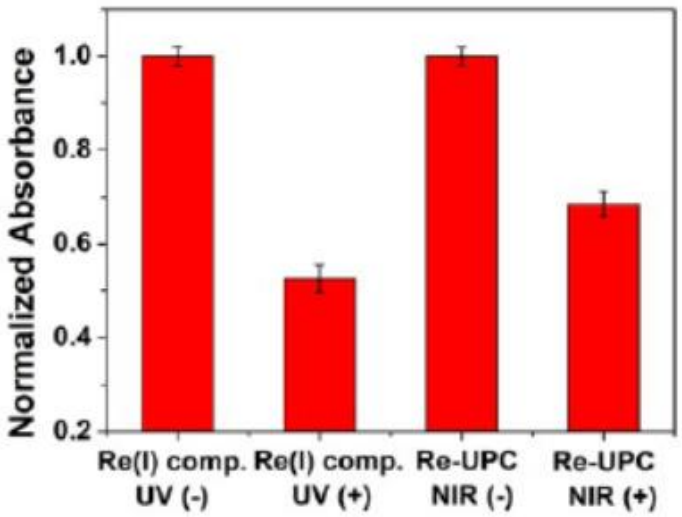

Fig 2.7 RNO/imidazole assay for investigation on mechanism of photoactivated cytotoxicity:Normalized absorbance (440 nm) of RNO (50 μM) in the presence of Re(I) complex (50 μM) or Re-UPC (500 μM) with or without light irradiation.

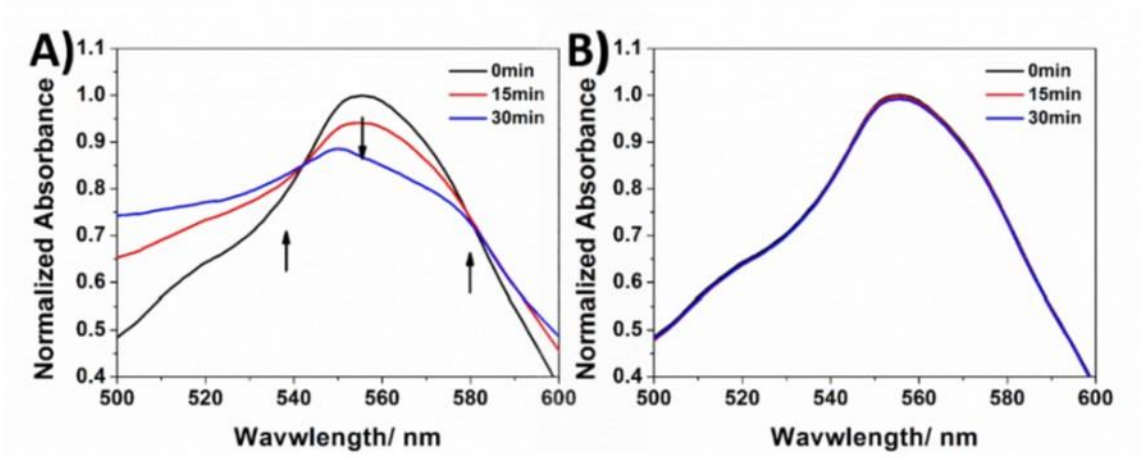

Fig 2.8 Time course of absorption spectra change of Myoglobin (50 μM) in PBS solution (pH 7.4)containing the rhenium (I) complex 15 μM A) with UV irradiation (365 nm) and B) without light irradiation

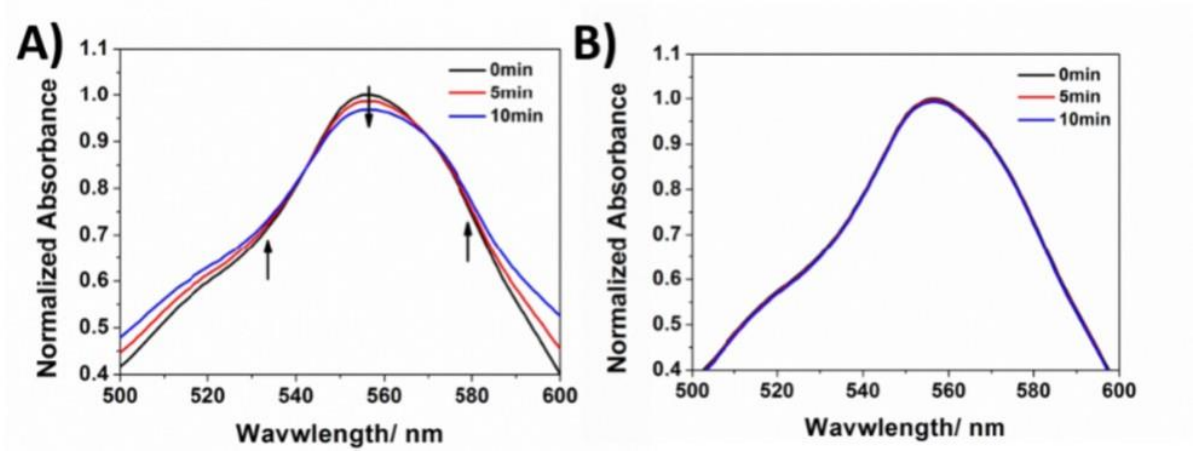

Fig 2.9 Time course of absorption spectra change of Myoglobin (50 μM) in PBS solution (pH 7.4) containing Re-UPC 15 μM A) with NIR irradiation (980 nm) and B) without irradiation

Furthermore, to study the mechanism of photoactivated cytotoxicity, N,N-dimethyl-4-nitrosoaniline (RNO) imidazole assay was carried out. In general, PBS solution containing RNO, imidazole and the Re(I) complex or Re-UPC were irradiated in fluorescence quartz cuvettes. Absorbance of N,N-dimethyl-4-nitrosoaniline at 440 nm was monitored by UV-VIS spectrometer. As shown in Fig 2.7, compared to sample

without light irradiation, an obvious decrease in the absorbance of RNO was observed when Re(I) complex was activated by UV. Similarly, Re-UPC under NIR irradiation also caused decreased absorbance of RNO, suggesting that the photo-activated cytotoxicity observed was probably associated with ROS generated during photoactivation.[16, 74] In addition, to better understand the mechanism concerning photoactivation of the Re(I) complex, experiments have been carried out to investigate the photochemistry of the complex. It has been reported that some rhenium complex will undergo ligand dissociation upon light irradiation.[75, 76] Therefore, myoglobin assay and NMR experiments were performed to study the photochemistry of the rhenium (I) complex. Myoglobin assay represents the principal method to determine CO release.[77] To exam whether CO ligand was released upon light irradiation, a solution containing 6 μM myoglobin(Mb), 10 mM dithionite and 1.5 μM of the Re(I) complex in PBS solution was prepared and irradiated by UV light (8.9 mW/cm^2). The dissociation of CO was tracked by monitoring the absorbance of Mb. The absorbance band at 557 nm of Mb decreased upon light irradiation (Fig 2.8 and Fig 2.9). In the meantime, two bands of MbCO adduct appeared at 540 nm and 577 nm. These results indicated the conversion of Mb to MbCO suggesting the dissociation of CO from the complex upon light irradiation. Moreover, the pyridyl group was monitored by ^{1}H NMR during photo activation. The NMR study revealed that signal associated with –CH_2 moiety on pyridyl group shown that, after one hour UV irradiation, a new species has been formed at 4.84 ppm. However, the signal of –CH2 moiety on the free pyridyl group was at 5.01 ppm, suggesting that the pyridyl did not dissociate from the metal center.

2.4 Conclusions

In summary we have demonstrated upconversion nanoparticle-based system for NIR activated cytotoxicity of Re(I) complex. Typically, UCNPs can be used to activate

the complex with upconversion luminescence triggered by NIR. The system can be effectively uptake by tumor cells via endocytosis. In addition, upon NIR irradiation, the locally activated drug exhibited enhanced cytotoxicity against both drug susceptible A2780 cells demonstrating that NIR irradiation combined with our system can achieve potent photoactivated cytotoxicity while minimizing unwanted photodamage to cells. Therefore, such combination of UCNPs and photoactivatable drug can provide a promising strategy to remotely control the activation of cytotoxicity to inhibit targeted tumor cells growth in both drug susceptible cells and cisplatin resistant cells and thus minimize the potential side effects.

2.5 Reference

1. T. C. Johnstone, K. Suntharalingam and S. J. Lippard, *Chem. Rev.*, 2016, **116**, 3436-3486.
2. Z. H. Siddik, *Oncogene*, 2003, **22**, 7265-7279.
3. P. C. Bruijnincx and P. J. Sadler, *Curr. Opin. Chem. Biol.*, 2008, **12**, 197-206.
4. J. S. Butler and P. J. Sadler, *Curr. Opin. Chem. Biol.*, 2013, **17**, 175-188.
5. N. Graf and S. J. Lippard, *Adv Drug Deliv Rev*, 2012, **64**, 993-1004.
6. W. Han Ang and P. J. Dyson, *Eur. J. Inorg. Chem.*, 2006, **2006**, 4003-4018.
7. S. K. Singh and D. S. Pandey, *RSC Adv.*, 2014, **4**, 1819-1840.
8. X. Wang and Z. Guo, *Chem. Soc. Rev.*, 2013, **42**, 202-224.
9. L. He, Y. Li, C.-P. Tan, R.-R. Ye, M.-H. Chen, J.-J. Cao, L.-N. Ji and Z.-W. Mao, *Chem. Sci.*, 2015, **6**, 5409-5418.
10. Y. Li, C. P. Tan, W. Zhang, L. He, L. N. Ji and Z. W. Mao, *Biomaterials*, 2015, **39**, 95-104.
11. J. N. Liu, W. B. Bu and J. L. Shi, *Acc. Chem. Res.*, 2015, **48**, 1797-1805.
12. H. Chen, J. Tian, W. He and Z. Guo, *J. Am. Chem. Soc.*, 2015, **137**, 1539-1547.
13. P. Zhang, Y. Chen, Y. Zeng, C. Shen, R. Li, Z. Guo, S. Li, Q. Zheng, C. Chu, Z. Wang, Z. Zheng, R. Tian, S. Ge, X. Zhang, N. S. Xia, G. Liu and X. Chen, *Proc. Natl. Acad. Sci. U. S. A.*, 2015, **112**, E6129-6138.

14. I. Chakraborty, S. J. Carrington, J. Hauser, S. R. J. Oliver and P. K. Mascharak, *Chem. Mater.*, 2015, **27**, 8387-8397.

15. A. Kastl, S. Dieckmann, K. Wahler, T. Volker, L. Kastl, A. L. Merkel, A. Vultur, B. Shannan, K. Harms, M. Ocker, W. J. Parak, M. Herlyn and E. Meggers, *ChemMedChem*, 2013, **8**, 924-927.

16. A. Leonidova, V. Pierroz, R. Rubbiani, J. Heier, S. Ferrari and G. Gasser, *Dalton transactions*, 2014, **43**, 4287-4294.

17. K. Wahler, A. Ludewig, P. Szabo, K. Harms and E. Meggers, *Eur. J. Inorg. Chem.*, 2014, **2014**, 807-811.

18. K. Yin Zhang, K. Ka-Shun Tso, M.-W. Louie, H.-W. Liu and K. Kam-Wing Lo, *Organometallics*, 2013, **32**, 5098-5102.

19. A. Leonidova and G. Gasser, *ACS Chem. Biol.*, 2014, **9**, 2180-2193.

20. K. Szacilowski, W. Macyk, A. Drzewiecka-Matuszek, M. Brindell and G. Stochel, *Chem. Rev.*, 2005, **105**, 2647-2694.

21. N. J. Farrer, L. Salassa and P. J. Sadler, *Dalton transactions*, 2009, 10690-10701.

22. R. Deng, X. Xie, M. Vendrell, Y. T. Chang and X. Liu, *J. Am. Chem. Soc.*, 2011, **133**, 20168-20171.

23. P. Huang, W. Zheng, S. Zhou, D. Tu, Z. Chen, H. Zhu, R. Li, E. Ma, M. Huang and X. Chen, *Angew. Chem. Int. Ed.*, 2014, **53**, 1252-1257.

24. L. Zhou, R. Wang, C. Yao, X. Li, C. Wang, X. Zhang, C. Xu, A. Zeng, D. Zhao and F. Zhang, *Nat Commun*, 2015, **6**, 6938.

25. Y. Yang, Q. Shao, R. Deng, C. Wang, X. Teng, K. Cheng, Z. Cheng, L. Huang, Z. Liu, X. Liu and B. Xing, *Angew. Chem. Int. Ed.*, 2012, **51**, 3125-3129.

26. L. Cheng, C. Wang, X. Ma, Q. Wang, Y. Cheng, H. Wang, Y. Li and Z. Liu, *Adv. Funct. Mater.*, 2013, **23**, 272-280.

27. Q. Liu, W. Feng, T. Yang, T. Yi and F. Li, *Nat. Protoc.*, 2013, **8**, 2033-2044.

28. H. Dong, S. R. Du, X. Y. Zheng, G. M. Lyu, L. D. Sun, L. D. Li, P. Z. Zhang, C. Zhang and C. H. Yan, *Chem. Rev.*, 2015, **115**, 10725-10815.

29. J. Rieffel, F. Chen, J. Kim, G. Chen, W. Shao, S. Shao, U. Chitgupi, R. Hernandez, S. A. Graves, R. J. Nickles, P. N. Prasad, C. Kim, W. Cai and J. F. Lovell, *Adv. Mater.*, 2015, **27**, 1785-1790.

30. G. Tian, Z. Gu, L. Zhou, W. Yin, X. Liu, L. Yan, S. Jin, W. Ren, G. Xing, S. Li and Y. Zhao, *Adv. Mater.*, 2012, **24**, 1226-1231.

31. P. Ma, H. Xiao, X. Li, C. Li, Y. Dai, Z. Cheng, X. Jing and J. Lin, *Adv. Mater.*, 2013, **25**, 4898-4905.

32. Y. Yang, F. Liu, X. Liu and B. Xing, *Nanoscale*, 2013, **5**, 231-238.

33. Y. Yang, B. Velmurugan, X. Liu and B. Xing, *Small*, 2013, **9**, 2937-2944.

34. X. Li, L. Zhou, Y. Wei, A. M. El-Toni, F. Zhang and D. Zhao, *J. Am. Chem. Soc.*, 2014, **136**, 15086-15092.

35. W. Fan, W. Bu, Z. Zhang, B. Shen, H. Zhang, Q. He, D. Ni, Z. Cui, K. Zhao, J. Bu, J. Du, J. Liu and J. Shi, *Angew. Chem. Int. Ed.*, 2015, **54**, 14026-14030.

36. N. M. Idris, M. K. Jayakumar, A. Bansal and Y. Zhang, *Chem. Soc. Rev.*, 2015, **44**, 1449-1478.

37. D. Yang, P. Ma, Z. Hou, Z. Cheng, C. Li and J. Lin, *Chem. Soc. Rev.*, 2015, **44**, 1416-1448.

38. L. Cheng, K. Yang, Y. Li, J. Chen, C. Wang, M. Shao, S. T. Lee and Z. Liu, *Angew. Chem. Int. Ed.*, 2011, **50**, 7385-7390.

39. N. M. Idris, M. K. Gnanasammandhan, J. Zhang, P. C. Ho, R. Mahendran and Y. Zhang, *Nat. Med.*, 2012, **18**, 1580-1585.

40. Y. Dai, H. Xiao, J. Liu, Q. Yuan, P. Ma, D. Yang, C. Li, Z. Cheng, Z. Hou, P. Yang and J. Lin, *J. Am. Chem. Soc.*, 2013, **135**, 18920-18929.

41. C. Wang, L. Cheng, Y. Liu, X. Wang, X. Ma, Z. Deng, Y. Li and Z. Liu, *Adv. Funct. Mater.*, 2013, **23**, 3077-3086.

42. W. Fan, W. Bu, B. Shen, Q. He, Z. Cui, Y. Liu, X. Zheng, K. Zhao and J. Shi, *Adv. Mater.*, 2015, **27**, 4155-4161.

43. X. Zhu, W. Feng, J. Chang, Y. W. Tan, J. Li, M. Chen, Y. Sun and F. Li, *Nat Commun*, 2016, **7**, 10437.

44. G. Chen, H. Qiu, P. N. Prasad and X. Chen, *Chem. Rev.*, 2014, **114**, 5161-5214.

45. Y. Min, J. Li, F. Liu, E. K. Yeow and B. Xing, *Angew. Chem. Int. Ed.*, 2014, **53**, 1012-1016.

46. S. Lu, D. Tu, P. Hu, J. Xu, R. Li, M. Wang, Z. Chen, M. Huang and X. Chen, *Angew. Chem. Int. Ed.*, 2015, **54**, 7915-7919.

47. X. Ai, C. J. Ho, J. Aw, A. B. Attia, J. Mu, Y. Wang, X. Wang, Y. Wang, X. Liu, H. Chen, M. Gao, X. Chen, E. K. Yeow, G. Liu, M. Olivo and B. Xing, *Nat Commun*, 2016, **7**, 10432.

48. L. D. Sun, Y. F. Wang and C. H. Yan, *Acc. Chem. Res.*, 2014, **47**, 1001-1009.

49. F. Wang, R. Deng and X. Liu, *Nat. Protoc.*, 2014, **9**, 1634-1644.

50. E. M. Chan, E. S. Levy and B. E. Cohen, *Adv. Mater.*, 2015, **27**, 5753-5761.

51. G. Chen, H. Agren, T. Y. Ohulchanskyy and P. N. Prasad, *Chem. Soc. Rev.*, 2015, **44**, 1680-1713.

52. X. Chen, D. Peng, Q. Ju and F. Wang, *Chem. Soc. Rev.*, 2015, **44**, 1318-1330.

53. A. Sedlmeier and H. H. Gorris, *Chem. Soc. Rev.*, 2015, **44**, 1526-1560.

54. B. Zhou, B. Shi, D. Jin and X. Liu, *Nat Nanotechnol*, 2015, **10**, 924-936.

55. S. Cui, D. Yin, Y. Chen, Y. Di, H. Chen, Y. Ma, S. Achilefu and Y. Gu, *ACS nano*, 2012, **7**, 676-688.

56. S. Wu and H. J. Butt, *Adv. Mater.*, 2016, **28**, 1208-1226.

57. S. He, K. Krippes, S. Ritz, Z. Chen, A. Best, H. J. Butt, V. Mailander and S. Wu, *Chem. Commun.*, 2015, **51**, 431-434.

58. A. E. Pierri, P. J. Huang, J. V. Garcia, J. G. Stanfill, M. Chui, G. Wu, N. Zheng and P. C. Ford, *Chem. Commun.*, 2015, **51**, 2072-2075.

59. E. Ruggiero, A. Habtemariam, L. Yate, J. C. Mareque-Rivas and L. Salassa, *Chem. Commun.*, 2014, **50**, 1715-1718.

60. Z. Chen, W. Sun, H. J. Butt and S. Wu, *Chem. Eur.J.*, 2015, **21**, 9165-9170.

61. E. Ruggiero, C. Garino, J. C. Mareque-Rivas, A. Habtemariam and L. Salassa, *Chem. Eur.J.*, 2016, **22**, 2801-2811.

62. P. T. Burks, J. V. Garcia, R. GonzalezIrias, J. T. Tillman, M. Niu, A. A. Mikhailovsky, J. Zhang, F. Zhang and P. C. Ford, *J. Am. Chem. Soc.*, 2013, **135**, 18145-18152.

63. H. Shi, T. Fang, Y. Tian, H. Huang and Y. Liu, *J. Mater. Chem. B*, 2016, DOI: 10.1039/c6tb01070a.

64. S. Perfahl, M. M. Natile, H. S. Mohamad, C. A. Helm, C. Schulzke, G. Natile and P. J. Bednarski, *Mol. Pharm.*, 2016, DOI: 10.1021/acs.molpharmaceut.6b00108.

65. J. D. Mase, A. O. Razgoniaev, M. K. Tschirhart and A. D. Ostrowski, *Photochem. Photobiol. Sci*, 2015, **14**, 775-785.

66. Y. Chen, G. Jiang, Q. Zhou, Y. Zhang, K. Li, Y. Zheng, B. Zhang and X. Wang, *RSC Adv.*, 2016, **6**, 23804-23808.

67. J. V. Garcia, J. Yang, D. Shen, C. Yao, X. Li, R. Wang, G. D. Stucky, D. Zhao, P. C. Ford and F. Zhang, *Small*, 2012, **8**, 3800-3805.

68. E. Ruggiero, J. Hernandez-Gil, J. C. Mareque-Rivas and L. Salassa, *Chem. Commun.*, 2015, **51**, 2091-2094.

69. B. Machura, M. Wolff, M. Jaworska, P. Lodowski, E. Benoist, C. Carrayon, N. Saffon, R. Kruszynski and Z. Mazurak, *J. Organomet. Chem.*, 2011, **696**, 3068-3075.

70. Y. Wei, F. Lu, X. Zhang and D. Chen, *Chem. Mater.*, 2006, **18**, 5733-5737.

71. H. Zhang, Y. Li, I. A. Ivanov, Y. Qu, Y. Huang and X. Duan, *Angew. Chem. Int. Ed.*, 2010, **49**, 2865-2868.

72. K. Baranowska and J. Okal, *Applied Catalysis A: General*, 2015, **499**, 158-167.

73. Y. Cheng, S. Yu, J. Wang, H. Qian, W. Wu and X. Jiang, *Macromol. Biosci.*, 2012, **12**, 1326-1335.

74. I. Kraljić and S. E. Mohsni, *Photochem. Photobiol.*, 1978, **28**, 577-581.

75. S. Sato, A. Sekine, Y. Ohashi, O. Ishitani, A. M. Blanco-Rodríguez, A. Vlček, T. Unno and K. Koike, *Inorg. Chem.*, 2007, **46**, 3531-3540.

76. P. V. Simpson, B. W. Skelton, P. Raiteri and M. Massi, *New J. Chem.*, 2016, DOI: 10.1039/c5nj03301b.

77. A. J. Atkin, J. M. Lynam, B. E. Moulton, P. Sawle, R. Motterlini, N. M. Boyle, M. T. Pryce and I. J. Fairlamb, *Dalton transactions*, 2011, **40**, 5755-5761.

Chapter 3: A bioinspired strategy for selective sensing of illicit date rape drug GHB

3.1 Introduction

Gamma-hydroxybutyric acid (GHB) is a short chain acid, which can function as depressant on the central nerve systems. GHB was used as anesthetic in 1960s[1, 2]. In addition, it has been utilized as pharmaceutical agent in the treatment of narcolepsy and alcohol withdraw[3, 4]. However, its use as therapeutic agent has been reduced mainly for the side effects such as amnesia and seizure[5]. In recent year, apart from the application as therapeutic agents, GHB has earned popularity as recreational drug due to its ability to induce euphoric feelings. It has been demonstrated that, the misuse of GHB may result in neurotoxic damage especially to maturing youths. In addition to the use as party drug, GHB has gained increasing attentions as a popular drug of abuse which is frequently related to drug-facilitated sexual assaults[6]. Considering the fact that GHB is colorless and odorless, it is barely detectable when spiked in drinks[7]. This makes it desirable to sexual offenders. In addition, its easy availability, low cost and rapid clearance from body make it one of the most commonly used date rape drugs in drug-facilitated sexual assaults[8].

Considering the potential physiological damage to human body and social impacts associated with GHB drug abuse, scientific researchers were greatly motivated to develop effective methods for sensing and detection of GHB. By right, methods based on Gas Chromatography-Mass Spectroscopy (GC/MS) or Liquid Chromatography-Mass Spectroscopy (LC/MS) have been well-established[9-11]. Although these procedures can be used for sensitive GHB detection, such methods require considerable sample treatment prior to analysis, which is laborious and may raise concerns of unwanted loss of significant information

of the original sample[12]. Moreover, most of the current methods do not distinguish GHB from its lactone precursor γ-butyrolactone (GBL) which is the point of interest in forensic applications[13]. Therefore, the development of alternative method for selective GHB analysis with minimal sample preparation would be highly desirable. In human body, GHB can be selectively oxidized through reactions catalyzed by specific enzymes (e.g. GHB dehydrogenase) and yield the oxidized form succinate semialdehyde and side reduced nicotinamide adenine dinucleotide (NADH)[14].

Inspired by this naturally occurring process, we introduce a simple yet effective approach based on highly specific enzymatic reaction for selective sensing of GHB. Typically, GHB molecules in either biosamples or spiked drinks can be recognized through specific enzyme-substrate interaction with GHB degydrogenase (GHB-DH) and undergo oxidation reaction generating NADH. As an ubiquitous reducing agent, the resulting NADH molecule can promote the reduction of gold(III) complex and form gold nanoparticles (AuNPs)[15-17]. Owing to the fascinating optical properties of AuNPs which is dependent on the morphological and physiological state (e.g. size, shape, aggregation state etc.) the distinct transformation from molecular metal complex into nanoscaled particles which is assisted by NADH reduction can be easily observed through the generation of Surface Plasmon Resonance (SPR) peak of AuNPs[18, 19]. In addition, the obvious colormetric changes accompanied by the formation of AuNPs allows simple GHB detection through naked-eye observation[20-22].

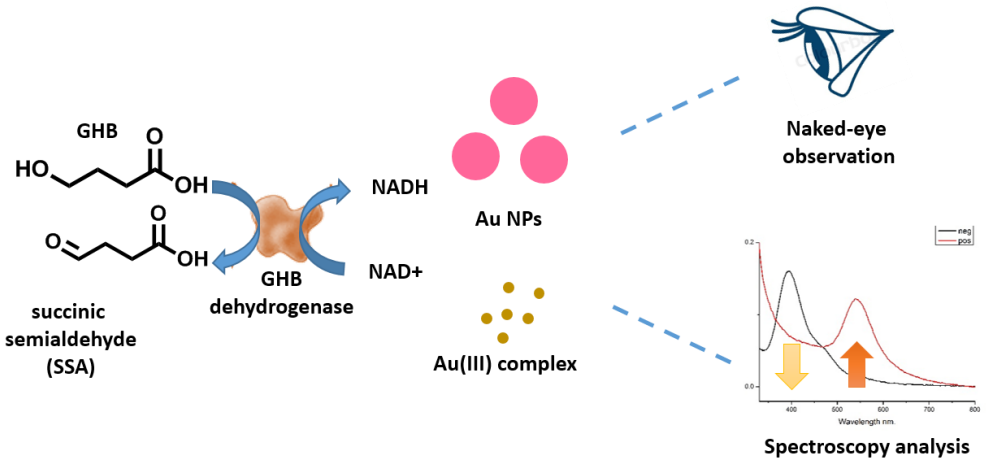

Fig 3.1 Scheme illustration of a bioinspired strategy for selective sensing of illicit date rape drug GHB.

3.2 Materials and methods

Materials

γ-butyrolactone (GBL), nicotinamide adenine dinucleotide (NAD^+) were purchased from TCI chemical (Japan). Tris(hydroxymethyl)aminomethane (Tris), Diaphorase (from Clostridium kluyveri), gold(III) chloride trihydrate ($HAuCl_4 \bullet 3H_2O$), cetrimonium bromide (CTAB), gold colloid (10 nm) were acquired from Sigma-Aldrich. GHB-DH was order from prima biomed (U.S.). All theese reagents indicated above were used directly without further purification.

Instruments.

NMR spectra were acquired on Bruker Avance 400 spectrometers. Mass spectra were obtained on a ThermoFinnigan LCQ Fleet MS. UV-VIS spectra were recorded on a SHIMAZU UV-1800 UV spectrophotometer. Fluorescence spectra were recorded on a Shimazu RF-5301PC spectrofluorophotometer.

Synthesis of GHB sodium salt

To a solution of GBL (23.2 mmol, 2 g) in EtOH (6 ml) a solution of NaOH (23.2 mmol, 928 mg) in water (4 ml) was added. The mixture was refluxed for 5 hours and the solvents were evaporated in vacuo. The product was white solid, 1.8 g (62%). 1H NMR (400 MHz, MeOD) δ 3.60 (t, *J* = 6.5 Hz, 2H), 2.26 (t, *J* = 7.4 Hz, 2H), 1.93–1.74 (m, 2H). M/Z=103.20 (negative mode)

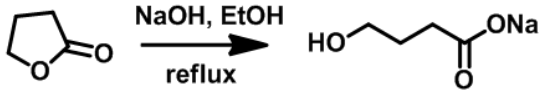

Fig 3.2 Synthetic scheme of GHB (sodium salt)

Enzymatic reduction of GHB

Enzymatic reduction of GHB sodium salt was monitored at 37℃ in 1mL of 1mM NAD+ in 50mM Tris-HCl buffer (pH 8.5) containing 0.24mg/mL GHB-DH. The reaction was triggered by the addition of GHB sodium salt to 20mM .The reaction process was monitored in a cuvette of 1cm light path by the absorbance of NADH centered at 334nm.

GHB-mediated formation of AuNPs

The GHB-mediated formation of AuNPs was carried out in 2 steps. Generally, a solution of Tris-HCl buffer 50mM (pH 8.5) containing NAD^+ (1mM), GHB-DH (0.24mg/mL) and different concentration of GHB was allow to react at 37℃. Then 100uL aliquot of the resulting mixture was added to a growth solution (1.25mL) containing CTAB (37mM), $HAuCl_4$ (0.09mM) and AuNPs (1.4 x 10^{-7}mM, 10nm). The reaction was performed at 30℃. The absorbance spectra of the solution were recorded at different time duration.

3.3 Results and discussion

Enzymatic oxidation of GHB

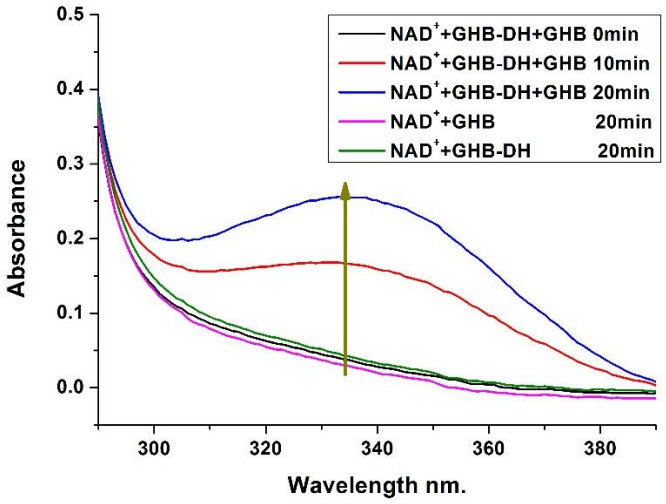

Fig 3.3 Absorbance spectra of enzyme (0.24 mg/mL) catalyzed production of NADH upon reduction of GHB (5 mM in 50 mM Tris-HCl buffer pH 8.5, containing 1mM NAD^+).

To achieve selective GHB detection, we started investigating enzymatic treatment of GHB with GHB dehydrogenase. Typically, to a solution containing 1mM NAD^+ and 0.24mg/mL GHB-DH in 50mM Tris-HCl buffer (pH 8.5), GHB substrate was added to trigger the reaction. In order to achieve optimum activity of GHB-DH, the reaction mixture was kept at 37℃ based on the manufacturer's protocol. The formation of NADH from NAD^+ catalyzed by GHB-DH through the oxidation GHB can be monitored by the absorbance peak of NADH at 334nm. As shown in Fig3.3, in the absence of GHB-DH, minimum change in absorbance spectra can be observed from the reaction mixture of GHB and NAD^+. Similarly, no obvious absorbance peak appeared in the mixture of NAD^+ and GHB-DH, even with prolonged incubation, suggesting the minimal production of NADH. In comparison, obvious increase in the absorbance at 334nm was observed upon enzymatic treatment GHB with NAD^+. The absorbance of NADH increase as incubation prolonged, exhibiting time-dependent spectra change, demonstrating the enzyme promoted generation of NADH. While NADH was efficiently produced upon enzymatic reduction of GHB, no significant amount of NADH was detected through enzyme catalyzed reaction (Fig 3.4), which suggest the generated NADH is largely based on the specific interaction between GHB and GHB-DH. Such specific enzyme-substrate recognition allows us to minimize interference from GHB derivative GBL, which is of special interest in some forensic analysis.

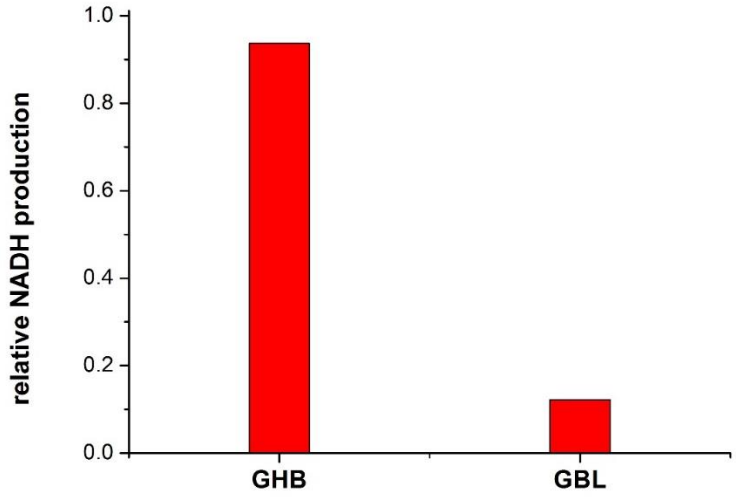

Fig 3.4 Relative amount of NADH produced by enzyme catalyzed reaction of substrate (GHB10 mM, GBL 10 mM).

Optimization of GHB triggered NADH production

To facilitate the future application in GHB sensing, the parameters such as reaction time, substrate concentration were optimized. Kinetic studies were performed to get the optimum reaction time of GHB with NAD^+ under the treatment of GHB dehydrogenase. As shown in Fig 3.5, upon the addition of GHB, the absorbance of NADH increased gradually suggesting the generation of NADH is dependent on GHB concentration. Rapid accumulation of NADH was observed within 80mins (Fig 3.5) upon addition of GHB. As reaction time prolonged, the rate of NADH production gradually decrease and finally reached a plateau. To facilitate sufficient amount of NADH for subsequent detection step as well as to ensure time efficiency, 75mins reaction time was chosen as the optimized reaction period of enzymatic oxidation of GHB. Under this optimized condition, the absorbance of NADH produced in the presence of GHB exhibited a linear increase with respect to the concentration of GHB within 1 to 16mM (**Fig. 3.6**).

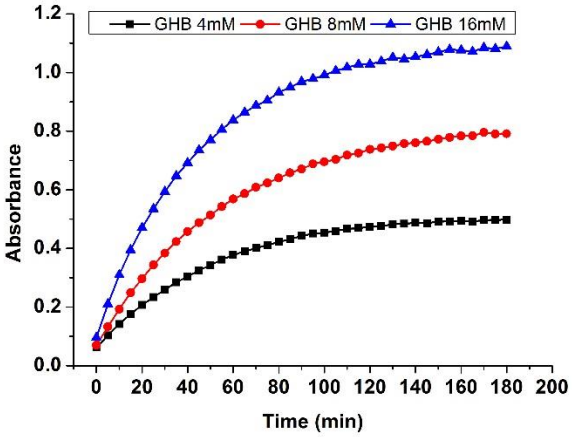

Fig 3.5 Absorbance of NADH produced through enzymatic oxidation of GHB of various concentration (50 mM Tris-HCl buffer pH 8.5, containing 1mM NAD^+).

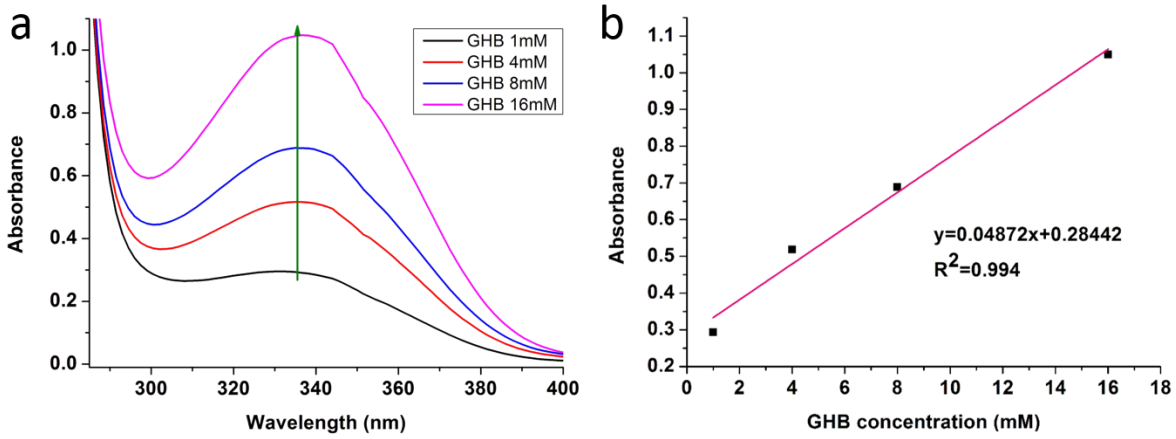

Fig 3.6 a) Absorbance spectra of NADH produced through GHB (1-16 mM) triggered enzymatic reaction under optimized conditions (75min, 50 mM Tris-HCl buffer pH 8.5) b) Linear correlation of NADH absorbance (334nm) *versus* GHB concentration.

GHB-mediated formation of AuNPs

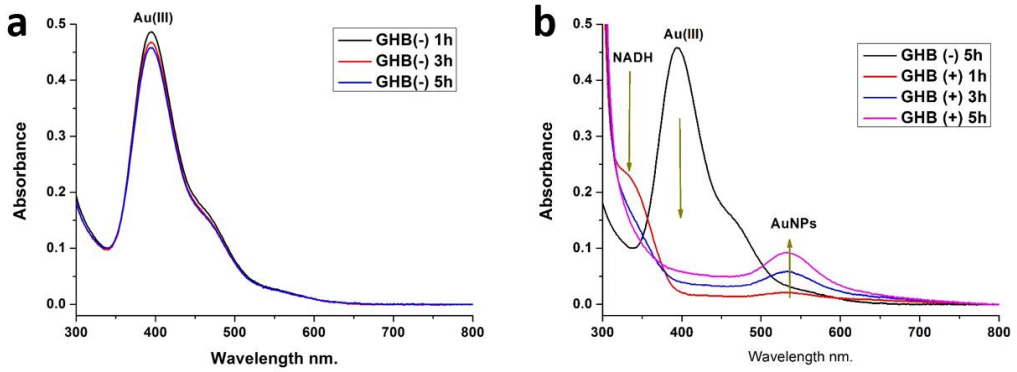

Fig 3.7 Absorbance spectra of growth solution (1.25mL) containing CTAB (37mM), $HAuCl_4$ (0.09mM) and AuNPs (1.4 x 10^{-7}mM) a) without NADH generated from enzyme catalyzed reaction (NAD^+ 1mM, GHB-DH 0.24 mg/mL), b) with NADH generated from enzyme catalyzed reaction (GHB 1.26 mg/mL 12.6 mM , NAD^+ 1mM, GHB-DH 0.24 mg/mL).

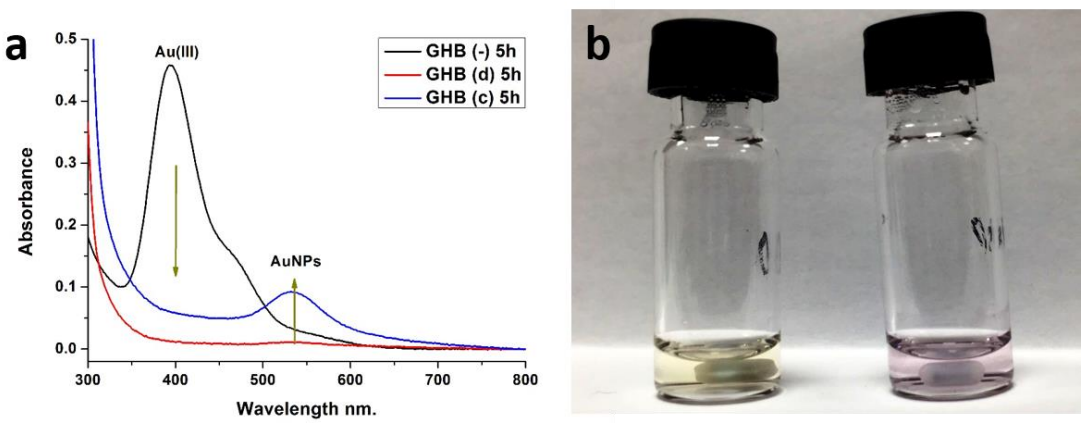

Fig 3.8 a) Absorbance spectra of growth solution (1.25mL) containing CTAB (37mM), $HAuCl_4$ (0.09mM) and AuNPs (1.4 x 10^{-7}mM) with NADH generated from enzyme catalyzed reaction (GHB 1.26 mg/mL 12.6 mM (blue curve)) or GHB 0.76 mg/mL 7.6 mM (red curve), NAD^+ 1mM, GHB-DH 0.24 mg/mL). b) Photograph of $HAuCl_4$ treated without (left) or with (right) NADH (induced by reduction of GHB)

Moreover, to explore the possibility of selective detection of GHB through the formation of AuNPs, we exploited the catalytic growth of AuNPs by NADH directly generated from enzymatic recognition of GHB. Generally, reaction mixture containing NADH was introduced into a solution containing CTAB (37mM), $HAuCl_4$ (0.09mM) and AuNPs (1.4 x 10^{-7}mM,

10nm). The reaction was allow to proceed at 30℃. As shown in Fig 3.7, without NADH, the solution exhibited a distinct absorbance peak at 392nm which is attributed to the presence of $AuCl_4^-$ species. However, upon treatment of NADH containing solution, the absorbance peak at 392nm gradually disappeared and the yellowish color of the reaction mixture was depleted. In addition, the absorbance of NADH at 334nm decreased (Fig 3.7b) simultaneously suggesting the rapid reduction of $HAuCl_4$ (equation 1) which is similar to previously reported studies[15].

$$AuCl_4^- + NADH \longrightarrow Au^I + 4Cl^- + NAD^+ + H^+ \quad (1)$$

$$2\,Au^I + NADH \xrightarrow{\text{Au seeds}} 2\,Au^0 + NAD^+ + H^+ \quad (2)$$

Furthermore, as the concentration of NADH further increase a distinct absorbance peak at ~539nm gradually appeared (Fig 3.8a). Upon prolonged incubation, the intensity of absorbance peak at 539nm gradually increased (Fig 3.7b). In the meantime, the colorless reaction solution gradually developed pinkish color (Fig 3.8 b), suggesting the growth of AuNPs (equation 2), which matches well with reported studies[15]. Moreover, the growth of AuNPs in the presence of GHB induced NADH was further confirmed by DLS analysis. The obvious increase in hydrodynamic diameter revealed the growth of AuNPs in the presence of NADH generated from enzyme catalyzed GHB reduction.

Optimization of AuNPs based GHB sensing

We have proved the concept of selective sensing illicit drug GHB through the growth of AuNPs. To better apply this strategy for the application of drug sensing in spiked drink, reaction of the sensing step (the formation of AuNPs) has been optimized. Kinetic investigations on the growth of AuNPs upon interaction with NADH were carried out. It can be observed that upon the addition of NADH, the absorbance of reaction mixture at 539 nm gradually increased (**Fig 3.9**), suggesting the formation of AuNPs is dependent on the concentration of NADH. Within the first 2 hours, no obvious increase in the absorbance was detected. As reaction time prolonged, the absorbance at 539 nm gradually increase over 24

hours (**Fig 3.9**). However, the slow reaction rate and limited sensitivity (relatively low absorbance) are the major concerns in future application. To address these issue, the growth of AuNPs in the presence of different concentration of Au seeds was evaluated. As shown in **Fig 3.9 b**, higher concentration (7.0 x 10^{-7}mM, 1.4 x 10^{-6}mM) of catalyst (Au seeds) can dramatically increase the absorbance of AuNPs within a shorter period of time (within 1 hour) suggesting the great improvement in the rate of AuNPs formation which is desirable for enhanced sensitivity and detection efficiency. Therefore, the amount of catalyst (Au seeds) was optimized as 1.4 x 10^{-7}mM. Under this condition, the absorbance of AuNPs formed in the presence of GHB exhibited a linear increase with respect to the concentration of GHB within 4 to 16 mM (Fig 3.10).

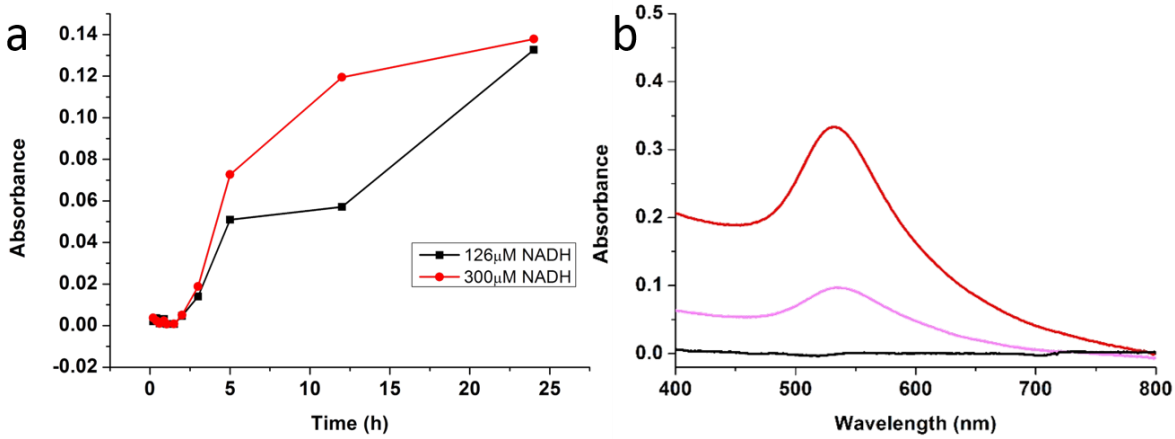

Fig 3.9 a) Absorbance spectra of AuNPs produced through reduction by NADH of various concentration (CTAB 37mM, $HAuCl_4$ 0.09mM and AuNPs 1.4 x 10^{-7}mM), b) Absorbance spectra of AuNPs formed via reduction of NADH (150uM) with different amount of catalyst (CTAB 37mM, $HAuCl_4$ 0.09mM, Au seeds/catalyst black: 1.4 x 10^{-7}mM, pink: 7.0 x 10^{-7}mM, red: 1.4 x 10^{-6}mM).

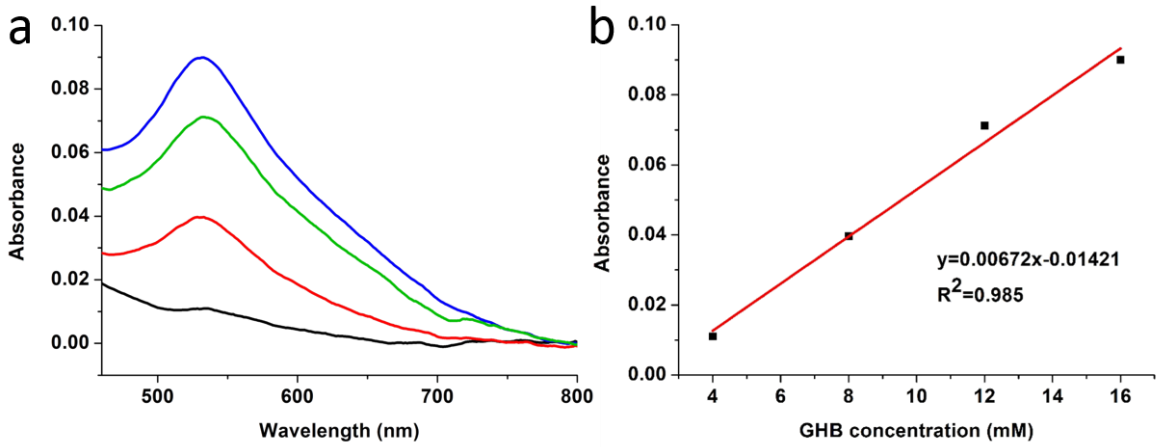

Fig 3.10 a) Absorbance spectra of AuNPs produced upon addition of GHB (4-16 mM) under optimized conditions (CTAB 37mM, $HAuCl_4$ 0.09mM, Au seed 1.4 x 10^{-6}mM and GHB black:4mM, red 8mM, green 12mM, blue 16mM.) b) Linear correlation of AuNPs absorbance (539nm) *versus* GHB concentration.

Moreover, the platform was utilized for the application of sensing and detection of GHB spiked in different types of drinks. Typically, GHB-free and GHB-spiked beverage was incubated with GHB dehydrogenase and NAD+ for 75min. The reaction mixture was subsequently used to reduce $HAuCl_4$ for the growth of AuNPs. As shown in **Fig 3.11**, pink color of AuNPs formed in the presence of GHB can be easily observed in various kind of drink including mineral water, soda and alcoholic drink (e.g. white wine and rice wine) suggesting the feasibility of such platform for the application of GHB sensing in a variety type of beverages.

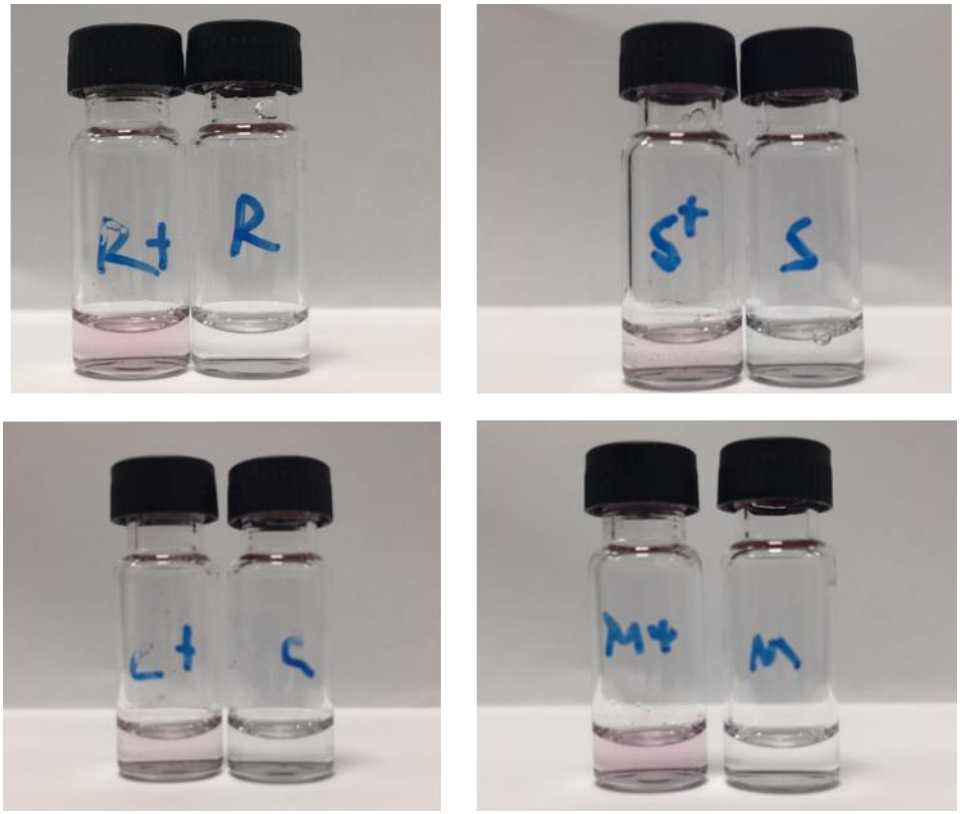

Fig 3.11 Photograph of drinks spiked with (R+, S+, C+, M+) or without (R, S ,C ,M) GHB (10 mM) R: rice wine, S: soda, C: chardonnay, M: mineral water.

3.4 Conclusion

To conclude, we have developed a simple yet effective approach based on highly specific enzymatic reaction for selective sensing of GHB. Typically, GHB molecules can be recognized through specific enzyme-substrate interaction with GHB degydrogenase (GHB-DH) and undergo oxidation reaction generating NADH. Subsequently, the resulting NADH molecule can facilitate the reduction of gold(III) complex and form AuNPs which can be analyzed through either absorbance spectrometer or naked-eye observation. Investigations have demonstrated the ability of such platform to detect GHS drug in a variety type of spiked drink suggesting the potential of our strategy in the application of illicit drug sensing.

3.5 Future work

A simple yet effective approach based on highly specific enzymatic reaction for selective sensing of GHB has been demonstrated. Although, the current system can be used for drug sensing in spiked drinks, future efforts are needed to further improve its sensitivity for drug detection in biosample such as urine or serum.

3.6 Reference

1. R. Neijzen, P. van Ardenne, M. Sikma, A. Egas, T. Ververs and E. van Maarseveen, *Eur. J. Pharm. Sci.*, 2012, **47**, 801-803.
2. K. L. Nicholson and R. L. Balster, *Drug Alcohol Depend.*, 2001, **63**, 1-22.
3. L. Gallimberti, N. Gentile, M. Cibin, F. Fadda, G. Canton, M. Ferri, S. Ferrara and G. Gessa, *The Lancet*, 1989, **334**, 787-789.
4. M. Mamelak, M. B. Scharf and M. Woods, *Sleep*, 1986, **9**, 285-289.
5. J. D. Miotto, Janice Basch, Shanna Murray, Jennifer Zogg, Richard Rawson, Karen, K. Miotto, J. Darakjian, J. Basch, S. Murray, J. Zogg and R. Rawson, *Am. J. Addict.*, 2001, **10**, 232-241.
6. M. Varela, S. Nogué, M. Oros and O. Miro, *Emerg. Med. J.*, 2004, **21**, 255-256.
7. Z. Németh, B. Kun and Z. Demetrovics, *J. Psychopharm.*, 2010, **24**, 1281-1287.
8. A. D. Brailsford, D. A. Cowan and A. T. Kicman, *J. Anal. Toxicol.*, 2012, **36**, 88-95.
9. A. A. Elian, *Forensic Sci. Int.*, 2002, **128**, 120-122.
10. S. Ferrara, L. Tedeschi, G. Frison, F. Castagna, L. Gallimberti, R. Giorgetti, G. Gessa and P. Palatini, *J. Pharm. Biomed. Anal.*, 1993, **11**, 483-487.
11. M. Wood, M. Laloup, N. Samyn, M. R. Morris, E. A. de Bruijn, R. A. Maes, M. S. Young, V. Maes and G. De Boeck, *J. Chromatogr.*, 2004, **1056**, 83-90.
12. C. L. Morris-Kukoski, *Toxicol. Rev.*, 2004, **23**, 33-43.
13. L. A. Ciolino, M. Z. Mesmer, R. D. Satzger, A. C. Machal, H. A. McCauley and A. S. Mohrhaus, *Journal of Forensic Science*, 2001, **46**, 1315-1323.
14. M. MAITRE, *Prog. Neurobiol.*, 1997, **51**, 337-361.

15. Y. Xiao, V. Pavlov, S. Levine, T. Niazov, G. Markovitch and I. Willner, *Angew. Chem.*, 2004, **116**, 4619-4622.

16. M. Baymiller and F. Huang, *Matters*, 2017, **3**, e201705000007.

17. X. Huang, I. H. El-Sayed, X. Yi and M. A. El-Sayed, *J. Photochem. Photobiol. B: Biol.*, 2005, **81**, 76-83.

18. E. Priyadarshini and N. Pradhan, *Sensors Actuators B: Chem.*, 2017, **238**, 888-902.

19. K. Saha, S. S. Agasti, C. Kim, X. Li and V. M. Rotello, *Chem. Rev.*, 2012, **112**, 2739-2779.

20. S. He, D. Li, C. Zhu, S. Song, L. Wang, Y. Long and C. Fan, *Chem. Commun.*, 2008, 4885-4887.

21. R. Cao, B. Li, Y. Zhang and Z. Zhang, *Chem. Commun.*, 2011, **47**, 12301-12303.

22. D. Vilela, M. C. González and A. Escarpa, *Anal. Chim. Acta*, 2012, **751**, 24-43.

Chapter 4: Nanoformulation of lanthanide complex, smart probe for persistent imaging in tumor cells

4.1 Introduction

It is known that the redox conditions within intracellular environment play crucial role in a variety of cellular processes, such as cell proliferation, differentiation, enzyme catalysis etc[1, 2]. Misregulation of cellular redox status is considered to be associated with various pathological processes. Studies revealed that there exists distinct reductive gradient between intracellular and extracellular compartment. In addition, studies also confirmed upregulated reducing agent in tumor cells. Glutathione tri-peptide (GSH), the most abundant reducing small molecule, is considered the major reason to produce the highly reductive intracellular environment.[3, 4]. Within normal cells, the GSH concentration (~ 2–10 mM) is considered higher than that of extracellular conditions[5]. In tumor cells, the GSH concentration is much higher (4 times) than in normal cells, creating a more reductive environment[6, 7]. Considering these facts, an effective strategy to monitor the intracellular reducing environment would be highly desirable.

By far, various luminescent probes have been reported for sensing and visualization in the intracellular reducing environment[8]. Generally these probes can be categorized into two major types based on their size: molecular probes and nanoscaled probes. Molecular probes exhibit promising advantages for their flexibilities in both chemical structures and functions. Basically, versatile desired properties such as tunable emissions, less photobleaching, long lifetime, deep penetration, good biocompatibility can be precisely fine-tuned through simple modifications of their structures[9-11]. In addition, small molecule complexes would allow easy and accurate characterization of their composition from single molecular level. Compared with moleclar probes, once internalized into cells, nanoprobes exhibited longer retention time[12], allowing

long term imaging. Considering the advantages of both types of probes, the development of new luminescent alternatives which allow fine tune of the optical properties through molecular design as well as prolonged retention in the intracellular compartment would be beneficial for sensing and visualization of intracellular reducing environment.

Recently, Rao and coworkers have reported a biocompatible condensation strategy through the reaction of cysteine and 2-cyanobenzothiazole (CBT)[13]. The covalent linkage between CBT and cysteine allows self-assemble nanostructures within live cells[14-16]. Inspired by these findings, we proposed a strategy by rational design of luminescent probe which can undergo reduction induced condensation and subsequently self-assembled into nanoscales probes within reducing intracellular environment. However, most of the molecular luminescent probes may encounter aggregation induced quenching once they were assembled into spatially confined nanoparticles[17]. Luminescent metal complexes can serve as molecular probes owing to their promising photophysical properties such as tunable emissions, good photostability, and long lifetime[18]. In addition, the large stokes shift of these type of probes can not only reduce the interference from excitation minimizing interference arise from excitation. More importantly, such large stokes shift can greatly help to avoid self-quenching at high concentration[19]. Based on such appealing optical properties of luminescent metal complex. We introduced a smart lanthanide metal complex **Tb-CBT.** Under reducing environment, the blocked cysteine moiety will be deprotected and undergo condensation with CBT group, promoting the self-assemble of condensed molecules into luminescent probe for long term sensing and visualization of intracellular reducing environment.

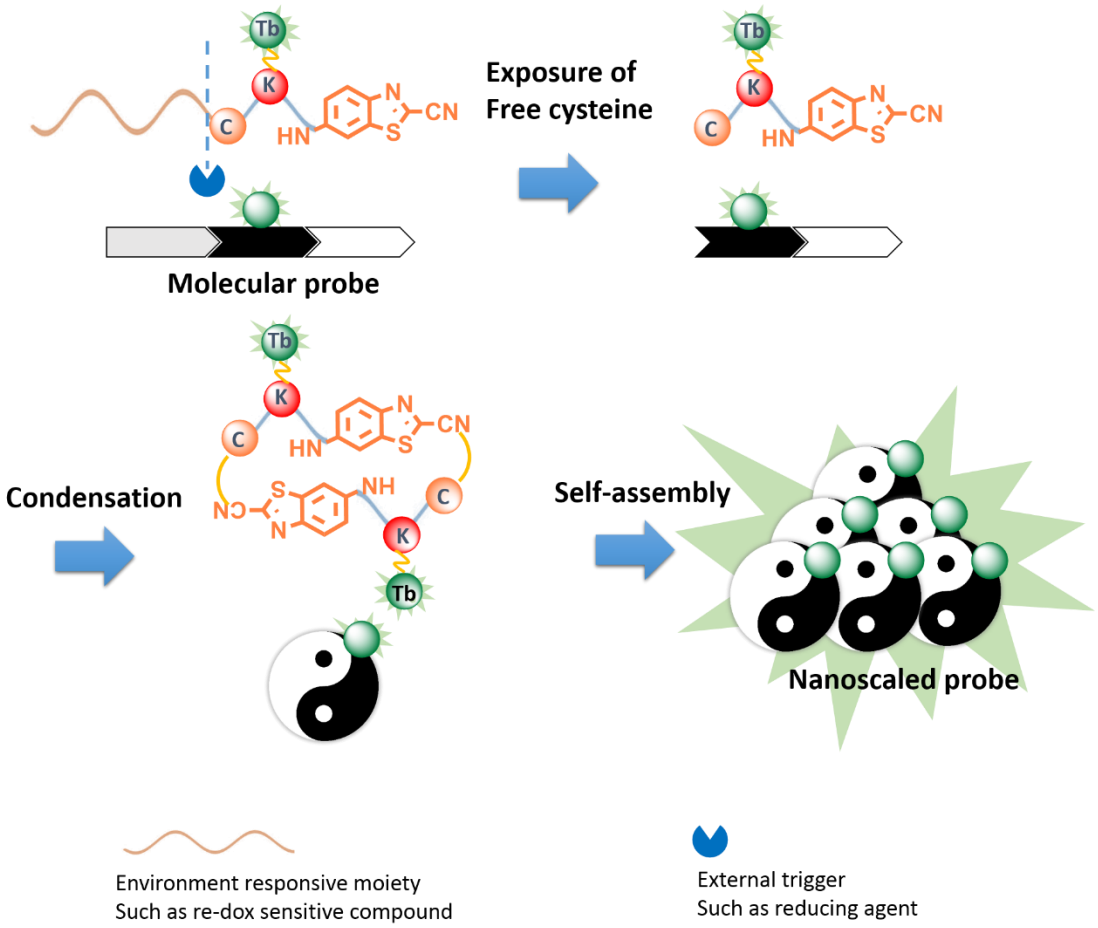

Fig 4.1 Scheme illustration of reduction induced condensation of luminescent lanthanide complex to self-assemble into nanoscaled probe for imaging in reducing intracellular environment.

4.2 Materials and methods

Materials

6-Amino-2-cyanobenzothiazole, Fmoc-Lys(Boc)-OH, isobutyl chloroformate, 4-methylmorpholine, triisopropylsilane, trifluoroacetic acid, EDC, HOBt, DIPEA, tri-tert-butyl 1,4,7,10-tetraazacyclododecane-1,4,7,10-tetraacetate, Piperidine, Fmoc-Cys(St-Bu)-OH, $TbCl_3$ were acquired from Sigma-Aldrich. All these reagents involved were directly used without further purification.

Instrument

NMR spectra were acquired on Bruker Avance 500 spectrometers. Mass spectra were obtained on a ThermoFinnigan LCQ Fleet MS. UV-Vis spectra were obtained on Cary 60 UV-Vis Spectrophotometer. Fluorescence spectra were recorded on a Varian Cary eclipse spectrometer. A FEI EM208S transmission electron microscope (Philips) was used to capture TEM images.

Synthesis of Fmoc-Lys(Boc)-CBT

To Fmoc-Lys(Boc)-OH (0.5 mmol, 1.5 eq, 351.4 mg) was added THF (1 mL) and was stirred over ice bath. 4-methylmorpholine (1 mmol, 2.0 eq, 109.9 µL) was added into the reaction mixture followed by isobutyl chloroformate (0.75 mmol, 1.5 eq, 94.85 µL), and was reacted under N_2 gas for 20 minutes. 6-Amino-2-cyanobenzothiazole (0.5 mmol, 1.0 eq, 87.6 mg) was dissolved with THF (4mL), and was transferred into the reaction mixture and allowed for reaction for 4 hours. The, the reaction mixture was extracted with ethyl acetate and water (2 x 30 mL). The organic layer was washed with brine (1 x 20 mL) and then dried over anhydrous magnesium sulphate. Excess solvent was removed *in vacuo* to yield a solid powder as the crude product (0.4750 g). The crude was purified through column chromatography (Hexane : Ethyl acetate 1:1) to yield Fmoc-Lys(Boc)-CBT as powder (0.2255 g, 72.07%). ^{1}HNMR (500MHz) δ 9.58 (s, 1H), 8.53 (s, 1H), 7.92 (d, 1H), 7.53 (d, 2H), 7.37 (t, 2H), 7.28 (t, 3H), 7.23 (d, 2H), 6.29 (d, 1H), 4.86 (s, 1H), 4.41 (m, 3H), 4.17 (t, 1H), 3.12 (s, 2H) 1.97 (d, 2H), 1.51 (m, 13H) M/Z = 648.18.

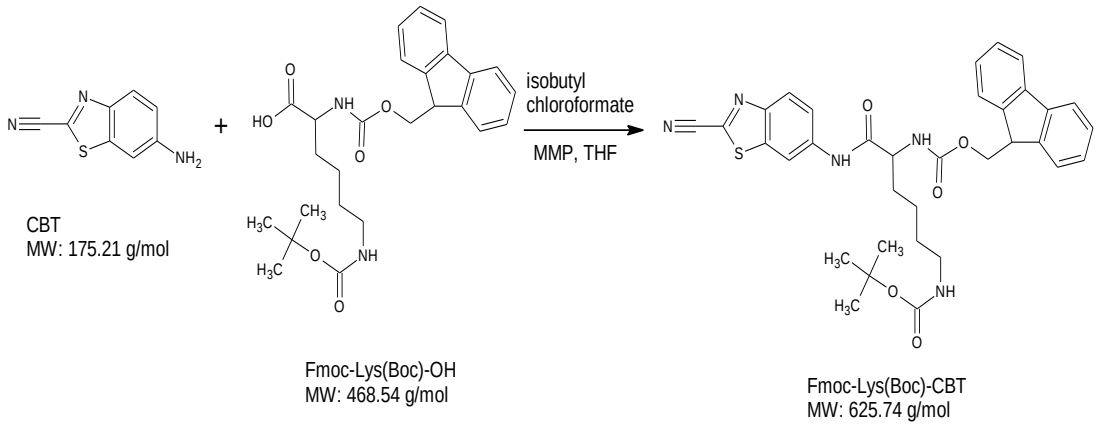

Fig 4.2 Synthetic scheme of Fmoc-Lys(Boc)-CBT

Synthesis of Fmoc-Lys-CBT

To Fmoc-Lys(Boc)-CBT (0.2255 g) was dissolved in trifluoroacetic acid (TFA) solution (95% TFA, 2.5% DCM, 2.5% triisopropylsilane) in a total of 3 mL and was stirred for 30 minutes. TLC (DCM: MeOH 9:1) was performed to check for the progress of reaction. The product was dried *in vacuo* to yield a solid powder product. Fmoc-Lys-CBT was used without further purification.

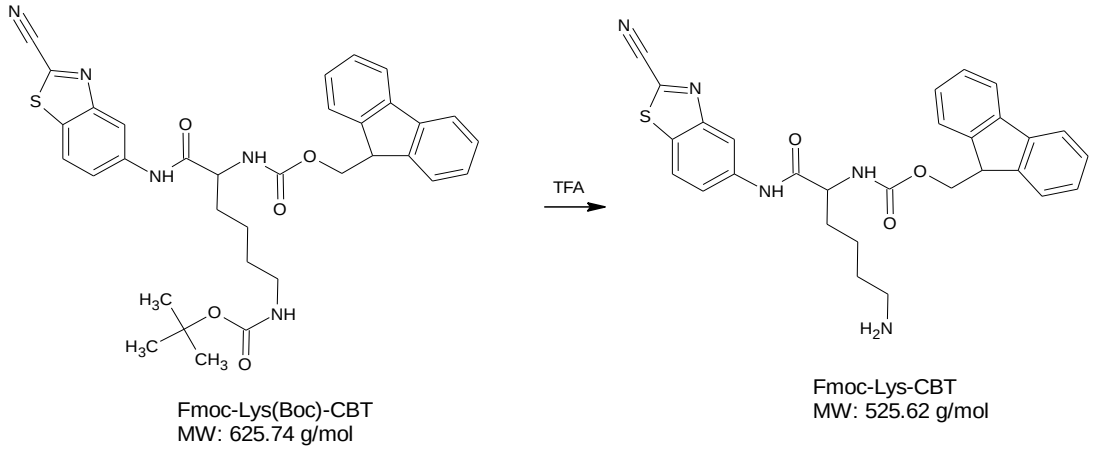

Fig 4.3 Synthetic scheme of Fmoc-Lys-CBT

Synthesis of Fmoc-Lys(DOTA-Boc)-CBT

To Fmoc-Lys-CBT (0.215 mmol, 1.0 eq, 112.75 mg) was added1-Ethyl-3-(3-dimethylaminopropyl)carbodiimide(EDC) (0.430 mmol, 2.0 eq, 66.75 mg), 1-Hydroxybenzotriazole (HOBt) (0.430 mmol, 2.0 eq, 65.85 mg), N,N-diisopropylethylamine

(DIPEA) (1.075 mmol, 5.0 eq, 188 µL) and DOTA-Boc(0.387 mmol, 1.8 eq, 221.65 mg). The reactants were dissolved in N,N-dimethylformamide (2.2 mL) to get the optimum molar concentration which is 100 mM. The reactants were stirred for 4 hours. TLC (DCM :MeOH 4:1) was performed to check for the progress of reaction. The product formed was extracted by the addition of ethyl acetate and water (2 x 30 mL). The organic layer was washed with brine (1 x 20 mL) and dried over anhydrous magnesium sulphate. The extract was filtered and was dried *in vacuo.* The crude product was then purified through column chromatography (DCM : MeOH 9:1) to yield Fmoc-Lys(DOTA-Boc)-CBT as oily liquid (0.0688 g, 35.34%). ^{1}HNMR (500MHz) δ 8.68 (s, 1H), 8.32(d, 1H), 8.07 (d, 1H), 7.68 (m, 6H), 7.32 (m, 3H), 6.85 (s, 1H), 4.66 (s, 1H), 4.32 (m, 4H), 2.5-3.5 (b, 26H), 1.67 (s, 6H), M/Z=1080.53.

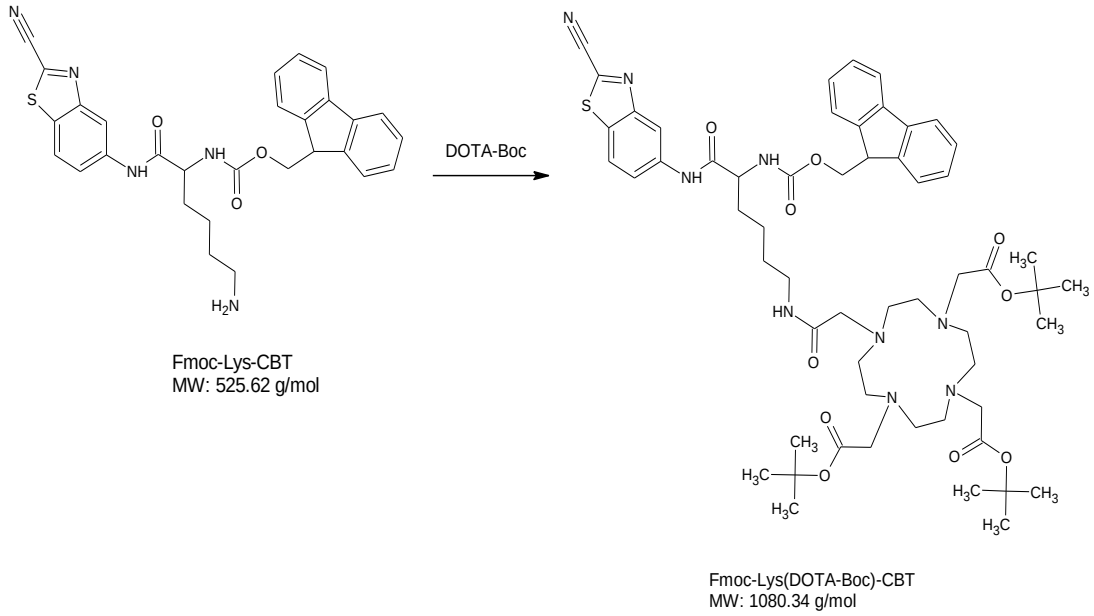

Fig 4.4 Synthetic scheme of Fmoc-Lys(DOTA-Boc)-CBT

Synthesis of H-Lys(DOTA-Boc)-CBT

Fmoc-Lys(DOTA-Boc)-CBT was transferred into a glass vial. To Fmoc-Lys(DOTA-Boc)-CBT (0.064 mmol, 1.0 eq, 68.8 mg) was added piperidine (0.128 mmol, 2.0 eq, 12.67µL) with 5% piperidine/DMF (253.4µL) and the reaction mixture was left to react for 20 minutes.Liquid-liquid extraction was done to by adding ethyl acetate (2 x 30 mL) and water (2

x 30 mL). The organic layer was extracted and treated with brine (1 x 20 mL). Then, anhydrous magnesium sulphate was added to remove excess water. The extract was dried *in vacuo* to yield a crude product as solid powder. Column chromatography (DCM: MeOH 9:1) was then performed to purify the crude product. The product H-Lys-(DOTA-Boc)-CB T appeared as solid powder which yields a total of 0.0181 g, 32.97%. M/Z=858.40

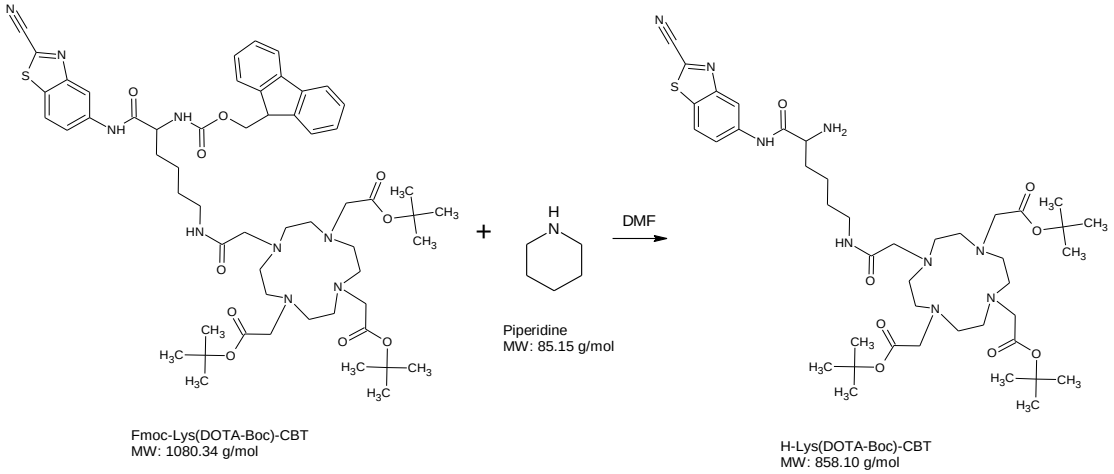

Fig 4.5 Synthetic scheme of H-Lys(DOTA-Boc)-CBT

Synthesis of Fmoc-Cys(St-Bu)-Lys(DOTA-Boc)-CBT

To H-Lys(DOTA-Boc)-CBT (0.0211 mol, 1.0 eq, 18.10 mg) was added Fmoc-Cys(St-Bu)-OH (0.0317 mol, 1.5 eq, 13.67 mg), EDC (0.0422 mol, 2.0 eq, 6.55 mg), and HOBt (0.0422 mol, 2.0 eq, 6.46 mg) in a MS tube. The reactants were dissolved in DMF (0.211 mL) and DIPEA (0.0317 mol, 1.5 eq, 5.51 µL) and was left to react for 4 hours. When the reaction was done, liquid-liquid extraction was performed by extracting the product with ethyl acetate (2 x 30 mL) and water (2 x 30 mL), then the organic layer was treated with brine (2 x 10 mL). Anhydrous $MgSO_4$ was added into the organic layer. The extract was filtered into a round bottom flask, and was dried *in vacuo*. The crude extract was purified through column chromatography (DCM :MeOH 4:1) to yield Fmoc-Cys(St-Bu)-Lys(DOTA-Boc)-CBT as a solid powder (17.3 mg, 64.48%). ^{1}HNMR (500MHz) δ 8.76 (s, 1H), 8.38 (s, 1H), 7.73 (s, 1H),

7.65 (m, 4H), 7.42(m, 5H), 6.97(s, 1H), 6.25(d, 1H), 4.71(d, 1H), 4.64 (s, 1H), 4.37(d, 2H), 4.21(d, 2H), 2.5-3.5(b, 28H), 1.68 (b, 6H), 1.47(s, 27H), 1.3(t, 9H). M/Z=1271.37

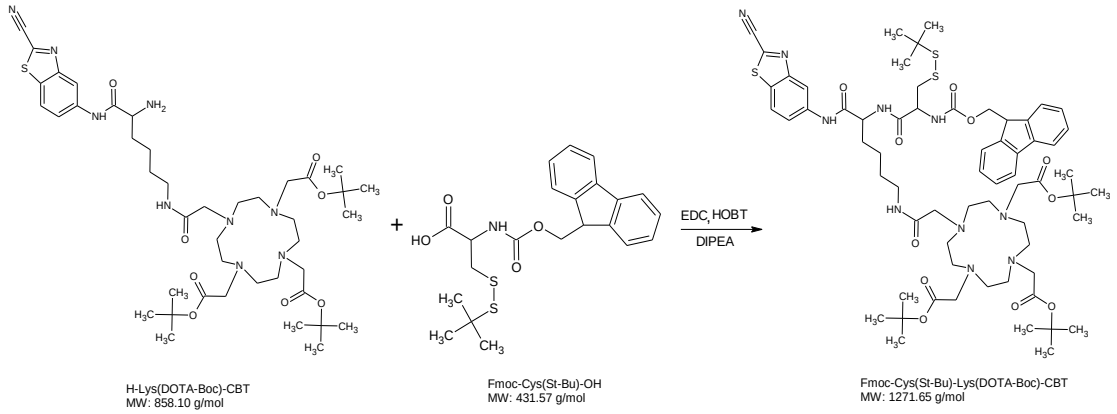

Fig 4.6 Synthetic scheme of Fmoc-Cys(St-Bu)-Lys(DOTA-Boc)-CBT

Synthesis of H-Cys(St-Bu)-Lys(DOTA-COOH)-CBT

To the solid powder, Fmoc-Cys(St-Bu)-Lys(DOTA-Boc)-CBT (0.0136 mmol, 1.0 eq, 17.3 mg) was added 5% piperidine/DMF (53.88 uL) and the reaction mixture was stirred for 20 minutes. TLC (DCM :MeOH 4:1) was performed.The product H-Cys(St-Bu)-Lys(DOTA-Boc)-CBT was then extracted with ethyl acetate (2 x 30 mL) and water (2 x 30 mL), followed by drying of water with brine (1 x 10 mL) and addition of anhydrous sodium sulphate into the extract. The extract was then filtered by gravity filtration and dried *in vacuo*.

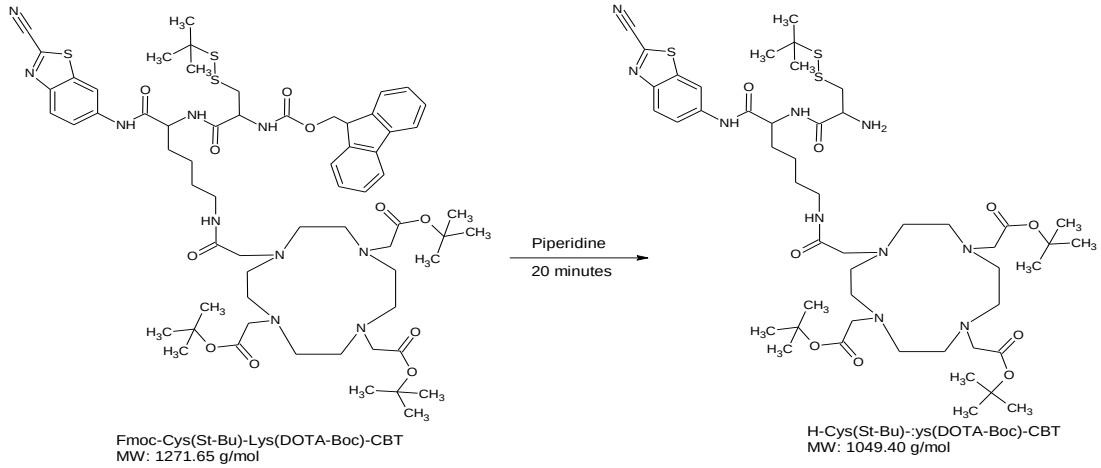

Fig 4.7 Synthetic scheme of Hc-Cys(St-Bu)-Lys(DOTA-Boc)-CBT

To the product H-Cys(St-Bu)-Lys(DOTA-Boc)-CBT was added 5 mL of 95% TFA, 2.5% DCM, 2.5% triisopropylsilane(TIPS) and was reacted for 2 hours. Reverse High Performance Liquid Chromatography (HPLC) was done to yield product **6**, H-Cys(St-Bu)-Lys(DOTA-CH_3-COOH)-CBT as pure solid powder (5.3 mg, 44.23%). M/Z=881.34

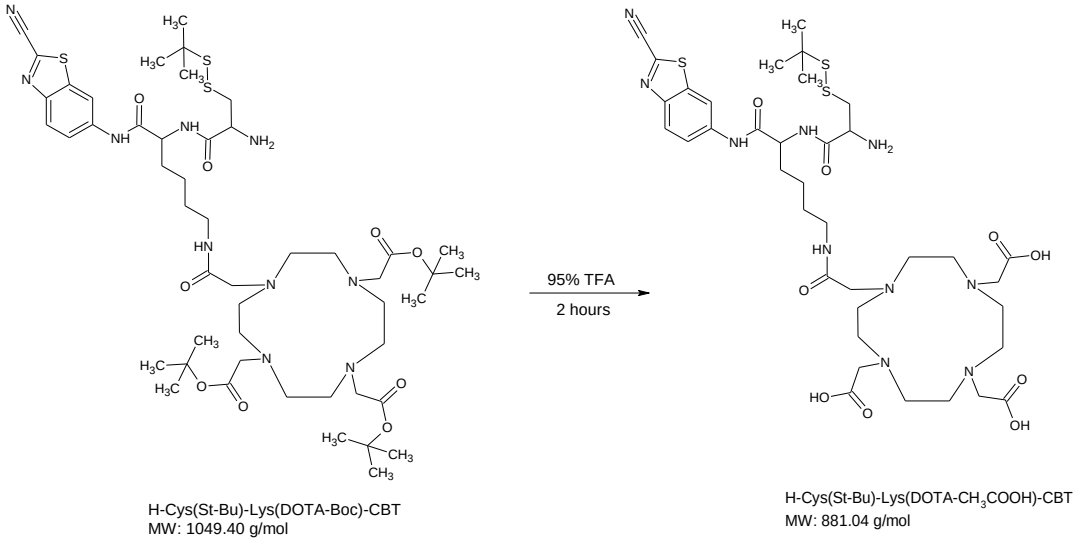

Fig 4.8 Synthetic scheme of Hc-Cys(St-Bu)-Lys(DOTA-COOH)-CBT

Synthesis of Tb-CBT

To H-Cys(St-Bu)-Lys(DOTA-CH_3-COOH)-CBT was added 0.5 mL of water to be fully dissolved. $TbCl_3$ was added into a glass vial. 400 µL of the dissolved H-Cys(St-Bu)-Lys(DOTA-CH_3-COOH)-CBT and 100 µL of water was mixed with $TbCl_3$ in the vial. To adjust the pH of solution to pH 6.0, 2 drops of 1 M Na_2CO_3 was added into the reaction mixture. The reaction mixture was left to stir and react for 24 hours. Reversed phase HPLC was done to yield a pure solid powder, Tb-CBT (0.6 mg, 28.3%). M/Z=1037.20.

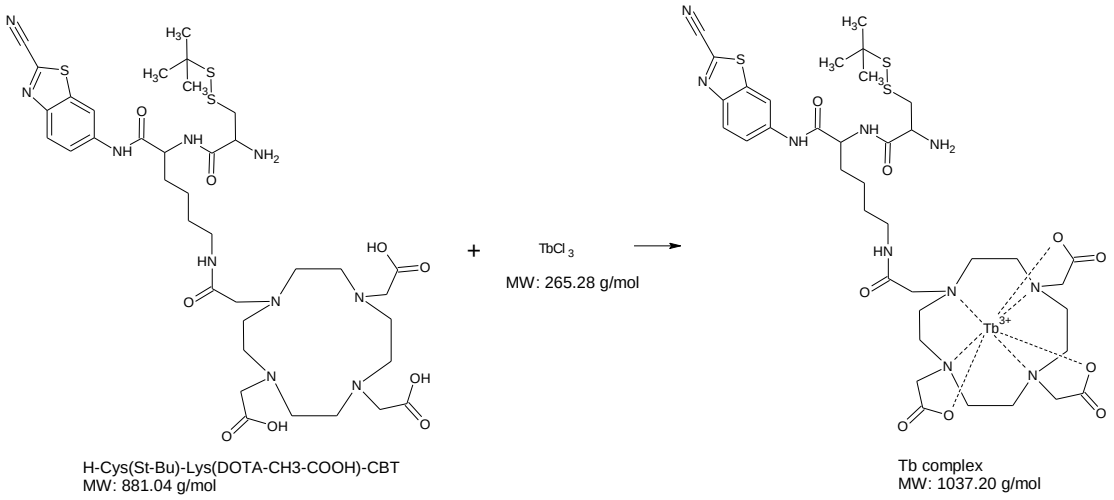

Fig 4.9 Synthetic scheme of Tb-CBT

Responsive condensation of Tb-CBT induced by reducing conditions

To Tb-CBT (0.6 mg) was added 0.2 M PBS buffer (pH=7.4) (116 μL) to yield an aqueous solution of 5 mM Tb metal complex. UV-VIS spectra of the 50 μM Tb metal complex solution was analyzed. Then, glutathione (GSH) was added to the prepared solution (final concentration 5mM). Luminescence spectra was analyzed and was recorded at different duration. The resulting mixture was kept in 37 ^{o}C water bath under vigorous magnetic stir. Fluorescence spectra were collected on an Agilent Cary Eclipse Fluorescence Spectrophotometer. MS analysis was also carried out to identify the condensation. M/Z=1949.4, 2035.9.

4.3 Results and discussions

Preparation of Tb-CBT

Tb-CBT probe was prepared following reported methods[20]. Typically, CBT was conjugated with Fmoc-Lys(Boc)-OH to afford Fmoc-Lys(Boc)-CBT. To allow for the functionalization with Tb chelating moiety, the protecting group was removed and gave rise to Fmoc-Lys-CBT. Subsequently, a precursor of chelating group DOTA was coupled with Fmoc-

Lys-CBT and yield to Fmoc-Lys(DOTA-Boc)-CBT. Deprotection of the resulting molecules enabled the linkage with a cysteine derivative and yield Fmoc-Cys(St-Bu)-Lys(DOTA-Boc)-CBT. After the removal of both fmoc and boc protecting groups, the ligand molecule H-Cys(St-Bu)-Lys(DOTA-COOH)-CBT was obtained. To afford the luminescent metal complex, Tb^{3+} ion was introduced to coordinate with the ligand and finally form the Tb-CBT probe.

In vitro studies of condensation of Tb-CBT in reducing environment

To investigate the potential condensation of Tb-CBT in response to reducing environment, glutathione was added to Tb-CBT containing solution. Typically, Tb-CBT was treated with GSH at 37 ^{o}C to induce the condensation. In the meantime, the luminescent property was monitored by measuring the fluorescence spectra. As shown in Fig 4.10a Tb-CBT exhibited intense emission at 426 nm. Upon treatment with GSH, no significant decrease was observed in the overall fluorescence intensity. In contrast, the luminescence intensity increased rapidly within the first 60 mins. As reaction proceed, the fluorescence intensity slowly increased and reached plateau after 3 hours. These results suggested that there was no aggregation-induced quenching among TB-CBT probe upon condensation in response to reducing environment.

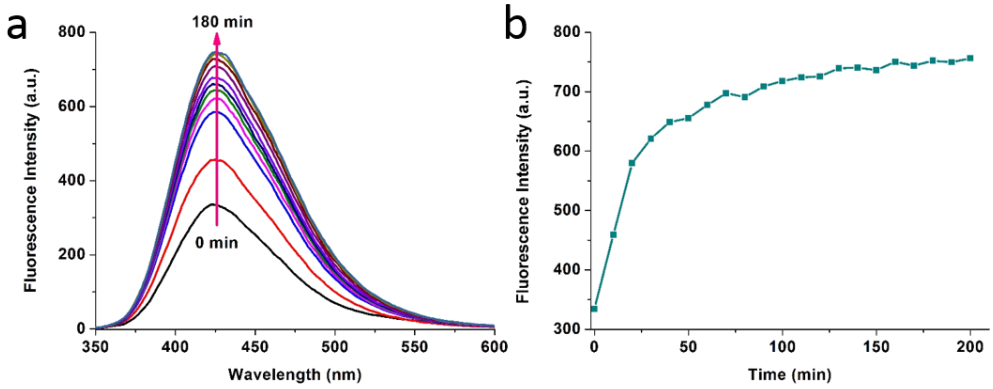

Fig 4.10 a) Fluorescence spectra of Tb-CBT (50 μM) treated with 5 mM of GSH at 37 ^{o}C in 0.2 M phosphate buffer (pH 7.4) λ_{ex} = 320 nm. b) Absorbance (426 nm) of Tb-CBT (50μM) treated with 5 mM GSH at 37 ^{o}C in 0.2 M phosphate buffer (pH 7.4) λ_{ex} = 320 nm.

In addition, the condensation of Tb-CBT probe was confirmed by TEM and MS analysis. TEM image clearly showed that nanoscaled particles were formed upon treatment of Tb-CBT in reducing environment (5 mM GSH) (Fig 4.11 b, c). The formed particles exhibited a spherical shape with diameter ranging from 100-300 nm. In comparison, no nano-sized structure was observed without the treatment of reducing agent (Fig 4.11 a). In addition, MS analysis revealed that during the process of condensation, Tb-CBT dimer was formed. These results indicated that, after treatment GSH, free thiol group of Cysteine would be exposed and allowed intermolecular condensation proceed to form oligomers (Fig 4.12). The formed oligomers would subsequently self-assemble into nanoscaled particles (Tb-NPs). Moreover, both free Tb-CBT complex and self-assembled particles exhibited great photostability. After 20-cycle measurement, no obvious decrease in the luminescence intensity of both Tb-CBT and Tb-NPs was observed, indicating that both molecular Tb-CBT and nano-sized Tb-NPs are quite stable upon excitation. The above *in vitro* evaluation demonstrated the successful condensation of molecular Tb-CBT and subsequent formation of nanoscaled luminescent probe under reductive condition.

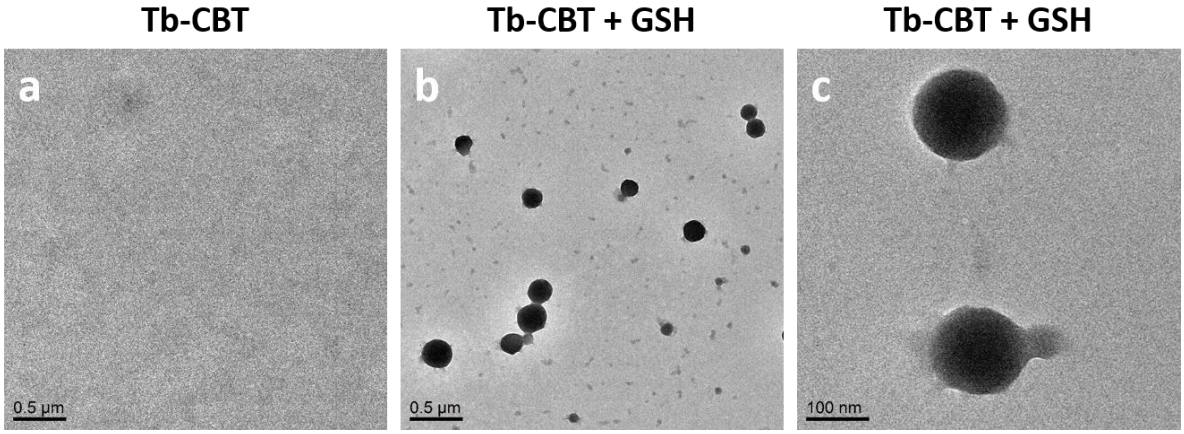

Fig 4.11 Representative transmission electron microscopy (TEM) image of the condensation of Tb-CBT in 0.2 M phosphate buffer (pH 7.4) a) without or b) and c) with treatment of 5 mM GSH.

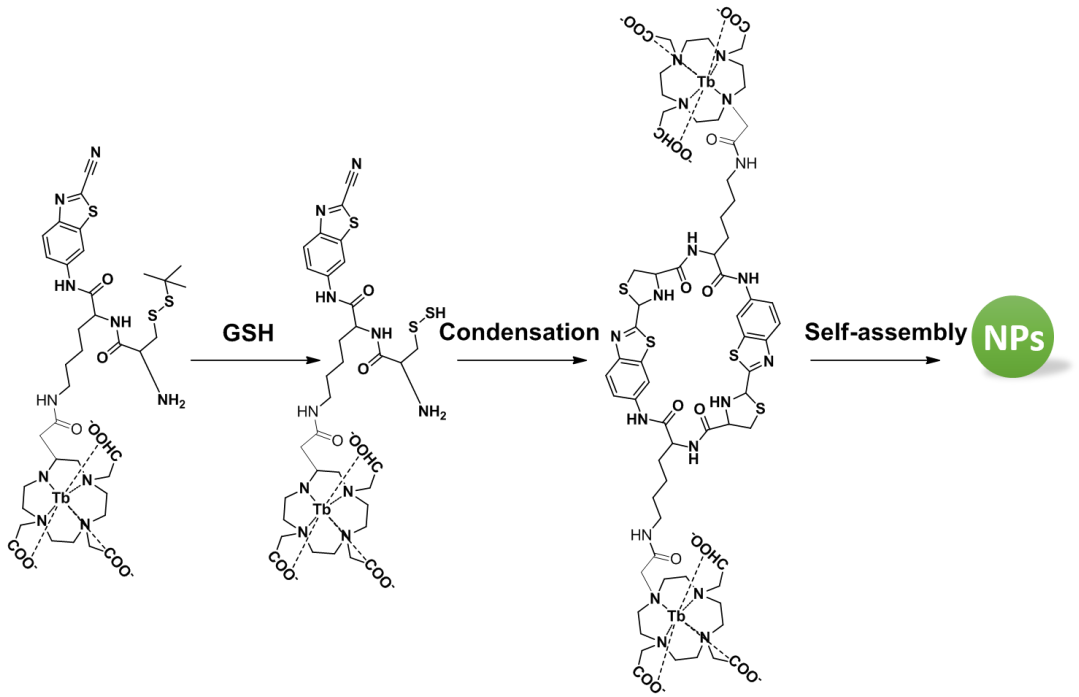

Fig 4.12 Scheme illustration of reduction-controlled condensation of Tb-CBT to self-assemble into Tb-NPs.

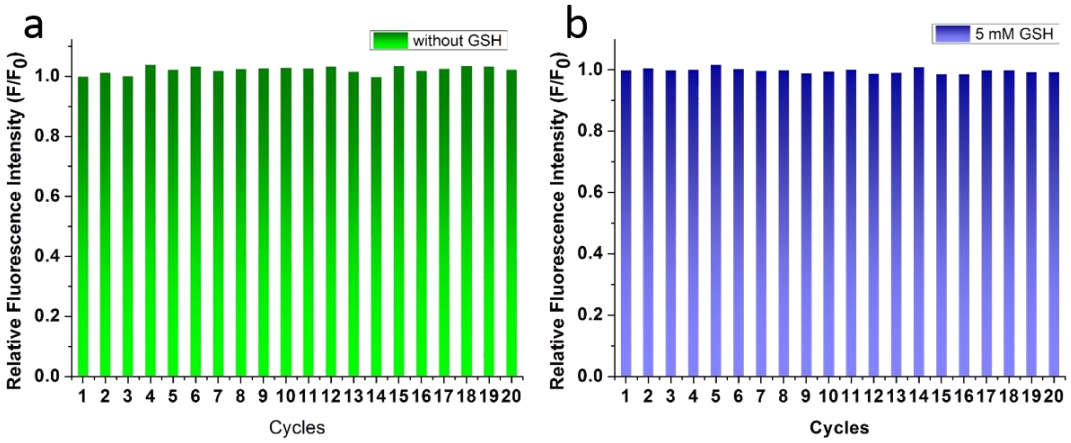

Fig 4.13 Luminescence intensity for 20 cycles of 50μM Tb-CBT a) before or b) after the treatment of GSH (5 mM) (in 0.2 M phosphate buffer (pH 7.4)).

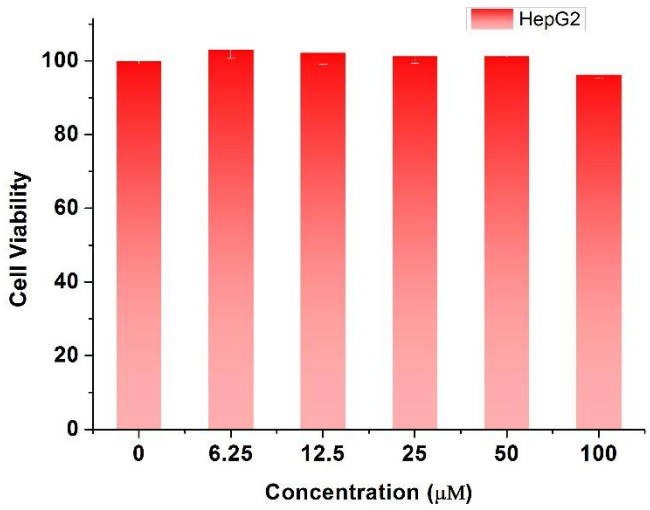

Fig 4.14 Cell viability of HepG2 cell incubated with Tb-CBT of various concentration for 24 hours.

After in vitro evaluation, we planned Tb-CBT for imaging in live cells. Before that, cytotoxicity of Tb-CBT was evaluated on thiol-overexpressing HepG2 cells. The viability of cells showed no obvious decrease at the concentration up to 100 μM Tb-CBT, suggesting the good biocompatibility for imaging. Then HepG2 cells were incubated with 20μM Tb-CBT for different time duration and washed 3 times with PBS. As shown in Fig 4.15, no obvious fluorescence signal was observed in HepG2 cells. Even at higher concentration, few signal can be captured, indicating the limited uptake of Tb-CBT into cells. In addition, flow cytometry analysis also confirm the lack of Tb-CBT fluorescence in HepG2 cells, suggesting the insufficient uptake of the current probe molecule Tb-CBT. Looking into the structure of current probe molecule, the use of macrocyclic chelator of multiple carboxylate moiety and amino acid contribute to the hydrophilicity of the probe. Besides, the overall charge of the current probe is zero. Considering the nature of plasma membrane, the lack of hydrophobicity and positive charge are the major concerns which limit the cellular uptake of Tb-CBT. To overcome this issue, functional group with hydrophobicity and positive charge should be introduced to facilitate the uptake through diffusion. For instance, the light emitting [Ru(II)(1,10-

phenanthroline)$_2$]$^{2+}$ complex can be introduced to replace the current Tb-containing moiety (Tb-DOTA). It can not only be used as luminescent moiety with excellent photophysical properties. Moreover, Ru(II) complex can serve as a hydrophobic cation to increase both lipophilicity, positive charges of the molecules, promoting the uptake of probe molecule. Alternatively, targeting group such as cell penetrating peptide can also be utilized to enhance the localization of the probe inside cells.

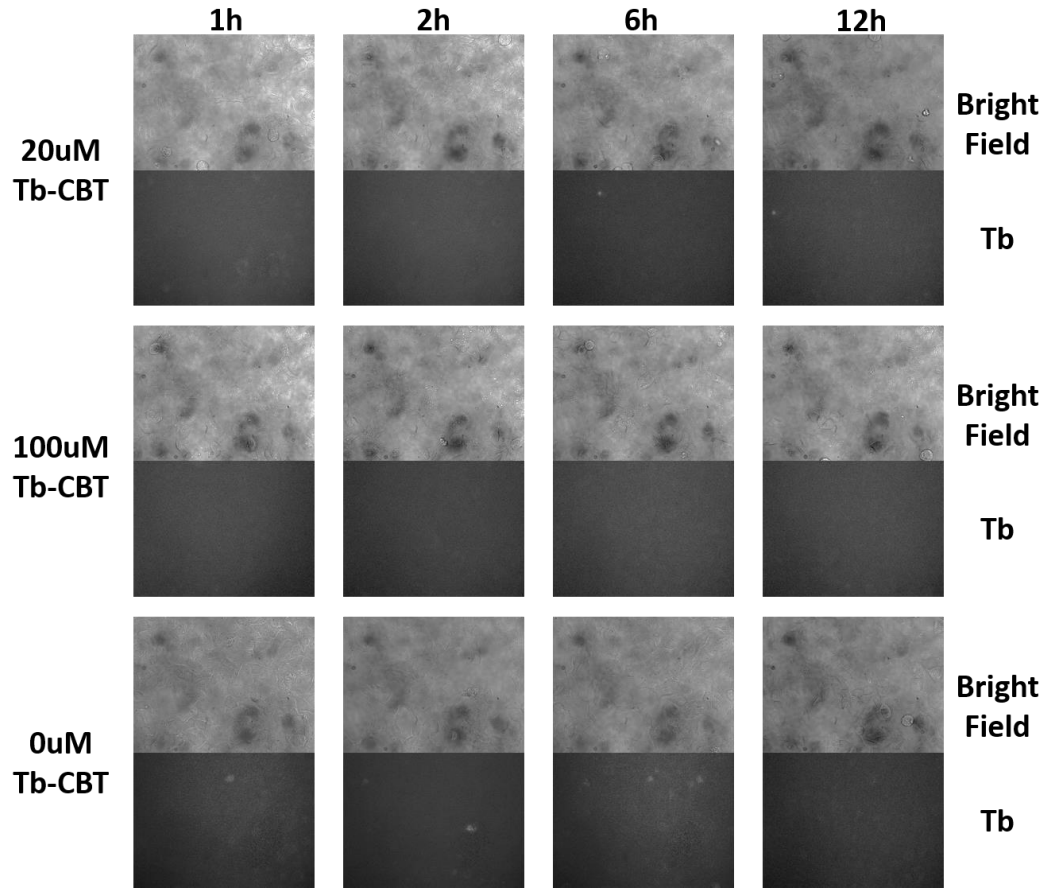

Fig 4.15 Fluorescence image of HepG2 cells incubated with different concentration of Tb-CBT

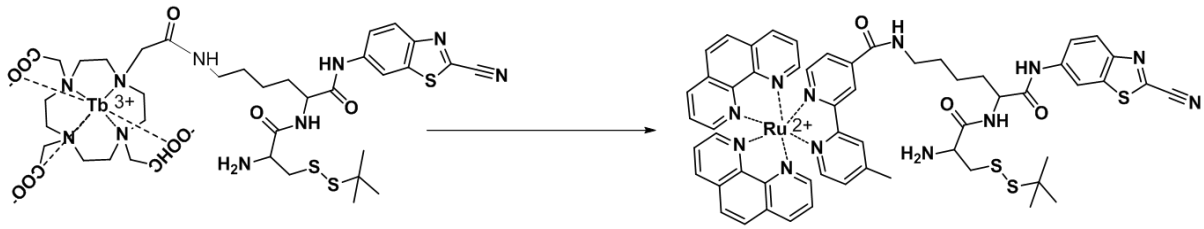

Fig 4.16 Proposed structure to improve cell uptake by replacing the hydrophilic and neutral Tb-containing moiety with hydrophobic cationic Ru complex.

4.4 Conclusion

In summary, we introduced a strategy by rational design of luminescent probe which can undergo reduction induced condensation and subsequently self-assembled into nanoscales probes within reducing intracellular environment for persistent imaging of tumor cells. To avoid potential self-quenching upon self-assembly into nanoprobes, lanthanide complexes were used as luminescent core mainly because of their large stokes shift. Under reducing environment, the blocked cysteine moiety will be deprotected and undergo condensation with CBT group, promoting the self-assembly of condensed molecules into nanoscaled probes which can serve as a persistent luminescent probe for imaging of tumor cells. In vitro experiment confirm the ability of Tb-CBT to self-assemble into nanosized structure. In addition, both molecular and nano-sized probes exhibited great photostsbility. However, the lack of hydrophobicity and positive charge may largely limit the uptake of current molecules for tumor cell imaging. Further efforts to improve the cell uptake of molecular probe with alternative design are needed for the development of smart probes for persistent imaging of tumor cells.

4.5 Future work

The current molecule Tb-CBT has limited cell uptake. In order to address this issue, alternative molecule with improved hydrophobicity and positive charge should be carefully designed. In addition, investigations to examine its ability to self-assemble and cytotoxicity are still necessary. Moreover, the cellular uptake and possible persistent imaging in tumor cells need to be explored.

4.6 Reference

1. C. C. Winterbourn, *Nat. Chem. Biol.*, 2008, **4**, 278.

2. T. Lu, Y. Pan, S.-Y. Kao, C. Li, I. Kohane, J. Chan and B. A. Yankner, *Nature*, 2004, **429**, 883.

3. F. Meng, W. E. Hennink and Z. Zhong, *Biomaterials*, 2009, **30**, 2180-2198.

4. M. A. Gauthier, *Journal*, 2014.

5. F. Q. Schafer and G. R. Buettner, *Free Radic. Biol. Med.*, 2001, **30**, 1191-1212.

6. G. K. Balendiran, R. Dabur and D. Fraser, *Cell Biochem. Funct.*, 2004, **22**, 343-352.

7. G. Saito, J. A. Swanson and K.-D. Lee, *Adv. Drug Del. Rev.*, 2003, **55**, 199-215.

8. Z. Lou, P. Li and K. Han, *Acc. Chem. Res.*, 2015, **48**, 1358-1368.

9. Y. Chen, Y. Bai, Z. Han, W. He and Z. Guo, *Chem. Soc. Rev.*, 2015, **44**, 4517-4546.

10. M. Beija, C. A. Afonso and J. M. Martinho, *Chem. Soc. Rev.*, 2009, **38**, 2410-2433.

11. H. Kobayashi, M. Ogawa, R. Alford, P. L. Choyke and Y. Urano, *Chem. Rev.*, 2009, **110**, 2620-2640.

12. M. Longmire, P. L. Choyke and H. Kobayashi, 2008.

13. G. Liang, H. Ren and J. Rao, *Nat. Chem.*, 2010, **2**, 54-60.

14. Z. Zheng, G. Li, C. Wu, M. Zhang, Y. Zhao and G. Liang, *Chem. Commun.*, 2017, **53**, 3567-3570.

15. Z. Hai, J. Wu, D. Saimi, Y. Ni, R. Zhou and G. Liang, *Anal. Chem.*, 2018, **90**, 1520-1524.

16. X. Ai, C. J. H. Ho, J. Aw, A. B. E. Attia, J. Mu, Y. Wang, X. Wang, Y. Wang, X. Liu and H. Chen, *Nat. Commun.*, 2016, **7**, 10432.

17. J. Mei, N. L. Leung, R. T. Kwok, J. W. Lam and B. Z. Tang, *Chem. Rev.*, 2015, **115**, 11718-11940.

18. M. Sy, A. Nonat, N. Hildebrandt and L. J. Charbonniere, *Chem. Commun.*, 2016, **52**, 5080-5095.

19. A. R. Sekhar, S. K. Sariki, R. R. Reddy, A. Bisai, P. K. Sahu, R. S. Tomar and J. Sankar, *Chem. Commun.*, 2017, **53**, 1096-1099.

20. D. G. McCafferty, B. M. Bishop, C. G. Wall, S. G. Hughes, S. L. Mecklenberg, T. J. Meyer and B. W. Erickson, *Tetrahedron*, 1995, **51**, 1093-1106.

Chapter 5: NIR-responsive metal Complexes for Precise Cell Activity Regulation

5.1 Introduction

Cell is known to has complex and heterogeneous structure. The membrane on its surface has a fluid and dynamic structure, which maintains the essential difference s between cytosol and extracellular environment. It has been well recognized that a variety of crucial cellular activities such as signal transduction, substance transportation, enzymatic activity etc., are critically dependent on cell membrane.[1] The misregulation of membrane-associated activities are involved in the progression of various degenerative diseases including cancer, atherosclerosis, and neurological disorder.[2, 3] Hence, the precise regulation of dynamic membrane associated processes would promote better understanding of fundamental physiological processes in living cells. More importantly it could also facilitate the development of therapeutic strategies for the treatment of various diseases. By right, chemical and genetic perturbation have been the major approaches to the studies of membrane-associated processes in biological systems.[4, 5] Although working successfully in principle, these strategies exhibited limited spatial and temporal resolution, which remains an inherent shortcoming for systematic analysis of dynamic biological phenomena due to the highly complex and heterogeneous nature of cells and living organisms[6].

Recently, optical manipulation of cell activities has gained considerable attention. As a unique strategy based on light stimulus, such high resolution optical control exhibits promising advantages to enable spatial and temporal manipulations of dynamic processes of protein activities and signalling pathways both *in vitro* and *in vivo*.[7, 8] However, most studies on optical regulation of membrane activities were achieved by using UV or visible light, which may raise the concerns of potential photo-damage, light toxicity, limited deep tissue penetration as well

as inherent absorption or scattering caused by endogenous biological molecules.[9, 10] Therefore, simple and specific light-mediated strategy that allows remote manipulation of membrane activities *in vitro* and *in vivo* through non-invasive and tissue-penetrable light irradiation remains a technical challenge. Recently, NIR light-responsive nanoparticles have been reported to regulate membrane associated processes within deep penetration and minimum light toxicity.[11, 12] Despite their initial success, the strategy may raise concerns associated with the use of nanomaterials such as their size, non-homogeneous composition, potential toxicity, limited batch-to-batch reproducibility etc.[13-15] Simple and robust small-molecule alternaives with properties such as strong luminescence, tunable emissions, less photo-bleaching, long lifetime, deep penetration, and good biocompatibility would be highly desirable and may be used for accurate optical control of cellular activities in living system.

As a promising alternative, small molecule complexes would exhibit promising advantages for their flexibilities in both chemical structures and functions. Basically, versatile desired properties such as tunable emissions, less photobleaching, long lifetime, deep penetration, good biocompatibility can be precisely fine-tuned through simple modifications of their ligands. In addition, small molecule complexes would allow easy and accurate characterization of their composition from single molecular level. More importantly, these comlexes would be able to covert NIR light into visible emissions upon two-photon excitation, which suggest the potential prospects of these simple and unique complexes towards optical regulation of cellular activities.

Herein, we introduce a simple yet effective approach based on small molecule complex for remote regulation of membrane activity. Generally, we first established simple and stable metal complex which have promising optical properties such as unique NIR light-converting proterties, intense emissions. To to achieve accurate modulation of the light-gated membrane

ion channel, the complex was localized on cell membrane through well-established bioorthogonal reaction (e.g. click reaction). Typically, we will introduce N_3-tagged glycans to cell surface through intrinsic metabolic pathways by simply adding a monosaccharide precursor, peracetylated N-azidoacetylmannosamine (Ac_4ManNAz) to cell culture medium. In addition, we will further engineer the complex with alkyne moiety on the ligand. To minize the potential damage to cells, a copper-free click reaction based on the dibenzocyclooctyne-conjugated complex as a bioorthogonal linkage will be used to covalently attach the complex on cell surface. As such, upon NIR light treatment, the complex on cell membrane would produce converted emission, activating light-responsive regulatory proteins on cell membrane and facilitate the regulation of subsequent cell activities both in vitro and in vivo.

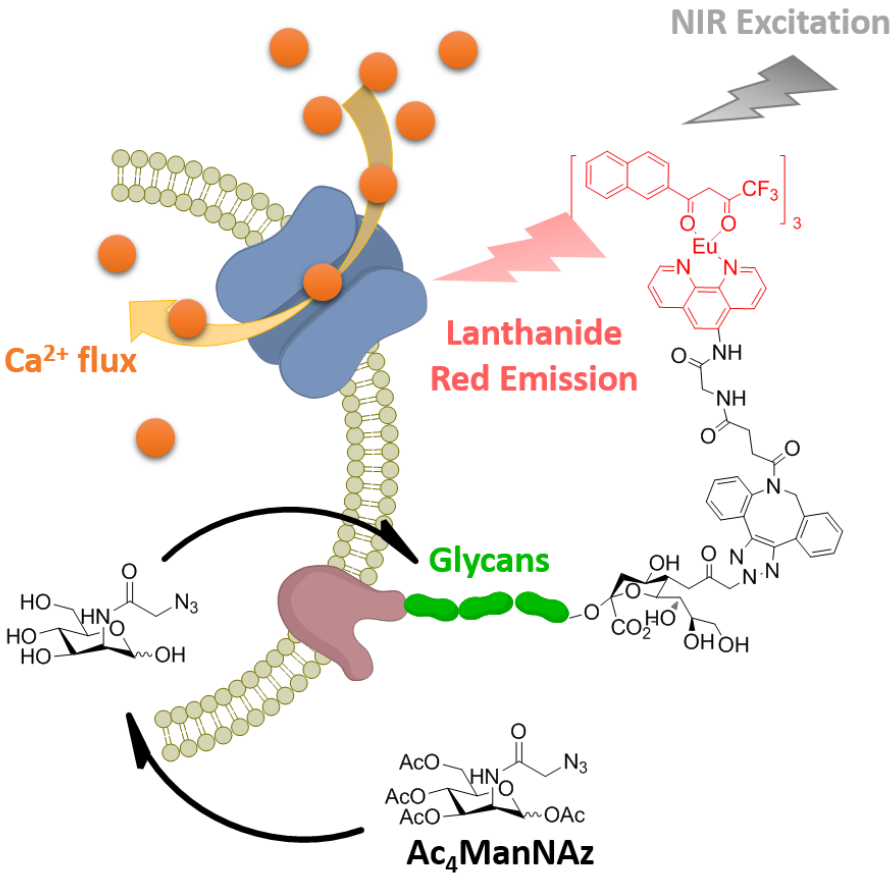

Fig 5.1 Scheme illustration of NIR-responsive metal Complexes for Precise Cell Activity Regulation

5.2 Materials and methods

Materials

Boc-glycine (Boc-Gly-OH), 1-[Bis(dimethylamino)methylene]-1H-1,2,3-triazolo[4,5-b]pyridinium 3-oxid hexafluorophosphate (HATU), N,N-Diisopropylethylamine (DIPEA), Trifluoroacetic acid (TFA), Europium(III) Chloride Hexahydrate (EuCl3.6H2O), 4,4,4-Trifluoro-1-(2-naphthyl)-1,3-butanedione (NTA), were obtained from Sigma-Aldrich. 1, 10-Phenanthrolin-5-amine, (Phen-NH2) was purchased from Santa Cruz. Dibenzocyclooctyne-N-hydroxysuccinimidyl ester (DBCO-NHS) and N-azidoacetylmannosamine-tetraacylated (Ac4ManNAz) were ordered from Click Chemistry Tools. Dulbecco's Modified Eagle Medium (DMEM), Reduced Serum Medium (Opti-MEM), fetal bovine serum (FBS), Antibiotic-Antimycotic, trypsin, Rhod-3 AM calcium imaging kit, Lipofectamine® 3000 transfection kit and PureLink® HiPure plasmid miniprep kit were obtained from Thermo Fisher Scientific. All the reagents indicated above were directly used without further purification.

Instruments.

NMR spectra were acquired on Bruker Avance 500 and Bruker Avance III 400 spectrometers. Mass spectra were obtained on a ThermoFinnigan LCQ Fleet MS. Fluorescence spectra were recorded on a Shimazu RF-5301PC spectrofluorophotometer. Two-photon emission spectrum was recorded at position perpendicular to the excitation beam (720 nm). The cell viabilities were tested on a microplate reader (BioTek). Fluorescence imaging and two-photon imaging of cells and zebrafish were carried out on a Nikon Eclipes TE2000-E microscope and Leica TCS SP5 X confocal microscope respectively. Light irradiation experiments were performed using either BLAK-RAY B-100AP/R UV lamp (365nm) or the Coherent Chameleon Ultra II pulsed laser (720nm).

Synthesis of Phen-Gly-Boc

1,10-Phenanthrolin-5-amine (80.0 mg, 0.410 mmol), Boc-Glycine-OH (78.9 mg, 0.451 mmol), HATU (311.8 mg, 0.820 mmol) and DIPEA (143 μL, 0.820 mmol) were dissolved in DMF (2 mL) in round bottom flask. The resulting mixture was then allowed to stir overnight at room temperature. After stirring, liquid-liquid extraction was carried out with H_2O-EA (v/v = 1:1) on the solution obtaining the organic layer for 4 times. The organic layer was washed with brine and dried with sodium sulphate. Excess EA was removed using rotary evaporator under reduced pressure. The compound was then dissolved in minimal amounts of EA and purified using silica column using stepwise elution with 150mL of 1%, 5%, 10%, 15%, 20% 25% MeOH in EA with 1% Ammonia as eluents respectively for each round. NMR and MS analysis was carried out to characterize the identity of the compound. 1H NMR (500 MHz, MeOD) of Phen-Gly-Boc: δ 9.12 (d, J = 3.5 Hz, 1H), 9.05 (d, J = 3.4 Hz, 1H), 8.65 (d, J = 8.2 Hz, 1H), 8.48 (d, J = 8.1 Hz, 1H), 8.13 (s, 1H), 7.82 (ddd, J = 10.7, 8.3, 4.4 Hz, 2H), 4.09 (s, 2H), 1.54 (s, 9H). M/Z = 353.30

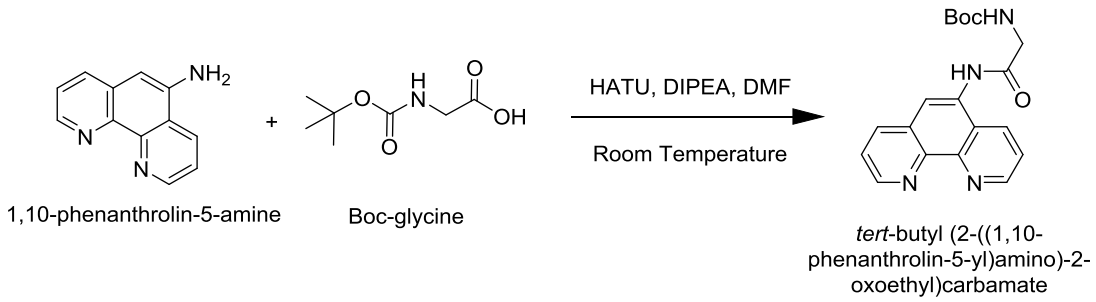

Fig 5.2 Synthetic scheme of Phen-Gly-Boc

Synthesis of Phen-Gly-DBCO

The removal of the Boc protecting group was achieved using DCM-TFA (v/v = 1:1, 16 mL). Excess TFA was removed by rotary evaporator under reduced pressure. The resulting

compound Phen-Gly-NH_2 was used in the following reaction without further purification. Typically, Phen-Gly-NH2 (6.80 mg, 0.0270 mmol), DBCO-NHS (12.0 mg, 0.0270 mmol) were added into a round bottom flask and dissolved in DMF with a 10-fold excess amount of DIPEA (2ml). The resulting mixture was then allowed to stir overnight at room temperature. After stirring, liquid-liquid extraction was carried out with H_2O-EA (v/v = 1:1) on the solution obtaining the organic layer for 4 times. The organic layer was washed with brine and dried with sodium sulphate. Excess EA was removed using rotary evaporator under reduced pressure to obtain the crude product. The crude compound was then dissolved in minimal amounts of DCM and purified using silica column using stepwise elution with 100mL of 0%, 1%, 2%, 3%, 4% 5% and 6% MeOH in DCM with 1% Ammonia as eluents respectively for each round. NMR and MS analysis was carried out to characterize the identity of the compound. 1H NMR (400 MHz, $CDCl_3$) of Phen-Gly-DBCO: δ 9.64 (s, 1H), 9.25 (dd, J = 4.3, 1.5 Hz, 1H), 9.20 (dd, J = 4.3, 1.6 Hz, 1H), 8.49 (dd, J = 8.4, 1.5 Hz, 1H), 8.33 (dd, J = 8.1, 1.6 Hz, 1H), 8.18 (s, 1H), 7.80 – 7.62 (m, 2H), 7.57 – 7.46 (m, 1H), 7.46 – 7.34 (m, 3H), 7.19 – 7.06 (m, 2H), 6.82 – 6.67 (m, 1H), 6.67 – 6.55 (m, 1H), 6.45 (d, J = 7.6 Hz, 1H), 4.52 (dd, J = 16.8, 7.5 Hz, 1H), 4.31 (d, J = 13.9 Hz, 1H), 3.82 (dd, J = 16.9, 5.1 Hz, 1H), 3.38 (d, J = 13.8 Hz, 1H), 2.49 – 2.28 (m, 2H), 2.13 – 1.85 (m, 3H). M/Z = 540.52.

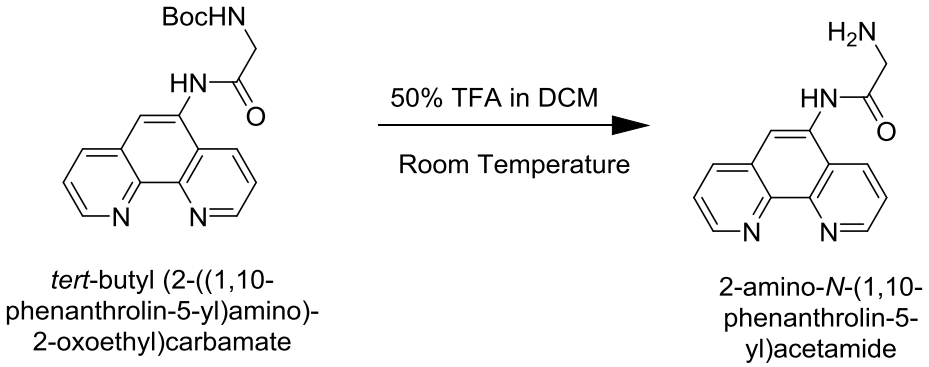

tert-butyl (2-((1,10-phenanthrolin-5-yl)amino)-2-oxoethyl)carbamate

2-amino-*N*-(1,10-phenanthrolin-5-yl)acetamide

Fig 5.3 Synthetic scheme of deprotection of Phen-Gly-Boc

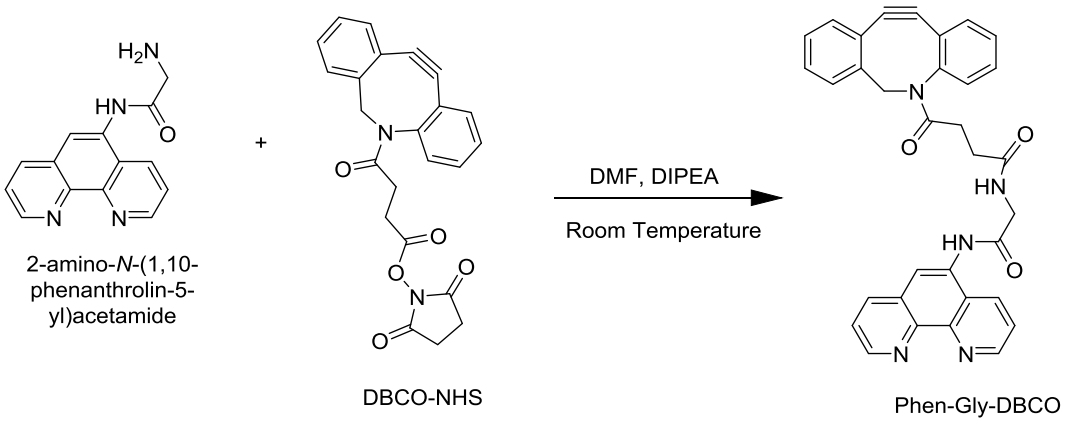

Fig 5.4 Synthetic scheme of Phen-Gly-DCBO

Synthesis of Eu(III) complex

EuCl3•6H2O (8.5 mg, 0.0232 mmol) dissolved in MeOH (400 μL) and added into a mixture of Phen-Gly-DBCO (12.6 mg, 0.0234 mmol) or Phenanthroline (4.2mg, 0.0233mmol) together with NTA (18.6 mg, 0.0699 mmol) that was dissolved in MEOH (600 μL) and DCM (200 μL). The mixture was allowed to be heated with reflux and stirred overnight. After heating with reflux overnight, the leftover MeOH and DCM were removed under reduced pressure using rotary evaporator. Minimum amount of MeOH was added to dissolve the compound. The resulting solution was then added into deionized water to obtain the Europium (III) complex precipitate. MS analysis were done to characterize the compound. M/Z = 1224.13 $[M\text{-}NTA]^+$.

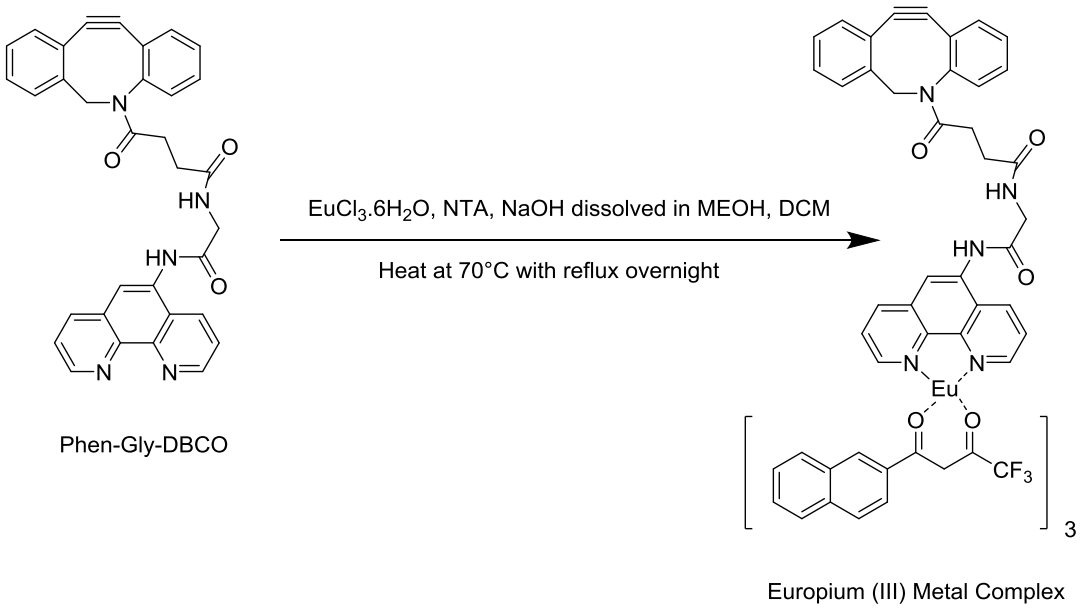

Fig 5.5 Synthetic scheme of Eu(III) complex **Eu-DBCO**.

Cell culture and metabolic labeling on cell membrane

The human embryonic kidney 293 (HEK293) cell lines were purchased from American Type Culture Collection (ATCC). The cells were cultured in Dulbecco's modified Eagle medium (DMEM) supplemented with 10% fetal bovine serum (FBS), 100 units mL^{-1} penicillin and 100 μg mL-^{1} streptomycin and maintained in a humidified incubator with 5% CO^2 at 37 °C. The cells were seeded at a density of 1×10^5 in 12-well plate and incubated with 50 μM of Ac_4ManNAz for 2 days. The cells were trypsinized and cultured in an ibidi dish (35 mm, plastic bottom) at 1×10^5 cells/well in 1 mL DMEM medium overnight. The azido-labeled cell membrane was stained with CellMask DeepRed (5 μM, 10 min) separately and imaged using confocal microscope. For cell viability test, HEK293 cells were seeded in 96-well plate (1×10^4 HEK293 cells per well) and incubated for 24 h. Then, cells were incubated with Ac_4ManNAz or Eu(III) complex of different concentrations for another 24 h and the cell viabilities were evaluated using TOX8 assay kit (resazurin based) by following standard manufacturer's protocol.

Membrane channel expression and covalent labeling of Eu-DBCO on HEK293 cell membrane

Generally, ChrimsonR-GFP plasmid was purchased from Addgene[16]. The plasmid DNA was replicated and purified with commercial available kit by following manufacturer's procedure. For ion channel expression, HEK293 cells were seeded with the density of 1×10^5 and incubated for 24 h. The commercial plasmid transfection reagant, Lipofectamine® 3000, was used according to the manufacturer's protocol in Opti-MEM medium.[17] After 4 h incubation, the medium was replaced with fresh DMEM medium containing Ac_4ManNAz (50 μM). The cells were cultured in incubator for 48 h and re-plated in ibidi dish (35 mm, 1×10^5 cells) for another 24 h. For confocal imaging experiments, cell samples were washed twice with DMEM medium and incubated with Eu-DBCO at a concentration of 60 μM for 3h at 37 °C. The cells were washed 3 times with DMEM medium prior to imaging (λ_{ex}=350±25nm).

Intracellular calcium analysis by Rhod-3 AM

Calcium imaging kit (Rhod-3AM) was dissolved in 100 μL DMSO to prepare a stork solution (10 mM). After Eu-DBCO labeling on transfected HEK293 cells, the samples in dishes (1×10^5 cells per well) were incubated with Rhod-3 AM (10 μM) for 30 min in the dark by following manufacturer's protocol. Then the cells were washed 3 times with serum-free DMEM medium and irradiated with 720 nm NIR light. [11]The intracellular calcium imaging was recorded on Leica TCS SP5 X confocal microscope (λ_{ex}= 560 nm).

***In vivo* animal studies and preparation:**

All the animal involved experiments were carried out by following the approved guidelines of Nanyang Technological Univercity Institutional Animal Care and Use Committee (IACUC). Typically, zebra fish embryos were kept in E3 media which contains 0.1% Methylene Blue, 0.33 mM $MgSO_4$, 0.33 mM $CaCl_2$, 0.17 mM KCl and 5 mM NaCl, pH 7.0−7.2. The fish

embryos were raised at 28.5 °C. Prior to experiments, the fish larvae were anesthetized at 48hours post fertilization by using 0.003% trcaine. Cells expressing ChrimsonR-GFP were incubated with Ca2+ indicator and harvested (5×10^6 cells/mL). The harvested cells were injected into the yolk sac of zebra fish larvae through pressurized microinjector (MPPI-3 Applied Scientific). After the implantation of cells, the larvae were washed with E3 media. The Eu(III) complex were injected into the yolk sac of these larvae which have been already implanted with cells. In Ca^{2+} imaging experiment, the anesthetized larvae were imaged in ibidi dish (35mm). The larvae were irradiated with NIR light (720nm) for different time durations. Fluorescence images of zebra fish larvae were captured on a Leica TCS SP5 X confocal microscope before and after NIR light stimulation.

5.3 Results and discussion

Covalent localization of Eu-DBCO on cell surface

To accurately manipulate membrane channel events, a light-sensitive ion channel ChrimsonR was incorporated onto cell surface in order to induce the influx of ions such as singaling cation Ca^{2+}. The successful incorporation of ChrimsonR on cell surface was monitored via the appearance of fluorescence signal from marker protein (GFP) through fluorescence imaging (Fig 5.6) and flow cytometry (FCM) (Fig 5.7) . In addition, similar cell staining was observed through a well-established membrane tracker CellMask Deepred, suggesting the successful expression of light-sensitive channel on cell surface. Furthermore, in order to induce NIR light controlled manipulation of membrane channel activities, lanthanide complex (e.g. Eu(III) complex) was utilize as light transducer mainly due to its two-photon optical proterties.

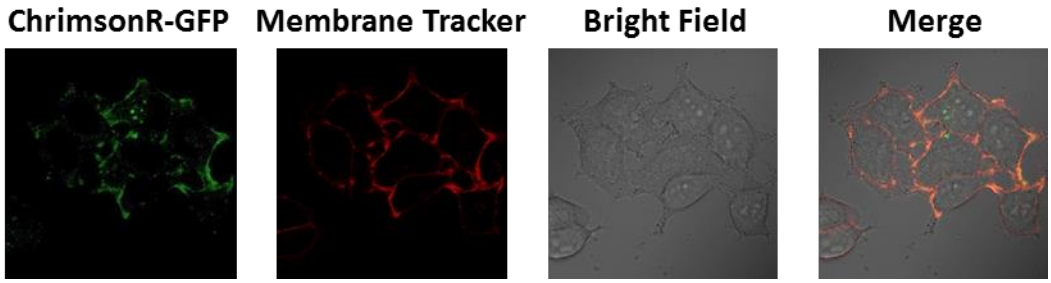

Fig 5.6 Confocal Imaging of HEK293 cells transfected with ChrimsonR-GFP Green: GFP (Ex: 488 nm, Em: 530/50 nm), red: CellMask DeepRed (Ex: 633 nm, Em: 670/50 nm).

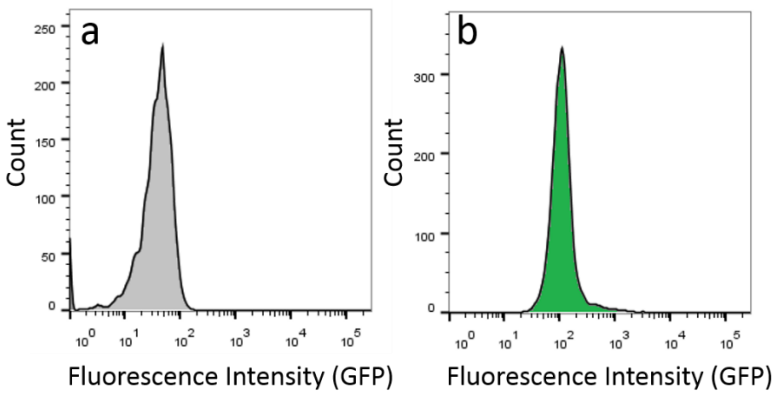

Fig 5.7 FCM analysis of ChrimsonR expression in HEK293 cells through marker protein GFP. a) HEK293 cells without ChrimsonR expression. b) HEK293 cells with successful incorporation of ChrimsonR.

To promote the localization Eu(III) complex on cell membrane, ring strained alkyne DBCO moiety was conjugated with the ligand molecule 1,10-Phenanthroline (Fig 5.2, Fig 5.3 and Fig 5.4). The resulting Eu(III) complex (**Eu-DBCO**) exhibited strong fluorescence emission at ~615nm upon excitation (350nm) (Fig 5.8). In addition, upon two-photon excitation condition (720nm), the strong red emission (615nm) was observed (Fig 5.9), which matched very well with the absorption maxima of ChrimsonR[16].

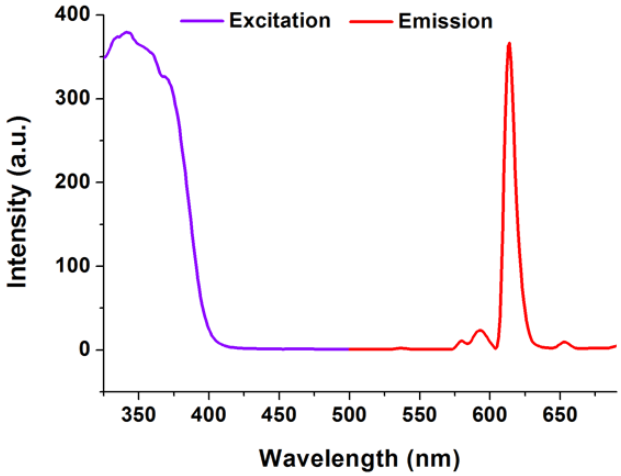

Fig 5.8 Fluorescence spectra of Eu-DBCO in HEPES buffer (1% DMSO), λ_{ex}=350nm, λ_{em}=615nm.

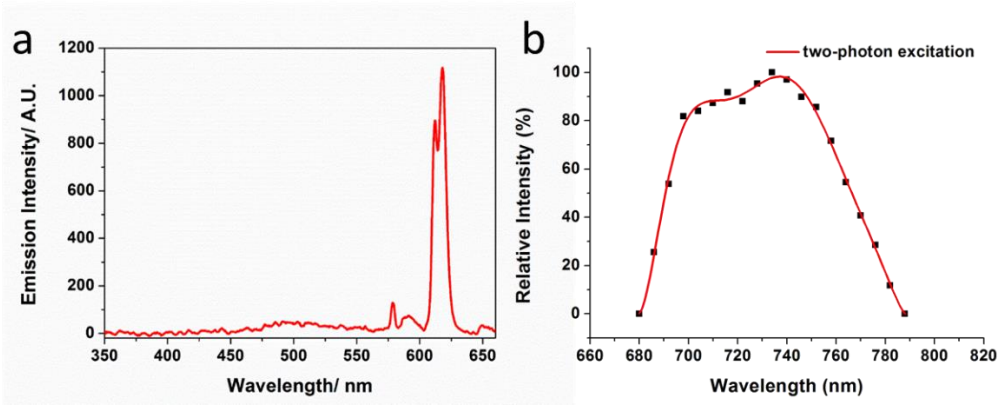

Fig 5.9 Fluorescence spectra of Eu-DBCO under two-photon excitation. a) Emission spectra of Eu-DBCO λ_{ex}=720nm, b) Excitation spectra of Eu-DBCO λ_{em}=615nm

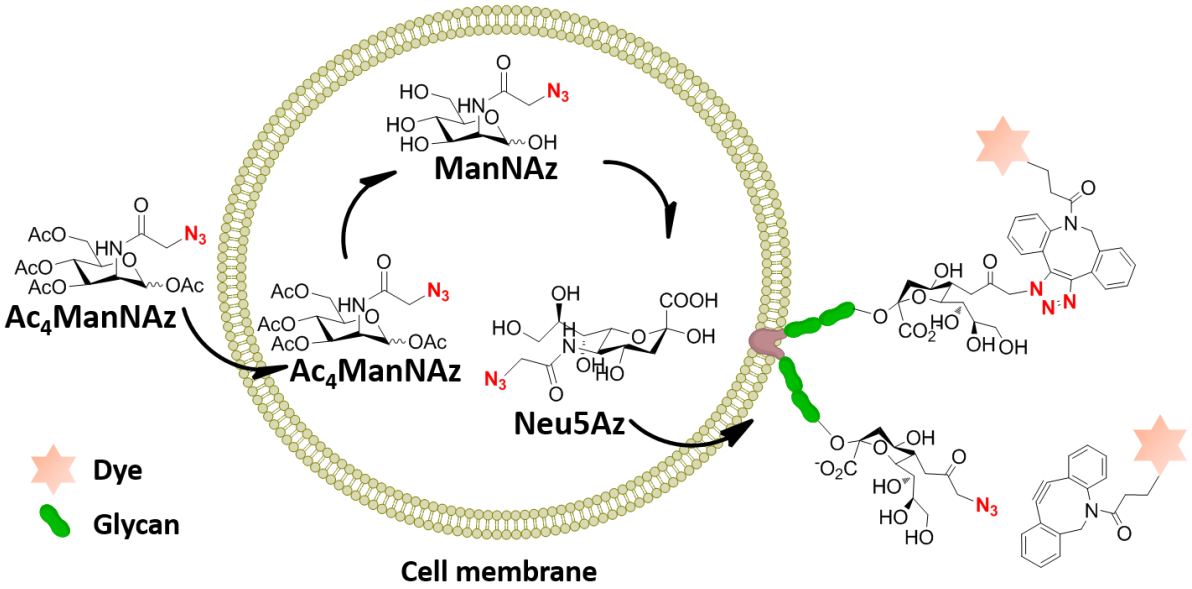

Fig 5.10 Schematic presentation of bioorthogonal labelling procedure of cells. Ac4ManNAz was incubated. It diffuse into cells and deacetylated by intracellular esterase. Subsequently, ManNAz is converted to Neu5Az and incorporated into glycan by sialytransferases and transported to cell surface. The cell surface labelled azide would allow further conjugation with alkyne-tagged dye through click reactions.

To accurate modulation of the light-gated ion channel, we started localizing Eu complex on cell surface. Firstly, cell surface glycans were covalently labeled with azido group via native metabolic biosynthesis pathways (Fig 5.10)[18, 19]. To introduce azide onto cell membrane, Ac_4ManNAz precusor was incubated with cells. Then, a copper free click reaction between DBCO-conjugated dye (for instance DBCO-conjugated Cy3 or Eu complex) and cell surface azide was performed. The cell surface labeling was observed through confocal microscopy and flow cytometry. As can be observed in Fig 5.11, bright yellow signal of DBCO-Cy3 can be captured on the surface of HEK293 cells which have been incubated with Ac_4ManNAz. In the meantime, similar staining pattern of cell surface was obtained by well-established cell membrane probe. In contrast, no obvious fluorescence signal was observed from cell which was cultured in the absence of Ac_4ManNAz, suggesting the successful conjugation of Azide and DBCO-Cy3 on cell surface. In addition, flow cytometry studies also confirmed the

increased signal of DBCO-Cy3 (Fig 5.12) from Ac_4ManNAz treated cells compared to cells without Ac_4ManNAz treatment. Besides, cell viability assay (Fig 5.13) revealed that, no obvious toxicity was observed towards HEK293 cells under the current conditions suggesting the feasibility of successful conjugation of functional molecules on cell surface through metabolic biosynthetic pathways.

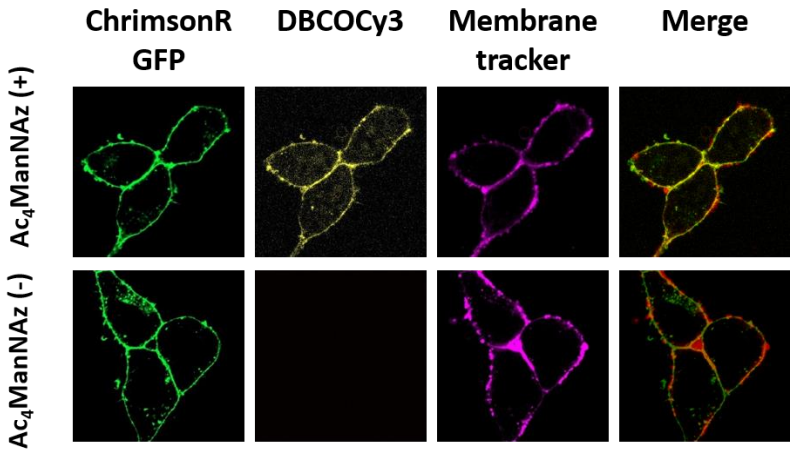

Fig 5.11 Imaging azido groups on the membrane of HEK293 cells stained with DBCO-Cy3 after treatment with (top) or without (bottom) Ac4ManNAz (50 μm). Green: GFP (Ex: 488 nm, Em: 530/50 nm), yellow: DBCO-Cy3 (Ex: 543 nm, Em: 580/50 nm), violet: CellMask DeepRed (Ex: 633 nm, Em: 670/50 nm).

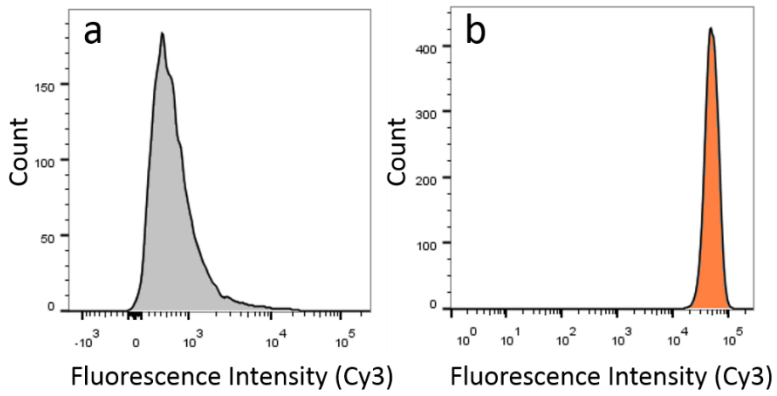

Fig 5.12 FCM analysis of DBCO-Cy3 labelled HEK293 cells after treatment a) with or b) without Ac_4ManNAz (50μM)

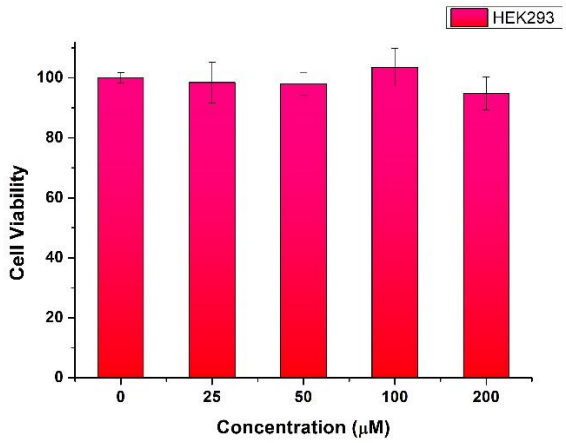

Fig 5.13 Cell viability of HEK293 cells treated with Ac4ManNAz of different concentrations.

Secondly, the copper-free reaction between cell-surface labelled azide and ring-strained alkyne (DBCO moiety) of **Eu-DBCO** allowed successful anchoring of Eu complex on cell membrane. It can be seen that, red fluorescence signal of **Eu-DBCO** (Fig 5.14, Fig 5.15 and Fig 516) appeared on the surface of HEK293 cells which had been incubated with Ac_4ManNAz. In addition, the obvious overlap (Fig 5.15) between Eu-DBCO and membrane tracker confirm the localization of Eu complex on cell membrane. In contrast, no obvious fluorescence signal was observed on the membrane of cells cultured without Ac_4ManNAz or azide tagged cells incubated with control molecule (**Eu-Phen)** without DBCO moiety. These resultes suggested the successful linkage of luminescent molecules (Eu-DBCO) on the cell surface by means of cell's intrinsic metabolic biosynthetic mechanism.

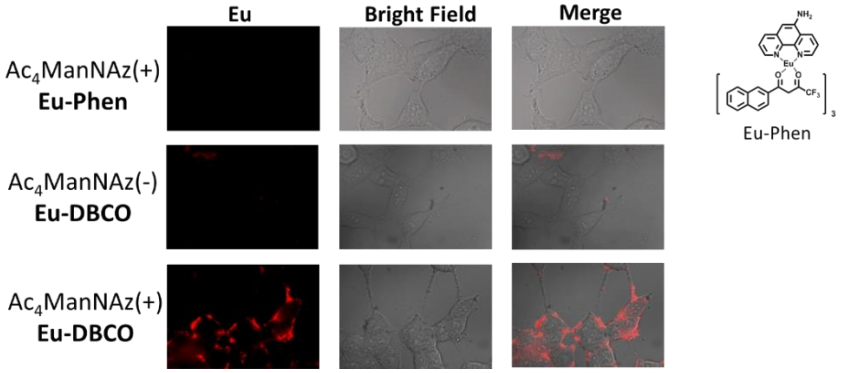

Fig 5.14 Fluorescence images of HEK293 cells labelled with Eu(III) complex (Ex=350nm, Em=610/50nm).

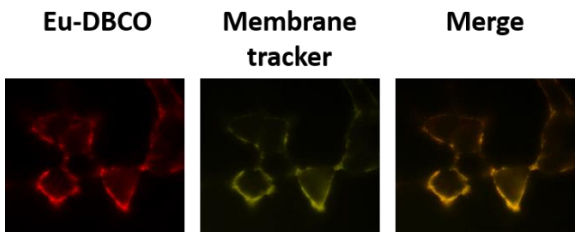

Fig 5.15 Fluorescence images of azide expressed HEK293 cells labelled with Eu-DBCO (Red: Ex=350nm, Em=610/50nm, yellow: Ex: 633 nm, Em: 670/50 nm).

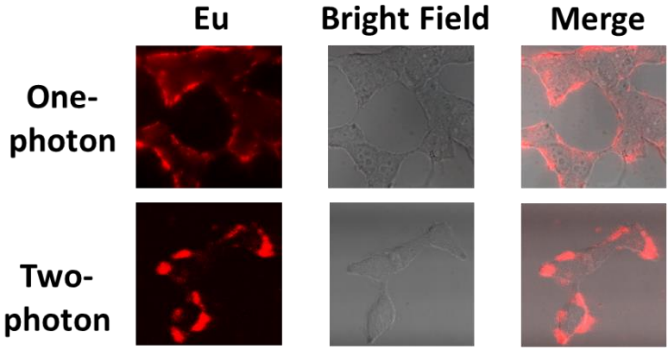

Fig 5.16 Fluorescence images of HEK293 cells labelled with Eu-DBCO (λ_{ex}=350nm, one-photon condition; λ_{ex}=720nm, two-photon condition).

Remote manipulation of membrane-associated activity on live cells

To evaluate the potential application of Eu(III) complex for precisely regulation of membrane-associated events, NIR light was applied to irradiate the Eu(III) complex labelled on the surface of transfected cells. Upon two-photon excitation, the red emission of the complex was utilized to stimulate the red light-sensitive membrane channel and induce cation influx (e.g. Ca^{2+}) into the intracellular compartment. In order to monitor the fluctuation of intracellular Ca^{2+}, a commercial Ca^{2+} fluorescent probe (Rhod-3 AM) was used to visualize the change of Ca^{2+} concentration inside cells. As illustrated in Fig 5.17, upon treatment of NIR light stimulation, ChrimsonR expressing cells (with Eu-DBCO labelled on their surface) exhibited obvious increase in the intracellular fluorescence signal, while cell treated with control molecule (Eu-Phen) exhibit no obvious enhance in intracellular Ca^{2+}. The elevated intracellular Ca^{2+} revealed that membrane-localized Eu(III) complex could be utilized as a

mediator to accurately manipulate the cation flow across cellular membrane. Additionally, cell viability assay revealed that no obvious toxicity to cells under similar condition of membrane activity manipulation (Fig 5.18), suggesting good biocompatibility of the probe.

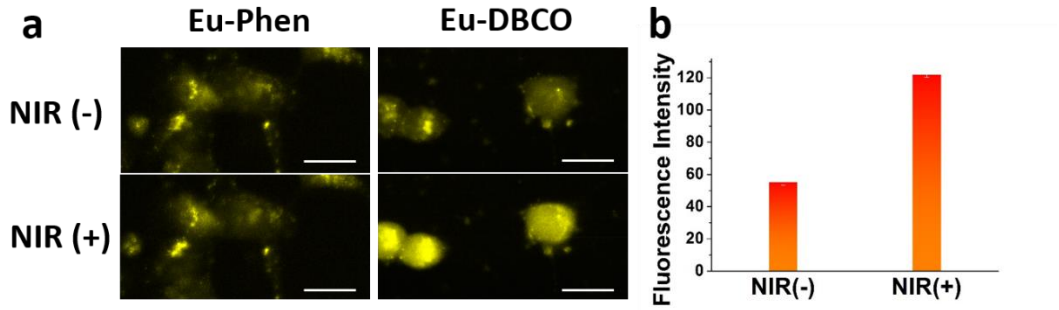

Fig 5.17 Cell activity manipulated through NIR two-photon illumination. a) Intracellular Ca^{2+} imaging before and after NIR light treatment. b) Fluorescence intensity of Ca^{2+} indicator before and after NIR light stimulation (Eu-DBCO).

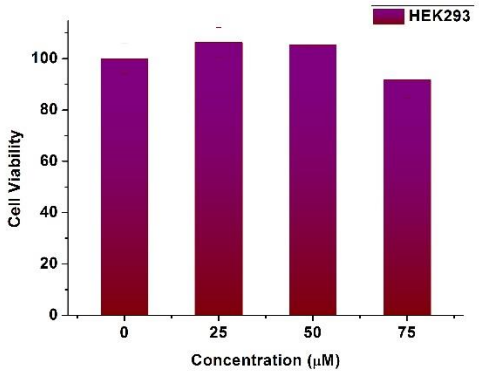

Fig 5.18 Cell viability of HEK293 cells treated with Eu-DBCO of various concentration.

Remote manipulation of membrane-associated activity within living animals

Furthermore, we also evaluate whether precise manipulation of membrane-associated activity can be induced through red-emissive lanthanide complex upon NIR light treatment. To this end, confocal microscopy was used to monitor the change of Ca^{2+} inside zebra fish. Generally, ChrimsonR transfected cells (labelled with N_3) with calcium probe (Rhod-AM3) were implanted into the yolk sac of zebra fish larvae at 48 hours post-fertilization. Then, Eu-DBCO was injected into the yolk sac of larvae to facilitate the localization of the complex on

cell surface. The obvious fluorescence signal in the abdominal area suggested the successful injection of Eu(III) complex into the larvae (Fig 5.19a). Upon 6h clearance, obvious fluorescence signal in larvae injected with **Eu-DBCO** could still be observed. However, negligible signal could be visualized in larvae injected with control molecule **Eu-Phen** without DBCO moiety (Fig 5.19a). Similarly, the effective localization of Eu complex was also revealed by quantitative analysis (Fig 5.19a); a higher mean fluorescence intensity in zebra fish larva injected with **Eu-DBCO** was observed after 6h clearance. The obvious difference in labelling effect in zebra fish larvae suggested that metabolic glycan labelling could effectively promote the accumulation of Eu(III) complex under in vivo conditions.

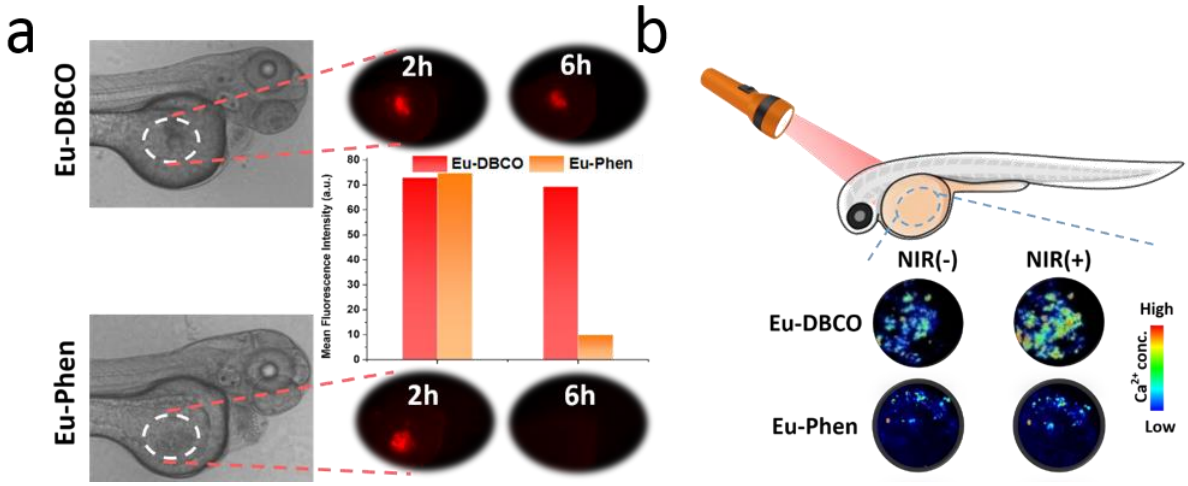

Fig 5.19 in vivo imaging and quantitative analysis of a) zebra fish injected with N3 labelled cells and Eu(III) complex (top: Eu-DBCO, bottom: Eu-Phen). b) Ca^{2+} imaging with or without NIR light treatment within zebra fish.

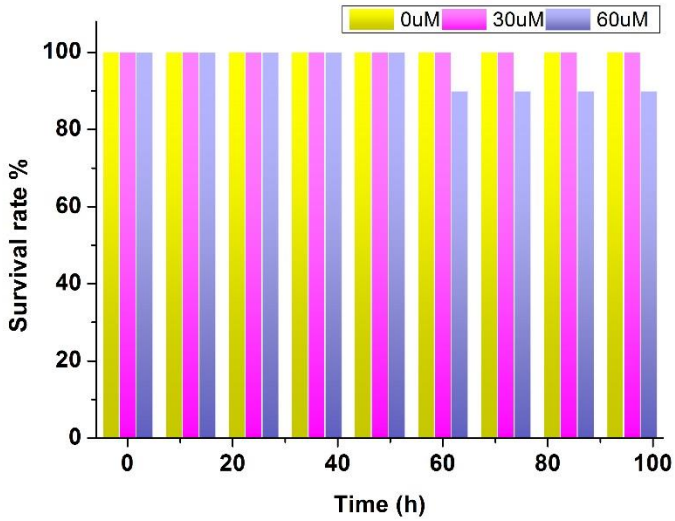

Fig 5.20 Survival rate of zebra fish larva after treatment with Eu-DBCO of various concentrations (each concentration n=10).

Moreover, to remotely manipulate the membrane channel activity in living animals, NIR light (720nm) was applied to irradiate the larvae. The Ca^{2+} flux in zebra fish was monitored by using observing the fluorescence signal of Rhod-AM3. As illustrated in Fig.5.12b, after NIR light treatment, fluorescence enhancement of Ca^{2+} probe can be observed in the larvae which were injected with Eu-DBCO. In contrast, little fluorescence change was observed in the larvae in the control group (Fig.5.19b). Additionally, the survival rate (Fig 5.20) of zebra fish larva treated with Eu-DBCO was monitored for 96 hours, revealing that no obvious toxicity to the larva under similar condition of membrane activity manipulation. These results demonstrated that the Eu-DBCO labelled in the larvae could successfully modulate the ion channel activity induced by the NIR light treatment under in vivo settings.

5.4 Conclusion

To summarize, we have developed novel strategy based on intrinsic metabolic synthesis pathways to achieve specific localization of NIR-light sensitive metal complex on cell surface by means of bioorthogonal reaction under in vivo conditions. Upon NIR light (720nm) stimulation, red emission from the metal complex could remotely modulate light responsive

membrane channel activity and regulate the ion flux in both live cells and animals. This strategy provides an effective and specific method for localization of luminescent complex on cell surface. In addition, it exhibits great potential to remotely manipulate biological events under in vivo settings. As such, these metal complexes have the potential to serve as tailored smart medicines for pathological disorders in the long run.

5.5 Reference

1. C. GM, in *The Cell: A Molecular Approach*, Sinauer Associates, Sunderland (MA), 2nd edition edn., 2000.
2. M. S. Brown, J. Ye, R. B. Rawson and J. L. Goldstein, *Cell*, 2000, **100**, 391-398.
3. A. Weihofen and B. Martoglio, *Trends Cell Biol.*, 2003, **13**, 71-78.
4. M. A. Shogren-Knaak, P. J. Alaimo and K. M. Shokat, *Annu. Rev. Cell. Dev. Biol.*, 2001, **17**, 405-433.
5. H. Wang, M. La Russa and L. S. Qi, *Annu. Rev. Biochem.*, 2016, **85**, 227-264.
6. M. Endo and T. Ozawa, *Journal of Photochemistry and Photobiology C: Photochemistry Reviews*, 2017, **30**, 10-23.
7. A. Bansal, H. Liu, M. K. G. Jayakumar, S. Andersson‐Engels and Y. Zhang, *Small*, 2016, **12**, 1732-1743.
8. X. Wu, Y. Zhang, K. Takle, O. Bilsel, Z. Li, H. Lee, Z. Zhang, D. Li, W. Fan and C. Duan, *ACS nano*, 2016, **10**, 1060-1066.
9. K. Szaciłowski, W. Macyk, A. Drzewiecka-Matuszek, M. Brindell and G. Stochel, *Chem. Rev.*, 2005, **105**, 2647-2694.
10. H. Kobayashi, M. Ogawa, R. Alford, P. L. Choyke and Y. Urano, *Chem. Rev.*, 2009, **110**, 2620-2640.
11. S. K. Mohanty, R. K. Reinscheid, X. Liu, N. Okamura, T. B. Krasieva and M. W. Berns, *Biophys. J.*, 2008, **95**, 3916-3926.

12. S. Hososhima, H. Yuasa, T. Ishizuka, M. R. Hoque, T. Yamashita, A. Yamanaka, E. Sugano, H. Tomita and H. Yawo, *Sci. Rep.*, 2015, **5**.

13. Y. Liu, Q. Su, X. Zou, M. Chen, W. Feng, Y. Shi and F. Li, *Chem. Commun.*, 2016, **52**, 7466-7469.

14. N. Desai, *The AAPS journal*, 2012, **14**, 282-295.

15. E. Papagiakoumou, F. Anselmi, A. Bègue, V. De Sars, J. Glückstad, E. Y. Isacoff and V. Emiliani, *Nat. Methods*, 2010, **7**, 848-854.

16. N. C. Klapoetke, Y. Murata, S. S. Kim, S. R. Pulver, A. Birdsey-Benson, Y. K. Cho, T. K. Morimoto, A. S. Chuong, E. J. Carpenter and Z. Tian, *Nat. Methods*, 2014, **11**, 338.

17. , https://tools.thermofisher.com/content/sfs/manuals/lipofectamine3000_protocol.pdf.

18. J. A. Prescher, D. H. Dube and C. R. Bertozzi, *Nature*, 2004, **430**, 873.

19. J. M. Baskin, J. A. Prescher, S. T. Laughlin, N. J. Agard, P. V. Chang, I. A. Miller, A. Lo, J. A. Codelli and C. R. Bertozzi, *Proc. Natl. Acad. Sci.*, 2007, **104**, 16793-16797.

Chapter 6: Conclusion

By now, nanotechnology exhibits unique advantages for research and development of effect and safer therapeutic and diagnostic modalities mainly for its ability to improve drug loading efficiency, pharmacokinetics as well as to minimize side effects. Considering the unique and desirable properties of different nanostructures, nanoformulation of traditional metal complex has been demonstrated promising strategy to solve the issues of currently used metal complex as therapeutic and sensing agents. In this dissertation, some intelligent platform were built based on stimuli-responsiveness of metal complex and nanostructures to facilitate the future advance of precise therapeutics and diagnostics.

Firstly, photo-sensitive Re(I) complex was incorporated onto light converting nanoparticles to construct a light mediated system which is capable of activating cytotoxic Re(I) complex for therapeutic purpose. Owing to the great spatial-temporal resolution of light irradiation, upon NIR stimulation, Re(I) complex can be locally activated within pathological side by upconverted UV light from nanoparticles and exert cytotoxic effect for precise treatment against both drug-susceptible and drug-resistant cancer cells, minimizing unwanted photo damage.

In addition, to selectively detect illicit drug Gamma-hydroxybutyric acid (GHB), we provide a bioinspired strategy based on stimuli-responsive formulation of AuNPs from Au(III) complex. Upon substrate-specific enzyme recognition of GHB, reduced nicotinamide adenine dinucleotide (NADH) would be generated and promoted the reduction of gold(III) complex to form gold nanoparticles. Thus allowing selective sensing of GHB through both spectroscopic analysis and naked-eye observation.

Thirdly, to develop a probe for long term sensing and imaging in response to reducing cellular environment, we introduced a strategy based on nanoformulation of lanthanide complex which can respond to reducing environment. Within reducing environment, the lanthanide complex would undergo inter-molecular cross linking and form dimer structure.

Further self-assembly of the lanthanide dimer yield luminescent nanoscaled particles which can potentially accumulate within cells for long term intracellular sensing and imaging purpose.

Finally, we provided a light induced strategy for remote manipulation of cell membrane activity. To precisely regulate membrane event, we started with site-specifically localize luminescent complex on cell surface through metabolic labelling and biorthogonal reaction. The luminescence of the metal complex could activate the light-sensitive ion channel on cell membrane and allow remote regulation of cation influx under both in vitro and in vivo settings. Such strategy can serve as a useful toolbox for accurate perturbation of biological event and promote in-depth understanding of the diverse biological processes in biomedical studies.

Publications

[1] **Hu, Ming**.;Ai, Xiangzhao.;Wang, Zhimin.;Zhang, Zhijun.;Cheong, Haolun.;Zhang, Wenmin.;Lin, Jun.;Li, Juan.;Yang, Huanghao.; Xing, Bengang. Nanoformulation of metal complexes: Intelligent stimuli-responsive platforms for precision therapeutics. *Nano Res.* **2018**, 10.1007/s12274-018-2138-1.

[2] **Hu, Ming**.;Zhao, Jixian.;Ai, Xiangzhao.;Budanovic, Maja.;Mu, Jing.;Webster, Richard. D.;Cao, Qian.;Mao, Zongwan.; Xing, Bengang. Near infrared light-mediated photoactivation of cytotoxic Re (I) complexes by using lanthanide-doped upconversion nanoparticles. *Dalton Trans.* **2016**, *45*, 14101-14108.

[3] Lyu, Linna.;**Hu, Ming**.;Fu, Afu.; Xing, Bengang. Extracellular Vesicles-Directed Exogenous Ion Channels Transport for Precise Manipulation of Biological Events. *Bioconj. Chem.* **2018**, 10.1021/acs.bioconjchem.8b00377.

[4] Ai, Xiangzhao.;**Hu, Ming**.;Wang, Zhimin.;Zhang, Wenmin.;Li, Juan.;Yang, Huanghao.;Lin, Jun.; Xing, Bengang. Recent advances of membrane-cloaked nanoplatforms for biomedical applications. *Bioconj. Chem.* **2018**, *29*, 838-851.

[5] Ai, Xiangzhao.;**Hu, Ming**.;Wang, Zhimin.;Lyu, Linna.;Zhang, Wenmin.;Li, Juan.;Yang, Huanghao.;Lin, Jun.; Xing, Bengang. Enhanced Cellular Ablation by Attenuating Hypoxia Status and Reprogramming Tumor-Associated Macrophages via NIR Light-Responsive Upconversion Nanocrystals. *Bioconj. Chem.* **2018**, *29*, 928-938.

[6] Lyu, Linna.;Liu, Fang.;Wang, Xiaoyong.;**Hu, Ming**.;Mu, Jing.;Cheong, Haolun.;Liu, Gang.; Xing, Bengang. Stimulus - Responsive Short Peptide Nanogels for Controlled Intracellular Drug Release and for Overcoming Tumor Resistance. *Chem.-Asian J.* **2017**, *12*, 744-752.

[7] Ai, Xiangzhao.;Lyu, Linna.;Mu, Jing.;**Hu, Ming**.;Wang, Zhimin.; Xing, Bengang. Synthesis of Core-shell Lanthanide-doped Upconversion Nanocrystals for Cellular Applications. *J. Vis. Exp.* **2017**, 10.3791/56416.

[8] Wang, Yifeng.;**Hu, Ming**.;Hayashi, Hirohito.;Xing, Bengang.; Chiba, Shunsuke. Linking of Alcohols with Vinyl Azides. *Org. Lett.* **2016**, *18*, 992-995.